

MOLECULAR MECHANISM OF
DEPHOSPHORYLATION
BY DUAL-SPECIFICITY PHOSPHATASES

by
Youngjoo Kim

A DISSERTATION

Presented to the Department of Biochemistry and Molecular Biology
and the Oregon Health & Science University

School of Medicine

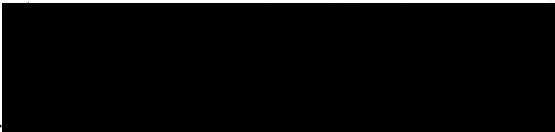
in partial fulfillment of
the requirements for the degree of
Doctor of Philosophy

Jan 2004

School of Medicine
Oregon Health and Science University

CERTIFICATE OF APPROVAL


This is to certify that the Ph.D. thesis of
Youngjoo Kim
has been approved



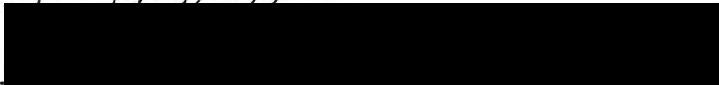
Dr. John Denu



Dr. Philip Stork



Dr. Richard Brennan



Dr. David Farrens



Dr. James Lundblad

TABLE OF CONTENTS

Table of Contents	i
List of Tables	iv
List of Figures	v
List of Abbreviations	vii
Acknowledgements	xii
Abstract	xiii
Chapter 1: Introduction	1
1.1 Introduction to protein phosphatases	2
1.2 Dual-specificity phosphatases (DSPs)	4
1.3 VHR	5
1.3.1 Structure	5
1.3.2 Mechanism	6
1.3.3 Regulation	7
1.3.4 Goals of the VHR project	8
1.4 MKP3	8
1.4.1 Activation of MKP3 by ERK binding	9
1.4.2 Structure	11
1.4.3 ERK; a physiological substrate of MKP3	12
1.4.4 Goals of the MKP3 project	13
Chapter 2: Intramolecular dephosphorylation of ERK by MKP3	24
2.0 Preface	24
2.1 Introduction	25
2.2 Materials and Methods	27
2.2.1 Protein preparation	27
2.2.2 <i>p</i> NPP assay	28

2. 2. 3	Generation of MKP3 antibody	28
2. 2. 4	Dephosphorylation of recombinant ERK2 proteins by phosphatases	28
2. 2. 5	Fluorescence anisotropy	30
2. 2. 6	Chemical cross-linking of C293S MKP3 and pERK	30
2. 2. 7	Dissociation constant of D316/319N ERK and L4A H176E ERK to MKP3	30
2. 3	Results	32
2. 3. 1	The N-terminal domain of MKP3 increases the effective pERK substrate concentration	32
2. 3. 2	Intramolecular dephosphorylation of pERK by MKP3	35
2. 3. 3	Stoichiometry of the substrate/enzyme complex of pERK-bound MKP3	38
2. 4	Discussion	41
2. 5	Acknowledgement	45
Chapter 3:	Probing the transition state structure of dual-specificity phosphatases using a physiological substrate mimic	76
3. 0	Preface	76
3. 1	Introduction	77
3. 2	Materials and Methods	79
3. 2. 1	Materials	79
3. 2. 2	Assays	79
3. 2. 3	Inhibition by <i>m</i> NBP	80
3. 2. 4	Isotope effect determinations	80
3. 2. 5	D ₂ O Solvent isotope effect	82
3. 3	Results and Discussion	83
3. 4	Acknowledgement	94

Chapter 4: Summary and Conclusions	109
4. 1 Mechanism of pERK dephosphorylation by MKP3	110
4. 2 Transition state structure of VHR using a physiological substrate mimic (<i>m</i> NBP)	113
References	115
Appendix. A continuous, nonradioactive assay for histone acetyltransferase	129

LIST OF TABLES

2. 1	<i>p</i> NPP hydrolysis activity by VHR, MKP3/VHR chimera, and wild-type MKP3	46
3. 1	Experimental values for $^{18}(V/K)_{\text{bridge}}$ and $^{18}(V/K)_{\text{nonbridge}}$	95

LIST OF FIGURES

1. 1	MAP kinase signaling cascade	14
1. 2	Domain organizations of PTPase	16
1. 3	Structural comparison between VHR and the catalytic domain of MKP3	18
1. 4	Catalytic mechanism of PTPs	20
1. 5	MKP3 catalytic mechanism for phosphoryl-enzyme intermediate formation	22
2. 1	The crystallographic model of phosphorylated ERK dimer	48
2. 2	Generation of MKP3/VHR chimera	50
2. 3	Binding affinity of ERK to MKP3 and an MKP3/VHR chimera	52
2. 4	Effect of fluorescent labeling on the binding of ERK to MKP3	54
2. 5	Time-dependent dephosphorylation of pERK by MKP3, VHR, and an MKP3/VHR chimera	56
2. 6	Time-dependent dephosphorylation of pERK by VHR and the MKP3/VHR chimera using a radioactive kinase assay	58
2. 7	Unphosphorylated ERK competes with phosphorylated ERK for binding at the N-terminal domain of MKP3	60
2. 8	Dephosphorylation of wild type and D316/319N mutant pERK by MKP3	62
2. 9	Glutaraldehyde cross-linking of C293S MKP3 and pERK	64
2. 10	Glutaraldehyde cross-linking of MKP3, ERK and the mixture of MKP3 and ERK	66
2. 11	Mobility differences in cross-linked species	68
2. 12	Bis[sulfosuccinimidyl]suberate (BS ³) cross-linking of MKP3, ERK, and the mixture of MKP3 and ERK	70
2. 13	Dephosphorylation of L4A H176E mutant pERK by MKP3	72
2. 14	Proposed model for pERK down-regulation involving the formation	

of a MKP3-pERK heterodimer and intramolecular dephosphorylation	74
3. 1 The substrates <i>p</i> -nitrophenyl phosphate and <i>m</i> -nitrobenzyl phosphate	97
3. 2 Isotopic isomers synthesized for measurement of the ¹⁸ O isotope effect	99
3. 3 The initial velocities of <i>p</i> NPP and <i>m</i> NBP hydrolysis by VHR	101
3. 4 pH dependency of the <i>V</i> / <i>K</i> value for VHR using <i>p</i> NPP and <i>m</i> NBP	103
3. 5 Solvent kinetic isotope effects of VHR-catalyzed hydrolysis of <i>p</i> NPP and <i>m</i> NBP in H ₂ O and D ₂ O	105
3. 6 Proposed transition state for VHR-catalyzed formation of the cysteinyl-phosphate enzyme intermediate from <i>m</i> NBP	107

LIST OF ABBREVIATIONS

A	alanine
α	alpha
Å	angstrom
Arg	arginine
Asn	asparagine
Asp	aspartic acid
β	beta
Bis-tris	[bis(2-hydroxyethyl)imino]tris(hydroxymethyl) methane
BS ³	bis[sulphosuccinimidyl]suberate
C	cysteine
C-	carboxyl-
°C	degrees Celsius
Cdk2	cell cycle dependent kinase 2
Cl	chloride
Cys	cysteine
D (protein context)	aspartic acid
D (chemical compounds)	deuterium
DNA	deoxyribonucleic acid
DSP	dual-specificity phosphatase
DTT	dithiothreitol
E	glutamic acid
EB	extracellular signal regulated kinase binding
EIE	equilibrium isotope effect
ERK	extracellular signal regulated kinase

FA	fluorescence anisotropy
Fe	iron
G	glycine
GEF	guanine nucleotide exchange factor
Glu	glutamic acid
GSH	reduced glutathione
GST	glutathione-S-transferase
H (protein context)	histidine
H (chemical compounds)	hydrogen
H ₂ O ₂	hydrogen peroxide
His	histidine
hr	hour
IPTG	isopropyl- β -D-thiogalactoside
JNK/SAPK	c-jun NH ₂ -terminal kinase/stress-activated protein kinase
K _d	equilibrium dissociation constant
K _i	inhibition constant
kDa	kilodalton
KIE	kinetic isotope effect
L	leucine
LAR	leukocyte antigen-related
μ L	microliter
μ M	micromolar
<i>m</i> -	<i>meta</i> -
M	molar
MAP	mitogen activated protein
MAPK	mitogen activated protein kinase

MBP	myelin basic protein
MEKK	mitogen activated protein/extracellular signal regulated kinase kinase kinase
MEK	mitogen activated protein/extracellular signal regulated kinase kinase
min	minutes
MKP	mitogen activated protein kinase phosphatase
<i>m</i> NBP	<i>meta</i> -nitrobenzyl phosphate
mP	multipolarization
mRNA	messenger ribonucleic acid
MW	molecular weight
N (protein context)	asparagines
N (chemical compounds)	nitrogen
N	normal
N-	amino-
Na	sodium
NGF	nerve growth factor
Ni	nickel
nm	nanometer
nM	nanomolar
NMR	nuclear magnetic resonance
O	oxygen
P	phosphorous
<i>p</i> -	<i>para</i> -
PAP	purple acid phosphatase
PBS	phosphate-buffered saline
PC12	phaeochromocytoma cell 12

PCR	polymerase chain reaction
pERK	phosphorylated extracellular signal-regulated kinase
%	percent
PI(3,4)P ₃	phosphatidylinositol-3, 4-diphosphate
PI(3,4,5)P ₃	phosphatidylinositol-3, 4, 5-triphosphate
PI(4,5)P ₃	phosphatidylinositol-4, 5-diphosphate
pNP	<i>para</i> -nitrophenolate
pNPP	<i>para</i> -nitrophenyl phosphate
PP	protein phosphatase
pT	phosphothreonine
PTEN	phosphatase and tensin homolog deleted on chromosome 10
pThr	phosphothreonine
PTP	protein tyrosine phosphatase
pTyr	phosphotyrosine
pY	phosphotyrosine
R	arginine
ROS	reactive oxygen species
s	seconds
S (protein context)	serine
S (chemical compounds)	sulfur
SAPK	stress-activated protein kinase
SDS-PAGE	sodium dodecyl sulfate-poly acrylamide gel electrophoresis
sec	seconds
Ser	serine
SH2	Src Homology2

SHP	Src homology 2 domain containing phosphatase
SKRP1	stress-activated protein kinase pathway-regulating phosphatase 1
SO ₄	sulphate
Sos	Son of sevenless
T	threonine
TBA	tris/bis-tris/acetate buffer
Thr	threonine
Tris	tris(hydroxymethyl)aminomethane
TS	transition state
Tyr	tyrosine
V	valine
VH1	<i>vaccinia H1</i>
VHR	<i>vaccinia H1</i> -related
X	any amino acids
Y	tyrosine
Zn	zinc

ACKNOWLEDGEMENTS

I am indebted to my advisor John Denu for being a wonderful mentor over the past five years. I thank him for providing guidance and advice that helped me overcome many difficult situations. He has created an intellectual environment that allowed me to acquire knowledge and independence. I would also like to thank members of my thesis committee: Richard Brennan, David Farrens, James Lunblad, and Philip Stork for providing ideas and for their support.

I was very fortunate to have wonderful lab members throughout the years. I could not forget my past and present lab members: Margie Borra, Kirk Tanner, Johanna Rigas, Michael Jackson, Manning Schmidt, and Clark Fjeld for their helpful discussions and for creating an enjoyable and inspiring environment. I especially thank Margie Borra who sympathized with me in difficult times.

I have enjoyed Taekwondo exercise during my graduate years. I thank my Taekwondo classmates, Lisa DiTommaso, Amanda Matsuda, Ngan Vo, Juan Sheu, Kelley Stewart, Mellisa Laughrey for their warm friendship.

I would like to give special thanks to my parents, Jongsoo Kim and Seook Kang. Without their endless love and support, I would not be here. They gave me many opportunities to achieve what I want. I would also like to thank my mother-in-law, Jongsup Lee, for her prayers for our family. Finally, I am grateful to my husband, Geunwon Lee, for his love, patience, and understanding. Hyun Lee, our first baby who was born in the most critical time of my graduate school, has given me a wonderful joy.

ABSTRACT

The dual specificity phosphatases belong to the large family of protein tyrosine phosphatases (PTPs) that contains the active site motif HCxxGxxR(S/T), but unlike the tyrosine-specific enzymes, DSPs are able to catalyze the efficient hydrolysis of both phosphotyrosine and phosphoserine/threonine residues. The dual specificity mitogen-activated protein kinase phosphatase MKP3 down-regulates mitogenic signaling through dephosphorylation of extracellular signal-regulated kinase (ERK). Like other MKPs, MKP3 consists of a noncatalytic N-terminal domain and a catalytic C-terminal domain. ERK binding to the N-terminal noncatalytic domain of MKP3 has been shown to increase (up to 100-fold) the catalytic activity of MKP3 towards small artificial substrates. We addressed the function of the N-terminal domain of MKP3 in either inter- or intramolecular dephosphorylation of pERK (phosphorylated ERK), and the stoichiometry of the MKP3/pERK Michaelis complex. These are important mechanistic distinctions given the observation that ERK exists in a monomer:dimer equilibrium which is shifted toward the dimer when phosphorylated, and given that MKP3 undergoes catalytic activation toward other substrates when bound to ERK. Wild type and engineered mutants of ERK and MKP3, binding analyses, reaction kinetics and chemical cross-linking studies were used to demonstrate that the monomer of MKP3 binds to the monomeric form of pERK, and that MKP3 within the resulting heterodimer performs intramolecular dephosphorylation of pERK. Catalytic activation and substrate tethering by MKP3 lead to a ≥ 4000 -fold rate enhancement (k_{cat}/K_m) for dephosphorylation of pERK.

Another dual-specificity phosphatase VHR (*vaccinia H1*-related) was used to examine its ability to catalyze hydrolysis reaction of a variety of small-molecule aryl and alkyl phosphates. It is unclear how DSPs accomplish similar reaction rates for phosphoesters whose reactivity (i. e. pK_a of the leaving group) can vary by more than 10^8 . We utilized the alkyl phosphate *m*-nitrobenzyl phosphate (*m*NBP), leaving group pK_a

14.9, as a physiological substrate mimic to probe the mechanism and transition state of the DSP, VHR. Detailed pH analyses of the V/K value for *m*NBP indicate that VHR reacts with the phosphate dianion of *m*NBP. The ^{18}O KIEs measured in the scissle bond demonstrate less bond cleavage in the transition state compared to *para*-nitrophenyl phosphate, a more labile substrate ($\text{p}K_{\text{a}} 7.1$). Supporting a distinct bridge-oxygen protonation step before P-O cleavage, an inverse solvent isotope effect of 0.52 with *m*NBP suggests that the ester oxygen is protonated by the conserved Asp-92 in a step prior to P-O fission. Though both monoanionic and dianionic forms of *m*NBP were shown to bind VHR, the mutant D92N was unable to catalyze measurable hydrolysis, consistent with the absolute requirement of Asp-92 to protonate the bridge oxygen for substrates whose leaving groups are more in line with physiological substrates.

Chapter 1

Introduction

1.1 Introduction to Protein Phosphatases

Protein phosphorylation and dephosphorylation are one of the most prevalent signal transduction mechanisms in the cell. This quick and reversible protein modification enables the cell to respond to extracellular stimuli rapidly and precisely. Protein phosphorylation and dephosphorylation are performed by protein kinases and phosphatases, respectively. Protein kinases form highly interactive networks to achieve the integrated function of cells in an organism. One family of protein kinases involved in signal transduction is the mitogen activated protein (MAP) kinases. MAP kinases are integral components of signaling pathways that transmit extracellular signals inside the cell and that elicit changes in gene transcription (see Figure 1. 1). Extracellular stimuli such as growth factors, mitogens, and stresses all activate MAP kinase pathways, via cell surface receptor protein tyrosine kinases. Activated receptors undergo autophosphorylation, thereby creating docking sites for the formation of multiprotein complexes where adaptor proteins such as Shc and Grb2 are recruited through their Src homology 2 (SH2) domains. SH2 domains, present in various signaling molecules, bind to the specific phosphotyrosine containing sequences in receptor proteins kinases. Formation of the complex between an activated receptor and Grb2 then leads to recruitment of a guanine nucleotide exchange factor (GEF) such as Son of Sevenless (Sos), that induces the Ras GTPase to exchange GDP for GTP. GTP-liganded Ras directly interacts with Raf, thereby increasing its kinase activity. Activated Raf then activates the MAP kinase kinase, MEK (MAP/ERK Kinase), through phosphorylation on two serine residues. MEK in turn activates the MAP kinase, ERK (extracellular signal-regulated kinase), by phosphorylation on tyrosine and threonine residues in its TxY motif. Activated ERK then enters the nucleus where it targets protein substrates such as other protein kinases, phospholipases, transcription factors, and cytoskeletal proteins by phosphorylating specific serines and threonines resulting in either up- or down-regulation of target protein's activity (1) (2) (3).

The phosphorylated protein substrates are dephosphorylated by protein phosphatases. There are two major classes of protein phosphatases: protein phosphatases (PPs) which specifically hydrolyze serine/threonine phosphoesters and protein tyrosine phosphatases (PTPs) which are phosphotyrosine-specific. Although both PPs and PTPs catalyze phosphoester hydrolysis, they are structurally different and have distinct catalytic mechanisms. Crystallographic structures of PPs (4) (5-7) revealed a common motif of a central β - α - β - α - β scaffold containing a dinuclear metal ion center located at the active site. An activated water molecule that is coordinated to the metal centers in PPs directly displaces the phosphate of substrate (8, 9) (10, 11). In the case of PTPs, the family members exhibit sequence diversity, although all structurally characterized PTPs share a common architecture containing a highly twisted β -sheet with four central parallel β -strands flanked by five anti-parallel β -strands, which is surrounded by six α -helices (12-14)(see Figure 1. 2 and 1. 3). PTPs are characterized by the signature motif HCX₅RT(S) within the catalytic domain, which resides between the β strand starting with C and the α helix beginning with RT(S). PTPs use the cysteine nucleophile of the HCX₅RT(S) signature motif to attack the phosphorous atom of the substrate, forming a phosphoenzyme intermediate (15) (16) (17). In particular, PTPs were shown to dephosphorylate target proteins such as MAP kinases and receptor kinases, leading to appropriate regulation of a variety of signal transduction pathways.

One exception to the common PTP structure is Cdc25, which catalyzes the activation of the cyclin-dependent kinases, causing initiation and progression of successive phases of the cell cycle. Cdc25A and Cdc25B catalytic domains form a small α/β -domain with a central five-stranded parallel β -sheet sandwiched by three α -helices from below and two α -helices from above (18, 19). This topology is identical to that of the sulfur transfer protein rhodanese, a highly conserved protein in bacteria and mitochondria whose exact function is unknown. A recent report from Rudolph *et al.* (20) showed that the monoprotonated phosphate of the protein substrate Cdk2-pTpY/CycA

provides the critical proton to the leaving group and identified Glu474 as a catalytic base, which plays an important role in proton transfer from the phosphate to the leaving group.

Besides PTPs and PPs, there are acid/alkaline phosphatases that dephosphorylate non-protein substrates such as thiophosphates, phosphomonoesters, and phosphates under acidic or basic conditions, respectively. Like PPs, the alkaline phosphatases are metalloenzymes that require zinc for activity (21) (22). Purple acid phosphatases (PAP), one subclass of acid phosphatases, also contain a dimetal center (either Fe or Zn), but not all of the acid phosphatases are metal dependent (23, 24). While the phosphate ester hydrolysis of alkaline phosphatase proceeds via a covalent phosphoseryl intermediate (25), acid phosphatases directly transfer the phosphoryl group of the substrate to a water molecule (8) in analogy to the proposed PP mechanism.

1.2 Dual-Specificity Phosphatases (DSPs)

Dual-specificity phosphatases are a subfamily of intracellular PTPs. Like other members of the PTP family, DSPs have a signature motif H₂CX₃RT(S) and appear to use the same basic catalytic mechanism in which the cysteine attacks the phosphorous atom of the substrate, forming a phosphoenzyme intermediate. While PTPs catalyze dephosphorylation of only phosphotyrosine residues, DSPs catalyze dephosphorylation of all three phospho-amino acids (phosphotyrosine, phosphoserine and phosphothreonine). Analysis of the human genome indicates that tyrosine-specific protein phosphatases and DSPs are one of the more abundant gene families (112 genes, ranked 29th overall) (26). Although PTPs and DSPs show limited sequence homology within the catalytic domain (Figure 1. 2), their overall structural folds in this region are amazingly similar. Since many of DSPs inactivate MAP kinases by dephosphorylating phosphoserine/threonine and phosphotyrosine, they are called MAP kinase phosphatases (MKPs). In this thesis, I will present two prototypical MKPs, VHR and MKP3, in regards to their molecular mechanisms in dephosphorylating their physiological substrates.

1.3 VHR

VHR, a human protein tyrosine phosphatase, was isolated using an expression cloning strategy (27). Since VHR showed limited sequence similarity to the *vaccinia* virus-encoded phosphatase VH1 (*vaccinia HI*) (28), it was named as *vaccinia HI*-related (VHR) phosphatase (27). In fact, a 30-amino acid stretch of 185 amino acids VHR (codons 115-144) exhibits 50 % identity to VH1 (see Figure 1. 2) (27), and has a minimal catalytic domain among PTPs. VHR is a nuclear dual-specificity phosphatase whose physiological substrate was shown to be ERK and JNK (Figure 1. 1) (29, 30).

1.3.1 Structure

The crystal structure of VHR was solved to 2.1 Å resolution by X-ray crystallography (Figure 1. 3)(31), and was found to consist of a single $\alpha + \beta$ domain. Although VHR has a shorter amino acid sequence than other PTPs and has sequence similarity only to the PTP active site consensus sequence (Figure 1. 2), the structure of VHR reveals a general fold that occurs in other PTPs such as human PTP1B (32, 33) and *Yersinia* PTP (34, 35). Structural features of PTPs have provided evidence for peptide substrate specificity and for selectivity toward the nature of the phosphorylated residue. Peptide specificity appears to be defined largely by residues both N- and C-terminal to the substrate pTyr residue. The structure of PTP1B in a complex with insulin receptor peptides indicates that a second pTyr residue adjacent to the substrate phosphorylation site plays a critical role in specificity (36). Similarly, VHR displays a preference for diphosphorylated peptide substrates based on the recent crystallographic model of VHR bound to a diphosphorylated peptide corresponding to the MAP kinase activation lip (37). Yuvaniyama *et al.* also pointed out that the depth of the active site cleft is potentially critical for substrate specificity (31). Compared to 9 Å deep active site clefts in PTP1B and *Yersinia* PTP, VHR has a shallower active site pocket (at most 6 Å), which allows for the hydrolysis of not only phosphotyrosine residues but also shorter phosphoserine/threonine residues. Although VHR is able to dephosphorylate

phosphoserine/threonine and phosphotyrosine residues, it prefers phosphotyrosine to phosphoserine/threonine (37). While most DSPs contain alanine and isoleucine in the X₂ and X₃ positions of the signature motif HCX₁X₂GX₃X₄RT(S), VHR harbors a glutamic acid and a tyrosine, respectively. The side chains of glutamic acid-126 and tyrosine-128 create a deeper and narrower active site than most DSPs, which provide higher phosphotyrosine dephosphorylation activity for VHR (37). In fact, attempts to dock a phosphothreonine into the active site of VHR result in steric clash. The smaller residues, isoleucine and alanine found in many DSPs, should allow phosphothreonine binding, thus explaining the dephosphorylation activity toward phosphoserine/threonine residues as well as that of phosphotyrosine residues. Another dual-specificity phosphatase family member, PTEN (phosphatase and tensin homolog deleted on chromosome 10), is unique among known PTPs, as it has two basic lysine residues within the signature motif. These positive charges are believed to interact with the negative charges of inositol phospholipid PIP₃ (phosphatidylinositol-3, 4, 5-triphosphate), the biological substrate for PTEN (38, 39).

1. 3. 2 Mechanism

Using site-directed mutagenesis, pH studies, and steady-state and rapid kinetics, the catalytic mechanism for VHR was determined using the small substrate *para*-nitrophenyl phosphate (*p*NPP) (Figure 1. 4 and Figure 3. 1) (40, 41). A thiolate of Cys-124 attacks the phosphate atom of a substrate to form a phosphoenzyme intermediate. A general acid Asp-92 located on a flexible loop donates a proton to the leaving group oxygen. Asp-92 then acts as a base to activate a water molecule for hydrolysis of the phosphoenzyme intermediate to generate free enzyme and inorganic phosphate (Figure 1. 4). Ser-131 could potentially hydrogen bond with Cys-124 in the phosphoenzyme intermediate, thereby making the thiolate a better leaving group through stabilization of the developing negative charge in the transition state (40). The invariant Arg-130 residue in the signature motif is important for both substrate binding and transition-state

stabilization, as it coordinates two of the oxygen atoms on the phosphoryl group via its guanidium side chain (42, 43). To obtain a detailed description of the transition-state structures involved in the dephosphorylation reaction by VHR, kinetic isotope effects (KIE) were measured (44). KIE studies demonstrated that the dephosphorylation reaction of *p*NPP by VHR proceeds through highly dissociative transition states with a large degree of bond cleavage to the leaving group, a metaphosphate-like structure of the transferring phosphoryl group, and very little bond formation to the nucleophile (44) (45).

1. 3. 3 Regulation

Although no general mechanism for regulating PTPs has been demonstrated, hydrogen peroxide (H_2O_2) has been shown to inactivate many PTPs such as VHR, PTP1, LAR (leukocyte antigen-related), SHP-2 (SH2 domain containing phosphatase), PTEN, and Cdc25C (cell cycle regulator) (46-52). Reactive oxygen species (ROS) appear to be transiently produced in response to growth factor stimulation. This change in cellular redox status was suggested to participate in downstream signal transduction. H_2O_2 , as one of the reactive oxygen species (ROS), was shown to play an important role in regulating tyrosine phosphorylation-dependent pathways (53-55). Inactivation of phosphatases was verified to be due to the formation of a nucleophile cysteine sulfenic acid intermediate by nucleophilic attack of the thiolate anion on H_2O_2 . A cysteine sulfenic acid intermediate was stabilized in the active site cleft. Oxidative inactivation of the above PTPs was completely reversible upon the addition of thiol-containing compounds such as dithiothreitol (DTT) and reduced glutathione (GSH). This suggests that the redox state within the cell may play a major role in the regulation of tyrosine phosphatase activity. A recent report by Salmeen *et al.* (51) showed that the sulphenic acid intermediate produced in response to PTP1B oxidation is rapidly converted into a sulphenyl-amide species where the sulphur atom of the catalytic cysteine is covalently linked to the main chain nitrogen of an adjacent residue. The large conformational changes in the catalytic site caused by the formation of this sulphenyl-amide species were

proposed to protect the active site cysteine from irreversible oxidation and permit redox regulation of the enzyme.

1.3.4 Goals of the VHR project

As reviewed above, the structure, function, and catalytic mechanism of VHR were extensively studied using the artificial substrate *p*NPP. *p*NPP, an aryl phosphomonoester, is a useful substrate because the reaction can be followed spectrophotometrically by the formation of product *p*NP (*para*-nitrophenolate) (Figure 3. 1). However, the low leaving group pK_a of *p*NPP (7.1), which can be easily hydrolyzed, does not represent physiological substrates such as phosphorylated serine/threonine and phosphorylated tyrosine residues whose leaving group pK_a s are 14 and 10, respectively. Despite differences in the reactivity of these substrates, which can vary by as much as 9 orders of magnitude, VHR can dephosphorylate both alkyl and aryl phosphomonoester substrates with similar efficiency. To examine how VHR compensates for the huge difference in reactivity based on leaving group pK_a , we used *meta*-nitrobenzyl phosphate (*m*NBP, Figure 3. 1) with a leaving group pK_a of 14.9, which is similar to that of the physiological substrates. *m*NBP was synthesized by our collaborator, Alvan Hengge and Piotr K. Grzyska, at Utah State University. In Chapter 3 of this thesis, we examine the mechanism and transition state structure of VHR using the physiological substrate mimic *m*NBP.

1.4 MKP3

MKP3 (mitogen activated protein kinase phosphatase 3) was first isolated from rat hippocampus as well as human brain by several laboratories independently (56-58). MKP3 contains the conserved PTP active site sequence H₃CX₃RT(S) and shows activity toward MAP kinases. MKP3 mRNA is induced during nerve growth factor-mediated differentiation but not during insulin or epidermal growth factor mitogenic stimulation in PC12 cells (56, 59). Unique among MKPs, MKP3 is neither an immediate early gene nor stress inducible, and it was the first DSP to be localized in the cytoplasm (Figure 1. 1)

(56-58). Furthermore, it exhibits substrate selectivity for the MAP kinases (58, 60, 61). MKP3 inactivates ERK, but has very low activity toward SAPK (stress-activated protein kinase) or p38 kinase. It has 38-58 % sequence identity to previously identified DSPs such as MKP1/CL100 (62), hVH2 (63), PAC1 (64), B23 (65), and VHR (27). The sequence identity among MKPs was found mostly in the C-terminal catalytic domain as well as in two N-terminal CH2 regions (66, 67), which display homology to the cell cycle regulator Cdc25 phosphatase (Figure 1. 2) (56, 57). Cdc25 dephosphorylates Tyr-15 and Thr-14 of p34/CDC2 kinase in a complex with cyclin B (68). The exact function of the CH2 domains is not known yet; however, it is thought that they provide an important role for substrate recognition.

1. 4. 1 Activation of MKP3 by ERK binding

Compared to VHR, which has a minimal catalytic domain (185 amino acids), MKP3 has an extended N-terminal noncatalytic domain attached to the catalytic domain (389 amino acids) (Figure 1. 2). Interestingly, although MKP3 has ~ 30 % sequence identity with VHR in its catalytic domain, including an identical HCX₅RT(S) signature motif, the catalytic activity of MKP3 was shown to be ~ 100-fold less than VHR toward the artificial substrate *p*NPP (69). Deletion of the N-terminal domain of MKP3 did not alter its catalytic activity toward *p*NPP, suggesting that the N-terminal domain is not inhibitory to the catalytic domain (69, 70). Based on the k_{cat}/K_m pH profile studies, it was shown that MKP3 displays a two ionization curve while VHR displays a three ionization curve (69). This suggests that MKP3 lacks an ionization of a general acid that must be protonated for catalysis (69).

The question of the lack of a general acid was starting to be elucidated when several groups showed that MKP3 is able to form a complex with ERK (58, 70, 71). Groom *et al.* showed that Pyst1 (an orthologue of MKP3) expressed in Cos-1 cells is able to block the serum-induced activation of MAP kinase and is able to form a physical complex with endogenous MAP kinase in these cells (58). Muda *et al.* reported that the

physical association of MKP3 and ERK (ERK1 and 2) is through the N-terminal noncatalytic domain of MKP3 (70). They also showed that at least 10-fold higher concentrations of purified MKP3 Δ N (deleted in N-terminal domain) than full-length MKP3 is required to inhibit ERK2 activity. At about the same time, the binding of ERK to the N-terminal domain of MKP3 was shown to increase dramatically the catalytic activity of MKP3 toward *p*NPP (71). Genetic analysis in *Drosophila* showed that a dominant gain-of-function mutation of the *rolled* MAP kinase gene, termed Sevenmaker (*rl*^{sevenmaker}), contains a single amino acid substitution of Asn for Asp-319 (D319N) (72). Camps *et al.* observed that one critical consequence of the ERK2 D319N mutation is an inability to bind and trigger catalytic activation of MKP3. All above observations suggest that binding of ERK to MKP3 may provide a general acid catalysis of MKP3.

Zhang's group as well as our lab determined the detailed mechanism of the catalytic activation of MKP3 upon binding of ERK to the N-terminal domain of MKP3 using the artificial substrate *p*NPP (Figure 1. 5) (42, 73). Site-directed mutagenesis, pH studies, Brønsted analysis, steady-state and rapid reaction kinetics determined that ERK-activated MKP3 utilizes general acid catalysis, enhancing the rate of P-O bond cleavage by 100-fold. ERK activates MKP3 through the stabilization of the active phosphatase conformation, inducing closure of the catalytic general acid loop. In the closed active conformation, the loop structure can participate efficiently in general acid/base catalysis, substrate binding, and transition-state stabilization (Figure 1. 5) (42, 73, 74). This type of binding and activation mechanism is also found in another MKP such as MKP1 (75) (76). This suggests that MKP3 and its activation by the substrate could serve as a model for other MKPs. Recently, PTEN was shown to follow a similar activation mechanism. PTEN is a tumor suppressor that inactivates phosphoinositide 3-kinase by catalyzing the removal of the 3' phosphate of phosphoinositide (77, 78). It has been shown that the binding of di-C8-phosphatidylinositol 4,5-P₂ (PI(4,5)P₂) to PTEN enhances its

phosphatase activity for the monodisperse substrates, PI(3,4,5)P₃ and PI(3,4)P₂, likely by an allosteric conformational change (50).

1.4.2 Structure

The crystal structure of the human Pyst1 catalytic domain (an orthologue of rat MKP3) (79) and the solution structure of the N-terminal domain of MKP3 (80) were solved independently. The catalytic domain of Pyst1 revealed a compact $\alpha + \beta$ structure comprising a six-stranded mixed β -sheet decorated with four helices on one face of the sheet and a single short helix on the other (Figure 1.3) (79). The catalytic active site is located within a cleft formed by a loop known as the phosphate-binding loop (PTP-loop) located between strand β 8 and helix α 5 (Figure 1.3) (79). Similar to VHR (6 Å), the cleft of Pyst1 is 5.5 Å which is a sufficient size to accommodate both phosphotyrosine and phosphothreonine/serine side chains; however, there is no evidence of a second phospho-binding site within the catalytic domain of Pyst1. The comparison of the catalytic domain of Pyst1 with VHR demonstrated that their 3-dimensional structures are similar even though their amino acid sequences are not (Figure 1.3). The major difference in the two structures resides in the so-called general acid loop where the general acid aspartic acid (residue 92 for VHR and 262 for MKP3) is located. Interestingly, in the crystal structure of Pyst1, D262 is disengaged from the other catalytic residues by over 10 Å, while D92 of VHR is close to the active site. It was suggested that major conformational changes occur to bring the catalytic residues together upon binding to ERK (79). It would be critical to have a crystallographic model of ERK bound MKP3 to explain the conformational changes in the general acid loop upon ERK binding.

The solution structure of the N-terminal domain of MKP3 was solved independently (80). The solution structure and biochemical analysis of the ERK2 binding (EB) domain of MKP3 show regions that are essential for ERK2 binding partly overlap with its sites that interact with the C-terminal catalytic domain, and that these

interactions are functionally coupled to the active site residues of MKP3 (80). Recently, the solution structure of the MKP PAC-1 catalytic domain was solved, which again revealed a similar type of activation mechanism where substrate binding induces conformational changes in the phosphatase active site, which is essential for its full enzymatic activity (81).

1. 4. 3 ERK; a physiological substrate of MKP3

The crystallographic structures of the unphosphorylated (82) and phosphorylated forms of ERK (phosphorylated on T183 and Y185) (Figure 2. 1) (83) reveal structural changes upon phosphorylation. Major changes occur in the “phosphorylation lip” region where T183 and Y185 are located. In the unphosphorylated (low activity) structure, the lip is folded to block the P+1 site and forces the domains into an open structure. Upon phosphorylation, the lip rearranges to promote domain closure and conformational changes in the L16 segment leading to the formation of a tight dimer. The residues involved in the dimer interaction are L333, L335, and L344, which form a hydrophobic zipper to lock the dimer together. The homodimerization of pERK (phosphorylated ERK at T183 and Y185 residues) was examined by Khokhlatchev *et al.* (84). The authors determined that the dissociation constant of ERK decreases from 20 μM to 7.5 nM when ERK is phosphorylated, and phosphorylation of ERK is sufficient for its nuclear translocation.

Nuclear translocation of ERK is important because there are many transcription factors that are regulated by ERK in the nucleus. Although monomeric ERK (42 kDa) freely diffuses in and out of the nucleus (85), dimeric pERK (84 kDa) whose molecular weight is much bigger than the nuclear pore size (~ 40 kDa) is not able to translocate to the nucleus. There are a few different models for the nuclear translocation of pERK; active transport of the dimer, a nuclear pore complex-mediated cytosol-independent pathway, and a carrier-independent mechanism (85-87).

1. 4. 4 Goals of the MKP3 project

The studies done with MKP3 reveal a unique activation mechanism whereby MKP3 obtains a high catalytic activity upon binding its cognate substrate to its noncatalytic domain. Extensive studies regarding the activation mechanism of MKP3 were done using an artificial substrate *p*NPP. It has been shown that ERK binding to the N-terminal noncatalytic domain of MKP3 increases dramatically the catalytic activity of MKP3 toward *p*NPP. On the other hand, dephosphorylation of pERK (a physiological substrate of MKP3) by MKP3 is very efficient with a V/K value of $10^6 \text{ M}^{-1}\text{s}^{-1}$ (88). Zhao *et al.* proposed that MKP3 dephosphorylates pERK in an ordered, distributive mechanism in which MKP3 binds diphosphorylated ERK, dephosphorylates the phosphotyrosine residue (Tyr-185) first, dissociates and releases the monophosphorylated ERK at threonine residue (Thr-183), which is then subjected to dephosphorylation by a second MKP3, yielding fully dephosphorylated ERK (88). However, the molecular mechanism of the pERK dephosphorylation reaction by MKP3 is not completely understood.

ERK forms a dimer upon phosphorylation by its upstream kinase MEK (83, 84), and ERK dimerization has been proposed as a necessary step for nuclear translocation (84) (85-87). As discussed above, ERK binds and activates MKP3 towards other substrates and is also dephosphorylated by MKP3, whose oligomeric state is not known. These observations raise two important questions concerning the dephosphorylation mechanism. Does MKP3 catalyze intra- or intermolecular dephosphorylation of pERK? For example, MKP3 could be activated by one molecule of ERK while it dephosphorylates a separate molecule. Alternatively, MKP3 may dephosphorylate the same ERK molecule to which it is bound through the N-terminus of MKP3. Another unknown is the stoichiometry of the relevant MKP3:ERK complex. In Chapter 2 of this thesis, we probe these important questions concerning the mechanism of pERK dephosphorylation reaction by MKP3.

Figure 1. 1 MAP kinase signaling cascade (see text for details, modified from (89)).

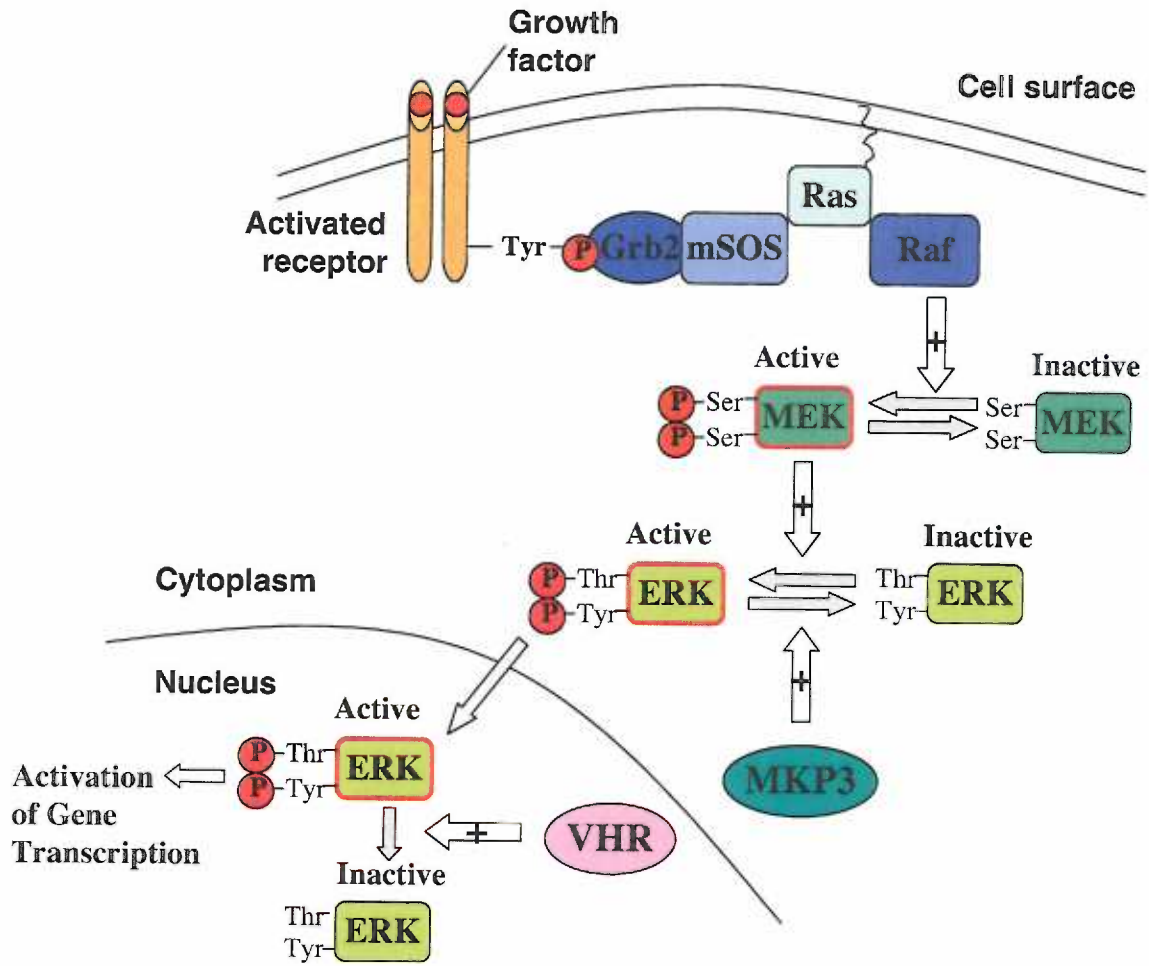


Figure 1. 2. Domain organization of PTPases. Red boxes indicate the signature motif which is characteristic for PTPase. Green rectangles indicate catalytic domains, and a yellow rectangle indicate a noncatalytic domain of MKPs. Two regions of homology (termed CH2A shown in light blue and CH2B shown in dark blue) were identified between sequences in the N-terminal noncatalytic domain of the MKPs and sequences flanking the active site of Cdc25 (see text for details).

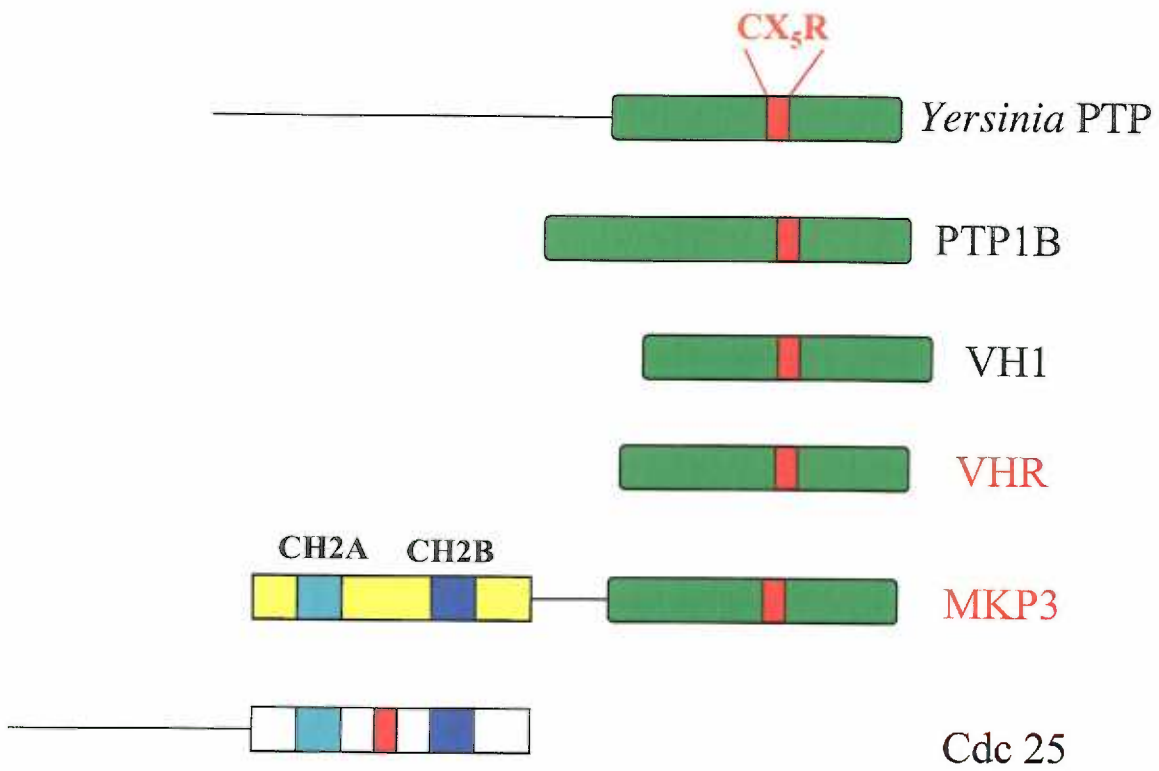


Figure 1. 3. Structural comparison between VHR (shown in yellow) and the catalytic domain of MKP3 (shown in light blue). Secondary structural elements are labeled for VHR (adapted from (31, 79)). A PTP loop containing a nucleophile cysteine residue and a general acid loop containing an aspartic acid residue are indicated. The side chains of aspartic acid and cysteine are shown in red and blue for VHR and MKP3, respectively.

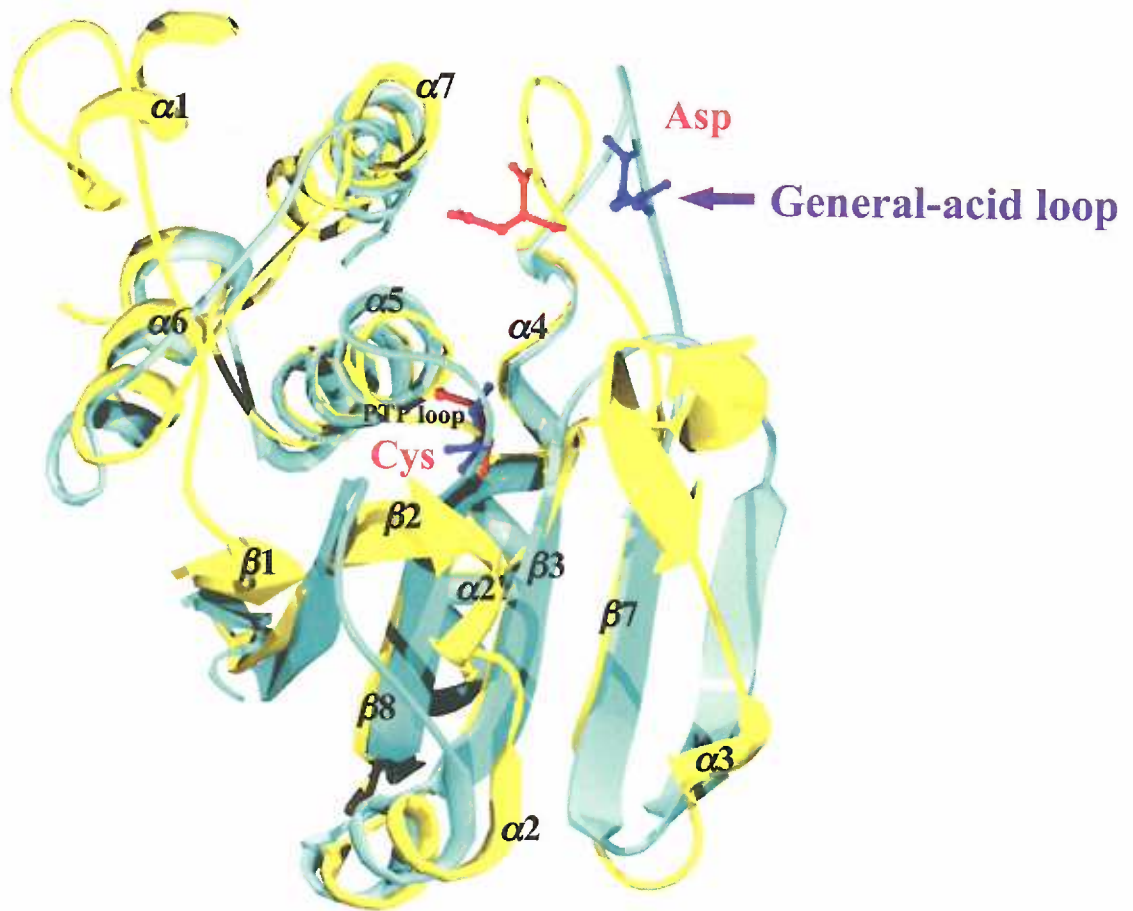


Figure 1. 4. Catalytic mechanism of PTPs. (see text for details, adapted from (138))

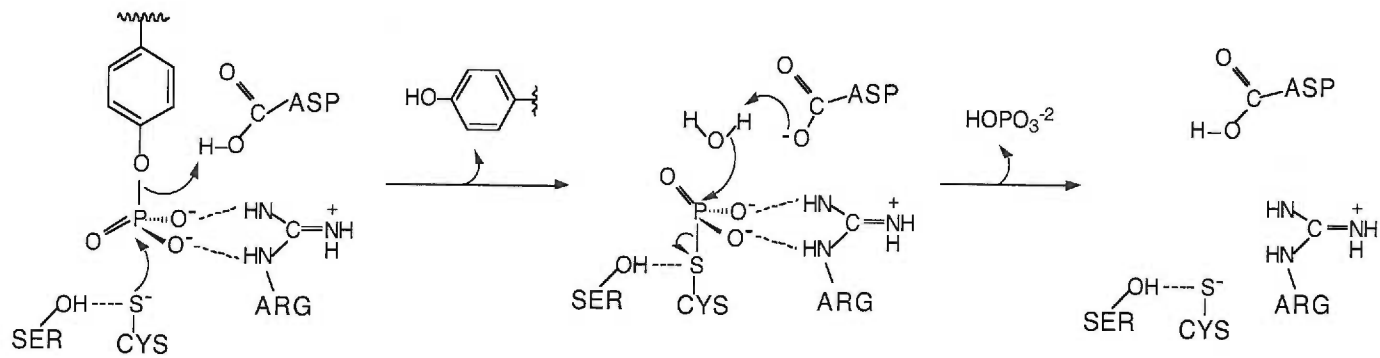
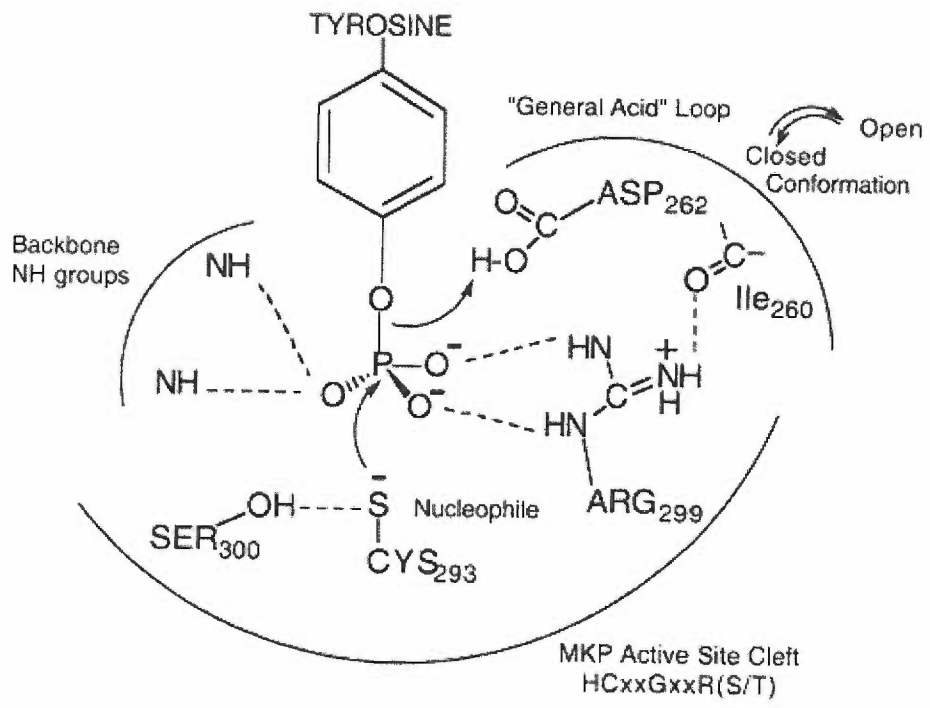


Figure 1. 5 MKP3 catalytic mechanism for phosphoryl-enzyme intermediate formation
(See text for details, adapted from (74)).



Chapter 2

Intramolecular dephosphorylation of ERK by MKP3

(Biochemistry 42: 15197-207, 2003)

2.0 Preface

I carried out all the experiments shown in this chapter. MKP3/VHR chimera construct was generated by Adrian Rice.

2.1 Introduction

Protein phosphorylation is one of the most fundamental regulatory mechanisms in living cells, and it is controlled by the opposing actions of protein kinases and phosphatases. Protein kinases referred to as the mitogen-activated protein (MAP) kinases are critical components in cellular signaling. The MAP kinase family comprises three structurally and functionally distinct enzyme classes: the extracellular signal-regulated kinases (ERK), c-Jun NH₂-terminal kinase/stress-activated protein kinase (JNK/SAPK), and p38/RK/CSBP (p38) (1-3). Full activation of the MAP kinases requires phosphorylation on both threonine and tyrosine residues in the TXY motif (90). Activated MAP kinases phosphorylate key regulatory proteins and transcription factors, leading to their activation. These activated MAP kinases are the targets for some dual-specificity phosphatases (DSPs). Since specific DSPs have been shown to inactivate MAP kinases (58) (91) (92) (93), many have been coined MAP kinase phosphatases (MKPs). Compared with protein tyrosine phosphatases (PTPs), which share the active-site motif HCxxGxxR(S/T), DSPs can be distinguished by their ability to hydrolyze all three major phosphorylated residues (phosphotyrosine, phosphothreonine, and phosphoserine). There are 12 distinct mammalian MKPs (94) (95), which have similar structural domains composed of an N-terminal noncatalytic domain and a C-terminal catalytic domain where the active-site motif, HCxxGxxR(S/T), is located. The amino-terminal domain has two short-sequence motifs (CH2A and CH2B) that display low homology to regions within the catalytic domain of the Cdc25 phosphatase (66, 95). Studies have shown that several MKPs display distinct *in vivo* substrate preferences for the various MAP kinases (58, 60, 96, 97). For example, it has been shown that MKP3 selectively targets ERK (58) while M3/6 (hVH-5) shows preference for JNK and p38 (60). Recently, SKRP1 (SAPK pathway-regulating phosphatase 1) was shown to inactivate the JNK pathway (98).

Several of these MKPs exhibit catalytic activation when bound to their reported kinase substrates (59) (61) (75, 76). In particular, MKP3 is a poor enzyme toward small phosphoesters such as *para*-nitrophenyl phosphate (*p*NPP). However, in the presence of ERK, the catalytic activity of MKP3 increases > 35-fold toward *p*NPP (42, 59, 73). It has been shown that this dramatic increase in MKP3 phosphatase activity towards synthetic substrates is mediated by the tight binding of ERK to the N-terminal domain of MKP3 (59) (42, 71, 73). Activation is due to the ability of ERK to stabilize the active conformer of the catalytic domain through closure of the “general acid” loop (42, 73). Positively charged amino acid clusters in the N-terminal domain of MKP3 have been shown to be required for the docking of ERK through negatively charged aspartic acid residues (99). It has also been suggested that the N-terminal domain of MKP3, as well as other MKPs, contribute to the substrate specificity observed toward various MAP kinase members (69, 79, 88). Although most detailed mechanistic evaluations of MKP3 have been done using the artificial substrate *p*NPP, few studies have been directed at understanding the dephosphorylation mechanism of its authentic substrate, pERK (phosphorylated ERK at residues threonine 183 and tyrosine 185) (Figure 2. 1). Recently, Zhao *et al.* (88) demonstrated that the catalytic efficiency of MPK3 for pERK was 6 orders of magnitude higher than that of the MKP3-catalyzed *p*NPP hydrolysis, due to the reported low K_m for pERK (~ 20 nM) (88).

Two important questions concerning the dephosphorylation mechanism remain unresolved. Does MKP3 catalyze intra- or inter-molecular dephosphorylation of pERK? And, what is the stoichiometry of the relevant MKP3:ERK complex? ERK is known to exist in equilibrium between monomeric and dimeric forms, which are shifted toward the dimeric form upon phosphorylation by its upstream kinase. ERK dimerization has been proposed as a requisite for nuclear translocation and function. The oligomeric state of MKP3 is not known, though MKP3 undergoes catalytic activation towards other substrates when bound to ERK. These observations suggest that MKP3 could be

activated by one molecule of ERK while it dephosphorylates a separate molecule, either free in solution or within an ERK dimer. Alternatively, MKP3 may dephosphorylate the same ERK molecule to which it is bound through the N-terminus of MKP3. In this study, we address these questions by examining the role of the N-terminal domain of MKP3, whether the reaction is catalyzed via inter- or intra-molecular dephosphorylation of pERK, and the stoichiometry of the MKP3/pERK Michaelis complex.

2.2 Materials and Methods

2.2.1 Protein preparation

MKP3 (69), VHR (100), and ERK (101) were expressed and purified as described previously. The MKP3/VHR chimera was generated by fusing the N-terminal domain of MKP3 to VHR using a PCR method. The fusion cDNA was generated using our existing pT7-VHR (100) and pT7-MKP3 His_{x6} expression vector (69) by standard PCR methods. The PCR fragment containing the VHR catalytic domain was inserted into pT7-MKP3, replacing the catalytic domain of MKP3. MKP3 and VHR were fused through the identical amino acid sequence 'SDGS'. The 'SDGS' sequence in VHR (17-20 in 185 residues VHR) is found in the loop between the first α helix and first β strand (31). In MKP3, 'SDGS' resides in the N-terminal domain close to the catalytic domain (193-196 in 381 residue protein; catalytic domain starts at 204 amino acid residue). The MKP3/VHR chimera was expressed and purified as described for MKP3 (69). D316/319N ERK was generated by single oligonucleotide site-directed mutagenesis, as described previously (102), and expressed and purified as described for wild type ERK (101). The expression vector for L4A H176E ERK (GST (Glutathione-S-transferase) tagged at the N-terminus and His_{x6}-tagged at the C-terminus) was a generous gift from M. Cobb (University of Texas, Southwestern Medical Center, Dallas, TX) (84). L4A H176E ERK was expressed as described for wild-type ERK (101). The bacterial lysate was incubated with glutathione-agarose resin (Sigma) for 30 minutes at 4 °C. The resin was washed with ERK buffer (50 mM sodium phosphate, 300 mM NaCl, 10 mM β -

mercaptoethanol) and incubated with thrombin (Sigma) for 1 hr at 25 °C to cleave the GST from L4A H176E ERK. Flow through containing L4A H176E ERK was collected and separated from thrombin using Ni²⁺-NTA agarose (Qiagen). L4A H176E ERK was batch eluted with 300 mM Imidazole and quantitated by SDS-PAGE. Phosphorylated L4A H176E ERK was able to phosphorylate myelin basic protein (MBP) with similar efficiency to that of wild type pERK, indicating that these mutations do not alter the function and overall structure of the kinase. All the proteins were aliquoted and stored at – 80 °C. Phosphorylation of recombinant rat wild type and mutant ERK2 proteins was performed as described previously (103).

2. 2. 2 *p*NPP assays

The assay buffer consisted of a three-component system containing 0.1 M acetate, 0.05 M Tris, and 0.05 M Bis-Tris. To determine the kinetic parameters k_{cat} , K_m and k_{cat}/K_m , the initial velocities were measured at increasing substrate concentrations. The apparent second-order rate constant k_{cat}/K_m describes the reaction between free enzyme and free substrate. The reactions were quenched with 10 N NaOH, and the production of *p*NP (*para*-nitrophenolate) was measured using a Multiskan Ascent microplate reader (Lab Systems) at 405 nm. The data were fitted to the Michaelis-Menten equation using software Kaleidagraph (Abelbeck Software) (Eq. 1). $v = [E_0] * k_{cat} * S / (S + K_m)$ (Eq. 1.)

2. 2. 3 Generation of MKP3 antibody

Chicken immunopurified anti-MKP3 antibody was generated by immunizing chickens with the full-length MKP3 protein. The IgY fraction was purified from egg yolks (Aves Labs). MKP3 antibody was purified over a column containing recombinant MKP3 conjugated to Affi-Gel 10 (Sigma). Chicken antibodies were eluted with 0.1 M sodium phosphate (pH 2.5) and stored in phosphate-buffered saline (PBS).

2. 2. 4 Dephosphorylation of recombinant ERK2 proteins by phosphatases

Recombinant MKP3, VHR, and the MKP3/VHR chimera were combined with 1 μ M recombinant phosphorylated ERK2 proteins (wild type, D316/319N, and L4A

H176E) in 0.1 M sodium acetate, 0.05 M Tris, and 0.05 M Bis-Tris (TBA) (pH 7.0 for MKP3 and pH 6.0 for VHR and MKP3/VHR Chimera) and incubated up to 1 hr at 25 °C. Aliquots were withdrawn at the indicated times and added to the tubes containing 5x Laemmli sample buffer to terminate the reactions. The samples were then subjected to western blot analysis as described previously to examine the phosphorylation state of ERK2 using an antibody specific to phosphorylated forms of p44/42 MAPK (Thr²⁰²/Tyr²⁰⁴) (New England Biolabs) (29). Changes in the phosphorylation state of ERK proteins were quantified by densitometry using a Bio-Rad GS-700 Imaging Densitometer and the Molecular Analyst Software (Bio-Rad). The identical samples were also coupled to a kinase assay to directly examine the effect of phosphatases on the activity of phosphorylated ERK as described previously (29). The amount of dephosphorylated ERK proteins was determined by subtracting the fraction remaining from 1 and multiplying by the initial concentration of phosphorylated ERK proteins. The data were fitted to the integrated Michaelis-Menten equation (Eq. 2) using software Kaleidagraph (Abelbeck Software) to obtain apparent second-order rate constant k_{cat}/K_m .

$t = p / k_{cat}E_0 + [K_m / k_{cat}E_0] \ln[p^\infty / p^\infty - p]$ (Eq. 2) where E_0 is the enzyme concentration, p^∞ is the product concentration upon complete reaction, p is the product concentration at time t . For the dephosphorylation of pERK by MKP3 and MKP3/VHR chimera, Eq. 2 was modified to Eq. 3. After MKP3 dephosphorylates pERK, the product (unphosphorylated ERK) builds up and binds to the N-terminal domain of MKP3 and inhibits the binding of pERK substrate. Therefore, we included an inhibition constant term in Eq. 2 and fitted the data using Eq. 3 (100).

$t = p / k_{cat}E_0 + [(1 + (p/K_i))K_m / k_{cat}E_0] \ln[p^\infty / p^\infty - p]$ (Eq. 3) where E_0 is the enzyme concentration, p^∞ is the product concentration upon complete reaction, p is the product concentration at time t , and K_i is the inhibition constant for ERK. We used 0.21 μ M and 0.23 μ M for the K_i for MKP3 and the MKP3/VHR chimera, respectively (described in the text).

2. 2. 5 Fluorescence Anisotropy

Wild type ERK and D316/319N ERK (120 μM) were labeled with fluorescein succinimidyl ester (5 mM) using a Fluorescein Amine Labeling Kit (Pan Vera, WI). Stoichiometry of labeling was 0.86 fluorescein succinimidyl ester per ERK monomer. The labeled proteins (30 nM) were titrated with either MKP3 or MKP3/VHR Chimera (0 to 1.6 μM). The changes in millipolarization were measured using a fluorescence anisotropy instrument (Pan Vera, WI). The total differential fluorescence polarization signal was 15 ~ 20 mP. Percent bound of labeled ERK proteins were plotted versus free MKP3 concentrations and data were fitted to Eq. 4. $[\text{ERK}\cdot\text{MKP3}] = \frac{([\text{ERK}]_0[\text{MKP3}]_{\text{free}})/(K_d + [\text{MKP3}]_{\text{free}})}{([\text{ERK}]_0[\text{MKP3}]_{\text{free}})/(K_d + [\text{MKP3}]_{\text{free}})} \text{ (Eq. 4)}$. MKP3 concentration that is bound to ERK was calculated by multiplying concentration of ERK to fractions of bound ERK. Free MKP3 concentrations were determined by subtracting bound MKP3 concentration from total MKP3 concentration.

2. 2. 6 Chemical Cross-Linking of C293S MKP3 and pERK

To assess the oligomeric state of MKP3 and ERK complex, the proteins were cross-linked with glutaraldehyde and bis[sulfosuccinimidyl]suberate (BS^3). The reactions were performed in 100 μL solutions containing 8 μM of C293S MKP3, pERK, or the 1:1 mixture of C293S MKP3 and pERK in 20 mM Tris \cdot Cl (pH 7.5) at 25 $^\circ\text{C}$. Cross-linking was initiated by adding glutaraldehyde to a final concentration of 5 mM and BS^3 to 200 μM . The cross-linking reactions were terminated at various time points (0-40 min) by adding Glycine (pH 9.0) at a final concentration of 0.2 M. The cross-linked proteins were subjected to SDS-PAGE, and detected by either coomassie staining or western blot analysis using chicken-polyclonal antibody specific to MKP3, and rabbit-polyclonal antibody specific to phosphorylated ERK.

2. 2. 7 Dissociation constant of D316/319N ERK and L4A H176E ERK to MKP3

The initial rates of *p*NPP hydrolysis in the presence of increasing concentrations of ERK proteins were measured spectrophotometrically at 405 nm. The k_{cat}/K_m values at

different concentrations of ERK proteins were determined by measuring the initial velocities at increasing substrate concentrations (0-2 μM) and fitting the data to Eq. 1. In order to obtain the amount of bound ERK, $(k_{\text{cat}}/K_m)/(k_{\text{cat}}/K_m)_{\text{max}}$ were multiplied by the concentration of MKP3. The bound ERK concentrations were plotted against free ERK concentration and the data were fitted to Eq. 4 to obtain the dissociation constant of ERK binding to MKP3.

2.3 Results

2.3.1 The N-terminal domain of MKP3 increases the effective pERK substrate concentration.

Initially, we addressed the role of the N-terminal domain of MKP3 in mediating either intra-or inter-molecular dephosphorylation of pERK. To accomplish this, it was necessary to separate catalytic activation from the evaluation of the catalytic advantage between intramolecular and intermolecular dephosphorylation. We generated a chimeric protein where the catalytic domain of MKP3 was replaced with the catalytic domain of human VHR (*vaccinia H1*- related) (Figure 2. 2). VHR represents the minimal, naturally occurring catalytic domain among dual-specificity phosphatases. pERK has been previously identified as an *in vivo* and *in vitro* substrate of VHR (29, 104). However, VHR does not contain the N-terminal domain of the MKPs (Figure 1. 2), and does not require catalytic activation, as it is fully active towards a variety of phospho-monoester substrates. We investigated the effect of fusing the N-terminal domain of MKP3 onto the catalytic domain of VHR. Generation of the chimeric protein is detailed in Materials and Methods (Figure 2. 2). We first measured the steady-state kinetic parameters (k_{cat} , K_m , k_{cat}/K_m) of MKP3, VHR, and the MKP3/VHR chimera using *pNPP* as a substrate. The MKP3/VHR chimera displayed catalytic efficiencies that were similar to those of wild type VHR using *pNPP* as a substrate (Table 2. 1). The k_{cat} value of the MKP3/VHR chimera was only 2.7 fold lower than that of VHR, whereas the K_m value was nearly identical. Because MKP3 can be activated by ERK binding to the N-terminal domain ((42, 71) (73) and Table 2. 1), we examined whether the catalytic activity of the MKP3/VHR chimera can be further activated by ERK binding. The addition of ERK in the reaction had no significant effect on the steady-state kinetic parameters of either the MKP3/VHR chimera or VHR, using *pNPP* as a substrate (Table 2. 1), consistent with constitutively active enzymes that do not require ERK binding for activation. These results demonstrate that we have successfully eliminated the catalytic activation step as a

necessary component for efficient dephosphorylation by the MKP3/VHR chimera, allowing us to now evaluate the direct contribution of the N-terminal domain towards either inter- or intra-molecular dephosphorylation of ERK.

However, we could not rule out the possibility that the MKP3/VHR chimera was incapable of binding ERK. To be certain that ERK binds to the N-terminal domain of the MKP3/VHR chimera, binding assays were performed using a fluorescent anisotropy method. ERK and a D316/319N ERK mutant were labeled with fluorescein as described in Materials and Methods. The labeled ERK proteins, at a concentration of 30 nM, were titrated with 0 to 1.6 μ M MKP3 or MKP3/VHR chimera. The change in millipolarization was measured, plotted against free phosphatase concentration, and the titration curves were fitted to Eq. 4 (Figure 2. 3). The D316/319N ERK mutant served as a negative control for establishing this binding method. These aspartic acid residues in ERK have been shown to be critical for binding to the N-terminal domain of MKP3 (99). Additional control experiments were performed to establish that labeling (\sim 1:1, fluorescein to ERK monomer) had no effect on the ability to bind to MKP3 (Figure 2. 4). The dissociation constants (K_d) for ERK binding to the wild type MKP3 (Figure 2. 3A) and the MKP3/VHR chimera (Figure 2. 3B) were $0.21 \pm 0.04 \mu$ M and $0.23 \pm 0.05 \mu$ M, respectively. These values were identical within experimental error. The K_d of MKP3 for ERK was similar to the value (0.17μ M) reported by Zhou *et al.* (105). No measurable binding of the D316/319N ERK mutant was observed under identical conditions (Figure 2. 3A). Our data indicate that ERK binds to both MKP3 and the MKP3/VHR chimera with similar affinity; however, binding does not cause an increase in the catalytic activity of the MKP3/VHR chimera. Like VHR, the MKP3/VHR chimera appears to be in a constitutively active state where ERK binding to the N-terminal domain does not further activate the enzyme toward small artificial substrates, like *p*NPP.

Having established that the chimera does not exhibit catalytic activation when bound to ERK, next we compared the catalytic activity of MKP3, VHR, and the

MKP3/VHR chimera toward an authentic protein substrate, pERK. Recombinant MKP3, VHR, and MKP3/VHR chimera, at a final concentration of 100 nM, were combined with 1 μ M recombinant pERK. Dephosphorylation was detected by western blot analysis using an antibody that specifically recognizes the diphosphorylated active form of ERK (a representative data set is shown in Figure 2. 5). The bands were quantitated by densitometry and the data were fitted to the integrated Michaelis-Menten equation (Eq. 2 or Eq. 3) as described in Materials and Methods. The k_{cat}/K_m values for pERK dephosphorylation by MKP3, VHR, and the MKP3/VHR chimera were $3.1 \pm 1.9 \times 10^6$, $20,530 \pm 1,300$, and $1.1 \pm 0.23 \times 10^6 \text{ M}^{-1}\text{s}^{-1}$, respectively. These values are an average of three or more separate experiments. The western blot analysis of pERK dephosphorylation was confirmed with a separate kinase assay as described in Materials and Methods. The k_{cat}/K_m values for pERK dephosphorylation by VHR and the MKP3/VHR chimera using the kinase assay were $9,750 \pm 923$ and $0.40 \pm 0.12 \times 10^6 \text{ M}^{-1}\text{s}^{-1}$, respectively (Figure 2. 6). These values are in reasonable agreement with the values obtained from the western blot analysis. Quite dramatically, the MKP3/VHR chimera was a more efficient enzyme (~ 40 -fold higher in k_{cat}/K_m) than wild type VHR in dephosphorylating pERK. This suggests that the N-terminal domain of MKP3 is contributing significantly to enhance catalysis of pERK through specific binding to the N-terminal domain. Since we have shown that the MKP3/VHR chimera was not catalytically activated by ERK binding (Table 2. 1), the increased k_{cat}/K_m value over wild type VHR is likely the result of an increase in the effective concentration of pERK. Although the chimera is an engineered enzyme, the fact that it exhibits “gain of function” behavior provides evidence for an intramolecular dephosphorylation mechanism of pERK by MKP3. The catalytic advantage of an increase in effective substrate concentration would be realized when the substrate and the enzyme are tethered within the same complex.

2. 3. 2 Intramolecular dephosphorylation of pERK by MKP3

To investigate whether pERK inactivation by MKP3 proceeds by intramolecular or intermolecular dephosphorylation, next, we examined the mechanism by which unphosphorylated ERK inhibits pERK dephosphorylation. If the reaction is intramolecular and involves MKP3 dephosphorylating the same pERK molecule to which its N-terminal domain is bound, then excess unphosphorylated ERK should inhibit dephosphorylation by competing with pERK at the N-terminus, and blocking an intramolecular reaction. Consistent with this, Zhao *et al.* (88) recently showed that unphosphorylated ERK acted as a classical competitive inhibitor of pERK dephosphorylation by MKP3. However, the basis for the observed inhibition was not established, since an excess amount of unphosphorylated ERK in the reaction could block the reaction by either binding the N-terminal domain, the catalytic domain or both.

Consistent with the results of Zhao *et al.* (88) we demonstrate that excess unphosphorylated ERK (10 μM) can readily inhibit pERK (1 μM) dephosphorylation by MKP3 (Figure 2. 7A). To investigate whether this inhibition was due to competition for binding at the N-terminal domain, we took advantage of a *Sevenmaker* type of mutant ERK (72), where we mutated two aspartic acid residues to asparagine residues (D316/319N ERK) (Figure 2. 1). These aspartic acid residues form negative clusters in ERK and have been shown to be critical for binding to the N-terminal domain of MKP3 (99). Once expressed and purified, we verified that D316/319N ERK does not bind tightly to the N-terminal domain of MKP3 by determining the ability of D316/319N ERK to activate MKP3 against *pNPP* substrate. There was minimal catalytic activation of MKP3 toward *pNPP* in the presence of D316/319N ERK at a 5-fold molar excess (Figure 2. 7B). In positive control experiments, MKP3 was activated approximately 50-fold when wild type ERK, at 2-fold molar excess, was present in the assay. In an effort to measure a dissociation constant of D316/319N ERK binding to MKP3, the initial rates of *pNPP* hydrolysis in the presence of increasing levels of D316/319N ERK were measured

and analyzed as described in Materials and Methods. Given the lack of significant binding, the estimated K_d with D316/319N ERK was $>10 \mu\text{M}$ (data not shown), suggesting that D316/319N ERK exhibits greatly diminished binding to the N-terminal domain of MKP3, consistent with the fluorescence polarization binding data of Figure 2. 3A. To verify that the D316/319N ERK mutant is structurally intact, the mutant was phosphorylated *in vitro* with its upstream kinase MEK and the ability of the activated kinase D316/319N pERK to phosphorylate myelin basic protein was compared to wild type pERK. Similar activities were observed (data not shown), suggesting that the double mutant D316/319N ERK is structurally and functionally intact, and that the loss of MKP3 binding reflects specific alterations in the binding interface.

In competition experiments similar to those described for wild type enzyme (Figure 2. 7A), excess D316/319N ERK exhibited only a very small inhibitory effect on the ability of MKP3 to dephosphorylate wild type pERK (Figure 2. 7A), which is likely due to some residual binding of D316/319N ERK to MKP3. These data provide strong support for the idea that the inhibition of pERK dephosphorylation by native ERK was due to ERK binding to the N-terminal domain of MKP3, and not due to competition at the active site of MKP3. Moreover, these data are consistent with an intramolecular dephosphorylation mechanism where pERK has to bind to the N-terminal domain of MKP3 to be effectively dephosphorylated by the catalytic domain of the same MKP3 molecule; however, the possibility existed that inhibition of pERK dephosphorylation in the presence of excess ERK might be due to dimerization between pERK and unphosphorylated ERK, leading to depletion of monomeric pERK as a substrate for MKP3, if the monomeric form is the relevant substrate. To rule out this possibility, we performed pERK dephosphorylation reactions in the presence of an excess of a dimerization mutant of ERK (L4A H176E), where four leucine residues (L333, 336, 341, 344) are mutated to alanine and one histidine residue is changed to glutamic acid (Figure 2. 1). These residues have been shown to be important in ERK dimerization upon

phosphorylation (84). We observed similarly inhibited rates of pERK dephosphorylation by MKP3 in the presence of the same concentration of either excess wild type ERK or dimerization mutant ERK (Figure 2. 7C). These data rule out mixed ERK dimerization as the source of inhibition and demonstrate that the observed inhibition by unphosphorylated ERK is derived from direct competition between pERK for the N-terminal domain of MKP3.

To further distinguish between inter and intramolecular dephosphorylation, we analyzed the ability of MKP3 to hydrolyze the phosphorylated form of the D316/319N ERK mutant under a variety of conditions where MKP3 is utilized in the basally-active state (MKP3 alone) or the activated state (MKP3 bound to unphosphorylated wild type ERK). Because D316/319N ERK does not bind tightly to MKP3, this mutant cannot activate MKP3 under the conditions employed. Therefore, dephosphorylation of D316/319N pERK by MKP3 should be greatly diminished. However, the efficiency of D316/319N pERK dephosphorylation by activated MKP3 (ERK-bound form) would depend on whether MKP3 performs inter or intramolecular dephosphorylation. If MKP3 utilizes an intermolecular mechanism, the activated form of MKP3 (ERK-bound) should be able to efficiently dephosphorylate D316/319N pERK, as there would be no additional requirement to bind to the N-terminal domain of MKP3, only to the catalytic domain. Alternatively, if MKP3 catalyzes intramolecular dephosphorylation, activated or basal MKP3 would not be able to efficiently dephosphorylate D316/319N pERK because of the inability to bind to the N-terminal domain of MKP3. To distinguish between these two mechanisms, we compared k_{cat}/K_m values of wild type pERK and D316/319N pERK dephosphorylation by MKP3 (both basal state and ERK-bound activated state). As shown in Figure 2. 8, the k_{cat}/K_m values with D316/319N pERK by both the basal and the activated state of MKP3 ($12,800 \pm 1,230 \text{ M}^{-1}\text{s}^{-1}$ and $13,510 \pm 1,443 \text{ M}^{-1}\text{s}^{-1}$, respectively) were similar, and were ~ 200 -fold lower than that of wild type pERK dephosphorylation ($3.1 \times 10^6 \text{ M}^{-1}\text{s}^{-1}$). These data provide additional evidence for an intramolecular

dephosphorylation mechanism, where substrate pERK must interact with the N-terminal domain of MKP3 to be dephosphorylated by the catalytic domain of the same molecule of MKP3.

2.3.3 Stoichiometry of the substrate/enzyme complex of pERK-bound MKP3

ERK exists in a monomer-dimer equilibrium that can be shifted in favor of the dimer upon phosphorylation by its upstream kinase MEK (84). In the cytoplasm, dimerization of phosphorylated ERK has been postulated as the trigger for translocation into the nucleus, where pERK can mediate transcriptional activation (85) (84) (86) (106). MKP3 has been shown to localize exclusively in the cytoplasm (61). Thus, MKP3 could encounter either the monomeric or dimeric form of pERK as the physiologically relevant substrate. To determine the stoichiometry of the pERK/MKP3 Michaelis complex, we used a chemical cross-linking approach. For this study, it was necessary to use the catalytic mutant of MKP3 (C293S, nucleophile cysteine 293 residue was mutated to a serine residue) to prevent dephosphorylation of the complex. This mutant has no detectable phosphatase activity, but displayed a similar binding constant ($K_d = 0.2 \mu\text{M}$) to that of wild type MKP3 for ERK. Similarly, other PTPs with this mutation are still able to bind their substrates (29, 33, 107, 108) (37).

MKP3(C293S), pERK, and a 1:1 mixture of MKP3(C293S) and pERK were subjected to glutaraldehyde cross-linking as described in Materials and Methods. The proteins were cross-linked at fixed concentrations of glutaraldehyde (5 mM) over time (up to 15 min). The cross-linked proteins were resolved by SDS-PAGE, and the gels were probed with antibodies against either MKP3 or phosphorylated ERK. Figure 2. 9A & B show western blots of representative data from the cross-linking analysis, which was performed no less than 3 separate times. Cross-linking of MKP3(C293S) alone indicated no significant amount of cross-linked species prior to 10 minutes, though faint bands were noticeable after longer periods of cross-linking (Figure 2. 9 & 2. 10). Strikingly, when MKP3(C293S) was mixed with an equal amount of pERK, an efficiently cross-

linked band whose molecular weight (80-90 kDa) corresponds to a heterodimer (predicted 86 kDa) of the two was detected (Figure 2. 9). This major cross-link band, which was clearly observable after only 1 minute, was immuno-reactive to both specific antibodies (Figure 2. 9A & B), in agreement with a 1:1 cross link of MKP3 and pERK. Consistent with previous reports that pERK can form a homodimer (84), cross-linking of pERK alone yielded a major cross-linked species at 80-90 kDa.

Due to the fact that both pERK and MKP3 are 43 kDa proteins, cross-linked species of homodimers and heterodimers exhibited only slight differences in mobility on SDS-PAGE (Figure 2. 11). However, these cross-linked species could be distinguished by differences in mobility on SDS-PAGE when loaded side by side (Figure 2. 11).

The western blot probed with the anti-pERK antibody displayed much weaker intensity of the cross-linked species than would be expected from the intensity of monomeric pERK (Figure 2. 9A) or from the same band probed with the anti-MKP3 antibody (Figure 2. 9A). To verify that the weaker signal is due to the loss of an epitope upon extensive cross-linking, the cross-linked proteins were detected by coomassie staining. Using coomassie detection, most (67 %) of the 1:1 protein mixture was cross-linked as the heterodimer under the conditions presented (Figure 2. 9C), suggesting that the western blot against pERK (Figure 2. 9B) had underrepresented the amount of pERK in the complex. The presence of weak higher oligomers (>dimer) were seen in both the 1:1 mixture and the sample containing only pERK (Figure 2. 9C). Interestingly, compared with the heterodimer, cross-linking of pERK alone revealed that much of pERK remained monomeric, as relatively small amounts of homodimer were cross-linked (Figure 2. 9C).

Using the identical analysis described above, we have performed cross-linking studies with unphosphorylated ERK, wildtype MKP3 and a 1:1 mixture of the two (Figure 2. 11). We found that unphosphorylated ERK and wild-type MKP3 can be efficiently cross-linked to form a similar heterodimer under the conditions used in the

above experiments. In addition to glutaraldehyde, we have used Bis[sulfosuccinimidyl] suberate (BS³) as a cross-linking agent. With ERK and MKP3 alone and in a 1:1 mixture, we observe (by coomassie staining) no significant cross-linked species with the proteins alone in solution, but we observe a strong cross-linked band at ~85 kDa in the 1:1 mixture (Figure 2. 12), similar to the results we have consistently observed using glutaraldehyde. Nonetheless, we cannot formally discount the possibility that MKP3 can bind dimers of ERK. Significant amounts of larger species (>85 kDa) were not observed. In support of the cross-linking studies, analytical ultracentrifugation experiments indicated that MKP3 existed as a monomeric species (calculated MW of 41,347 kDa of a single ideal component), which when combined with pERK produced a complex consistent with a heterodimer (data not shown).

To provide additional evidence for the idea that MKP3 binds and dephosphorylates the monomeric form of pERK, we utilized the dimerization mutant of ERK (L4A H176E). We investigated the efficiency of MKP3 to dephosphorylate the monomeric form of pERK (L4A H176E pERK). To ensure that the L4A H176E ERK mutant does not display altered binding to MKP3, or diminished ability to activate MKP3, we measured the rate of *p*NPP hydrolysis by MKP3 in the presence of increasing concentrations of either wild type or L4A H176E ERK (as described in Materials and Methods). As is evident from Figure 2. 13A and B, the L4A H176E ERK mutant displayed binding/activation curves that were indistinguishable (within error) from wild type ERK. The calculated dissociation constants of binding wild type or L4A H176E ERK to MKP3 were $0.27 \pm 0.06 \mu\text{M}$ and $0.20 \pm 0.07 \mu\text{M}$, respectively (Figure 2. 13A & B). Utilizing the fluorescence binding assay described in Figure 2. 3, we determined a K_d of $0.15 \pm 0.02 \mu\text{M}$ between L4A H176E ERK and MKP3. The K_d of $0.27 \mu\text{M}$ is in good agreement with the value of $0.21 \mu\text{M}$ obtained for wild type ERK using the fluorescent anisotropy binding experiment described above. There is also excellent agreement between K_d values $0.20 \mu\text{M}$ and $0.15 \mu\text{M}$ obtained with the L4A H176E ERK mutant

using the activation-based assay and the fluorescent anisotropy binding assay, respectively. More importantly, similar dissociation constants for MKP3 binding to L4A H176E or wild type ERK indicate that overall binding and activation of MKP3 are unaffected by these mutations. To test the ability of MKP3 to dephosphorylate L4A H176E pERK, we compared the k_{cat}/K_m values with wild type pERK and L4A H176E pERK as substrates. The k_{cat}/K_m value ($0.88 \pm 0.23 \times 10^6$) using L4A H176E pERK was only ~3-fold lower than that observed with wild type pERK ($3.1 \pm 1.9 \times 10^6$) (Figure 2. 13C & D). This similarity in k_{cat}/K_m values provides additional support that the monomeric form of pERK is the relevant substrate for MKP3. Together, our studies suggest that the heterodimer of MKP3 and phosphorylated ERK is the physiologically relevant complex.

2.4 Discussion

In addition to its role in mediating catalytic activation of the carboxy terminus, we have demonstrated that the N-terminal domain of MKP3 mediates intramolecular dephosphorylation between the monomeric form of phosphorylated ERK and a monomer of MKP3 (Figure 2. 14). Thus, monomeric pERK binds to the N-terminal domain of MKP3 and is dephosphorylated by the same molecule of MKP3. By tethering pERK to the N-terminal domain of MKP3, the C-terminal catalytic domain enjoys an increase in effective substrate concentration. Using the MKP3/VHR chimera protein (Table 2. 1 & Figure 2. 5) to estimate this catalytic advantage, the increased effective concentration contributes about ~40-fold to the k_{cat}/K_m value. This is probably a lower estimate given the potential sub-optimal substrate orientation of the chimera relative to MKP3. Binding of ERK to MKP3 also induces catalytic activation, which contributes ~100 fold rate acceleration in the k_{cat}/K_m value (42, 59, 73). Even ignoring the basic contribution of the initial tight-binding affinity ($K_d \leq 210$ nM) between ERK and MKP3, the intramolecular dephosphorylation mechanism creates a reaction that is ~4000 fold more efficient

towards its target substrate. MKP3 is an exquisite example of both regulated and specific catalysis, creating a virtual “magic bullet” towards pERK.

Our general model for pERK dephosphorylation by MKP3 is depicted in Fig 2.

14. Several additional insights can be gleaned from this model. It has been shown that ERK exists in a monomer-dimer equilibrium (84), which can be shifted toward dimer formation when ERK is phosphorylated by MEK. The crystallographic model of pERK was solved as a dimer (83). Consistent with these observations, our data indicate that pERK is (minimally) in a monomer-dimer equilibrium state. Dimerization of pERK is thought to provide the molecular switch that allows dimeric pERK to translocate from the cytosol to the nucleus (84). Here, cross-linking studies along with other presented data, are entirely consistent with a simple heterodimeric complex between pERK monomer and MKP3, and provide strong evidence for the heterodimer as the functionally relevant Michaelis complex. However, we cannot rule out the possibility that MKP3 can bind and dephosphorylate dimeric ERK. Future studies will be directed at exploring this possibility. When pERK and MKP3 are present at equal-molar concentrations, monomeric MKP3 complexes with pERK (i.e., little of the monomer remains) to generate a species that is almost exclusively the heterodimer. Together these data suggest that the binding between pERK and MKP3 is tighter than the binding between pERK monomers, and that binding may be mutually exclusive. Although for technical reasons we were unable to measure a K_d value between pERK and MKP3 (C293S), Zhao *et al.* have reported a Michaelis constant K_m of $0.022 \pm 0.005 \mu\text{M}$ (88). Khokhlatchev *et al.* (84) have reported a K_d value of 7.5 nM for pERK dimerization. Given the significant amount of pERK monomer reported by Khokhlatchev *et al.* (84) in the latter study, we believe the K_d value from equilibrium sedimentation data may be a high estimate of the actual binding affinity between pERK monomers (84). Our data are consistent with the idea that MKP3 binding to pERK or ERK may prevent the ability of ERK to dimerize. We have used molecular modeling of the available x-ray/NMR structures of VHR (37),

pERK (83), the N-terminal domain of MKP3 (79), and the C-terminal domain of MKP3 (80) to examine the idea of mutually exclusive binding. The N-terminal noncatalytic domain and the C-terminal catalytic domain of MKP3 were solved separately. The structure of the linker region (~50 amino acid residues) between two domains has not been solved. Using the VHR-phosphopeptide structure (37) as a guide, we oriented the catalytic domain of MKP3 (79) onto a monomer of pERK (83). The location of the N-terminal domain binding-site on pERK was modeled, in part, using the Arg residues (Arg 64/65) in the N-terminal domain of MKP3, which were shown to be important in interacting with ERK (80, 105), through Asp residues (Asp 316/319) located on the opposite face of the TxY phosphorylation motif (99). When the two domains of MKP3 and the pERK monomer were docked as described above, the catalytic domain of MKP3 interacts with one side of pERK (TxY motif) and the N-terminal domain of MKP3 interacts on the opposite side of pERK (via Asp 316/319). This interaction is schematically drawn in the bottom half of Figure 2. 14. To connect the two domains of MKP3, the 50 unaccounted for amino acids in the linker could be predicted to traverse the dimerization domain of pERK, preventing homo-dimerization, although the N-terminal domain and not the linker region may be involved in mutually exclusive binding. Future investigations will examine the idea of mutually exclusive binding and whether MKP3 can bind and dephosphorylate a covalently fused ERK dimer. If mutually exclusive binding is established, then additional studies will address whether the linker region, the N-terminal domain alone, or both regions are required to prevent ERK homodimerization.

The formation of a heterodimeric complex of MKP3 and ERK has several important implications in the regulation of ERK function, as well as nuclear translocation. There are three different postulated mechanisms for nuclear import of MAP kinase: passive diffusion of monomer, active transport of a homodimer, and a nuclear pore complex-mediated, cytosol-independent transport (85, 87, 106). Formation

of a heterodimer between MKP3 and pERK in the cytoplasm might prevent pERK translocating to the nucleus by anchoring pERK in the cytoplasm. Interestingly, this mode of regulation does not require MKP3 to be active as a phosphatase. Indeed, Brunet, A. *et al.* showed that overexpression of an inactive form of MKP3 (C293S MKP3) could sequester ERK in the cytoplasm (109). Similarly, it has been shown that MEK anchors unphosphorylated ERK in the cytoplasm (110-112). The localization and the function of ERK may be ultimately determined by which protein(s) are associated (85, 106, 113). Tanoue, T. *et al.* suggested that there is a docking domain in MAP kinases common to substrates, activators, and regulators, including MEK1, MNK1, and MKP3 (99). Others proposed that conserved docking sites in MEKs and substrate proteins mediate high affinity binding to MAP kinases (114-116). Using short synthetic peptides, recent studies by Bardwell *et al.* provided evidence that the regulators of ERK such as MEK1/2, Elk-1, and MKP1/2 bind to an overlapping region in ERK (117). Studies by Zhang *et al.* showed mutually exclusive binding of MKP3 and MEK to ERK using GST pull-down assays (118). Together, these studies support a model where formation of a heterodimer between MKP3 and ERK might prevent further activation of ERK by blocking the binding site for MEK (Figure 2. 14). Consistent with this idea, we have observed that unphosphorylated ERK bound to C293S MKP3 is highly resistant to phosphorylation by active MEK (Denu *et al.* unpublished observation). Thus, MKP3 not only down-regulates pERK function by substrate-activated, intramolecular dephosphorylation, but may also prevent pERK homo-dimerization and further activation by its upstream kinase MEK. However, it should be noted that Brunet *et al.*, using a transient transfection system, concluded that inactive MKP3 (C293S) blocks MAPK nuclear translocation without affecting its phosphorylation by MEK (109). Although this contradictory observation may have resulted from the use of an artificially high activation of the MEK pathway, additional studies are needed to explore this potential mode of regulation.

This work provides a framework for understanding the general and specific mechanisms employed by the MKP family of enzymes that regulate MAP kinases. The MKPs share similar structural domains consisting of the N-terminal noncatalytic domain and C-terminal catalytic domain. Given the observed specificity (60, 119) (75, 96) (61) and the catalytic activation seen with other MKPs (42, 71, 73) (61, 75, 76), many of the reaction and regulatory mechanisms described here for MKP3 may be a general feature of other MKPs. Future work focusing on protein complex formation among and between the MKPs and the MAP kinases will provide additional insight into the exquisite regulation of these enzymes.

2.5 Acknowledgements

We thank Johanna Rigas for generating the antibody against MKP3, Melanie Cobb (University of Texas Southwestern) for providing the pGEX-KG H176E L₄A ERK2 Plasmid, Jeffrey Hansen and Virgil Schirf (University of Texas Health Sciences Center) for performing the sedimentation velocity analysis.

Table 2. 1. *p*NPP hydrolysis activity by VHR, MKP3/VHR chimera, and wild-type MKP3. pH 6.0 at 25 °C. The initial velocities were measured using 100 nM enzymes at increasing substrate concentrations (0- 20 mM) to determine the kinetic parameters k_{cat} , K_m and k_{cat}/K_m . ERK was added as 2-fold excess to the enzymes (200 nM). The reactions were quenched with 10 N NaOH, and the production of *p*NP (*para*-nitrophenolate) was measured using a Multiskan Ascent microplate reader (Lab Systems) at 405 nm. The data were fitted to the Michaelis-Menten equation using software Kaleidagraph (Abelbeck Software). $v = [E_0] * k_{cat} * S / (S + K_m)$

The values are averaged from three separate experiments.

	VHR	VHR + ERK	chimera	chimera + ERK	MKP3	MKP3 + ERK
$k_{cat} (s^{-1})$	6.20 ± 0.43	6.25 ± 0.23	2.30 ± 0.12	2.84 ± 0.11	0.024 ± 0.005	0.45 ± 0.08
K_m (mM)	2.17 ± 0.42	2.32 ± 0.31	3.25 ± 0.41	2.30 ± 0.25	5.12 ± 1.01	1.5 ± 0.14
k_{cat}/K_m ($M^{-1}s^{-1}$)	2863 ± 390.4	2694 ± 252	742 ± 59.4	1235 ± 91.0	4.69 ± 1.34	305 ± 78.5

Figure 2. 1 The crystallographic model of phosphorylated ERK dimer (adapted from (83)). Residues important in dimerization are shown in blue (H176, L333, L336, L341, and L344). Residues that are phosphorylated are shown in light blue (T183 and Y185). Residues that are important in interacting with the N-terminal domain of MKP3 are shown in green (D316 and D319). Structures were generated as a ribbon diagram using Swiss Pdb Viewer v3. 7 and POV-Ray v3. 5.

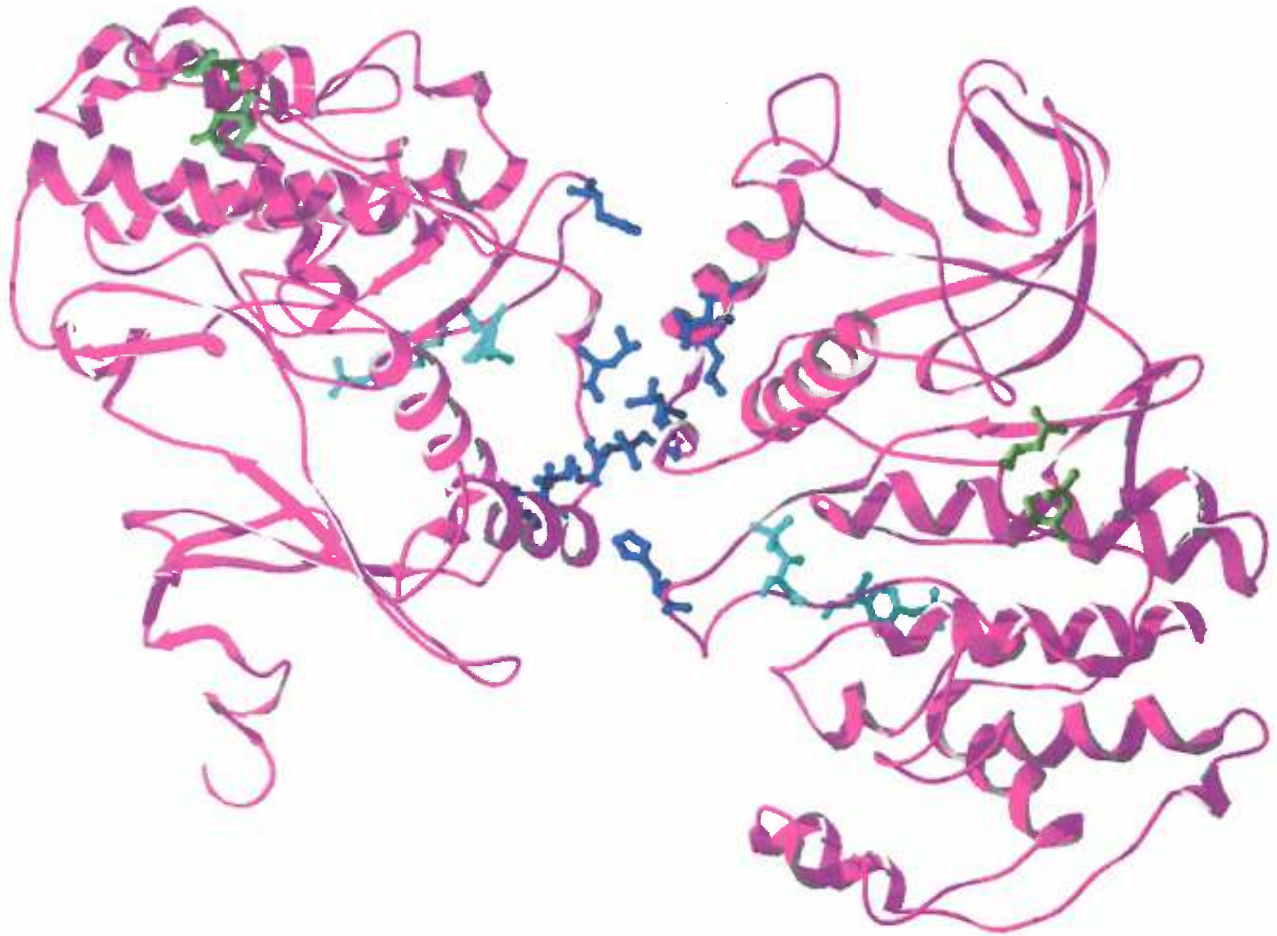
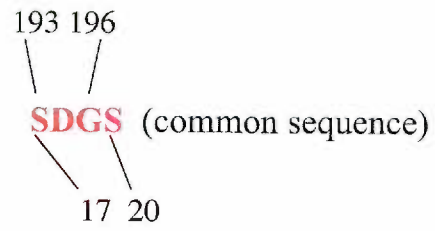


Figure 2. 2 Generation of MKP3/VHR chimera. The MKP3/VHR chimera was generated by fusing the N-terminal domain of MKP3 to VHR using a PCR method. The fusion cDNA was generated using our existing pT7-VHR and pT7-MKP3 His_{x6} expression vector by standard PCR methods. The PCR fragment containing the VHR catalytic domain was inserted into pT7-MKP3, replacing the catalytic domain of MKP3. MKP3 and VHR were fused through the identical amino acid sequence 'SDGS'. The 'SDGS' sequence in VHR (17-20 in 185 residues VHR) is found in the loop between the first α helix and first β strand. In MKP3, 'SDGS' resides in the N-terminal domain close to the catalytic domain (193-196 in 381 residue protein; catalytic domain starts at 204 amino acid residue).



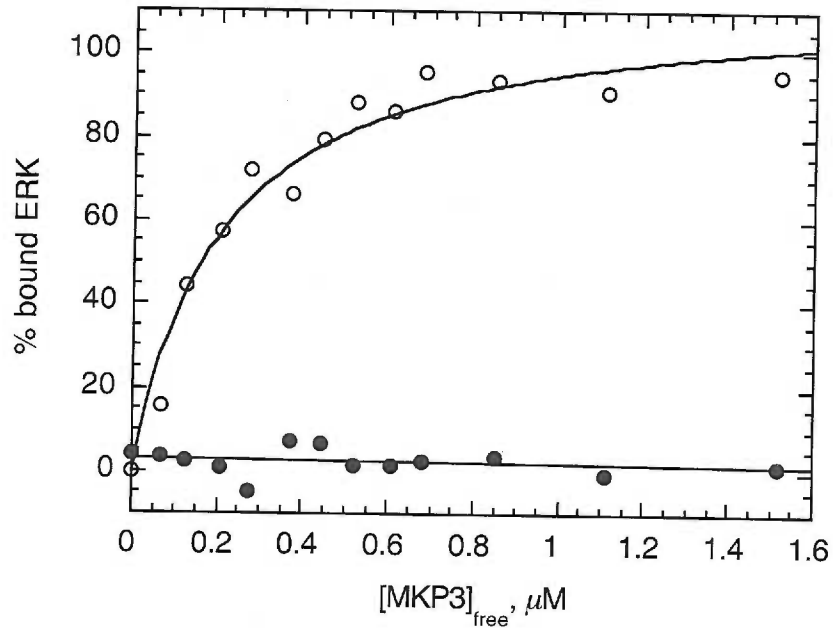
MKP3/VHR Chimera



-HCxxGxxR(T/S)- active site motif

Figure 2. 3 Binding affinity of ERK to MKP3 and an MKP3/VHR chimera. Wild-type ERK and D316/319N ERK were labeled with fluorescein as described in Materials and Methods. The labeled enzymes (30 nM) were titrated with 0 to 1.6 μ M MKP3 (A, open circles) or MKP3/VHR Chimera (B, filled circles). Binding data for the D316/319N ERK mutant are shown in A, filled circles. The changes in millipolarization were measured using a fluorescent anisotropy instrument, and plotted against phosphatase concentrations. Percent bound of labeled proteins were plotted versus free MKP3 concentrations and data were fitted to Eq. 4 using Kaleidagraph. The binding constants for ERK to the wild-type MKP3 and the MKP3/VHR chimera were $0.21 \pm 0.04 \mu$ M and $0.23 \pm 0.05 \mu$ M, respectively. These values are an average of three separate experiments.

(A)



(B)

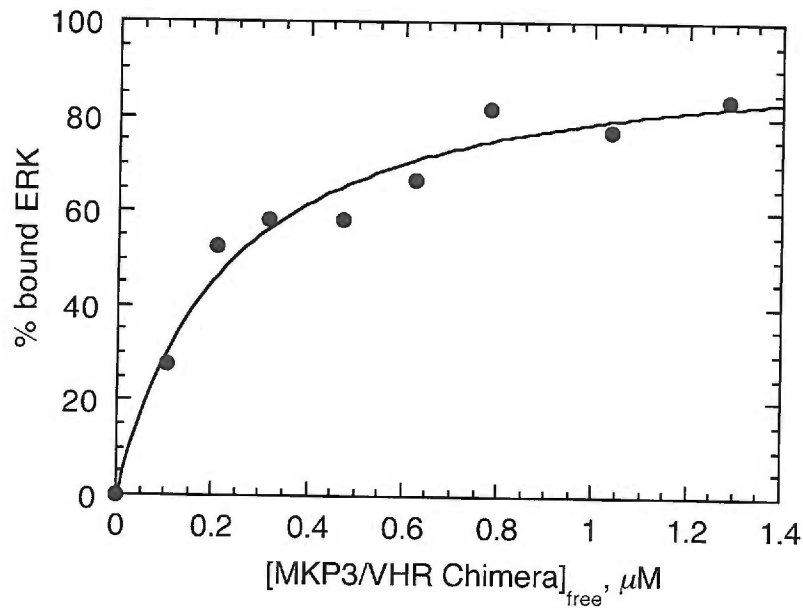


Figure 2. 4 Effect of fluorescein labeling of ERK on the ability to bind and activate MKP3. Fluorescein labeling of ERK proteins have no significant effect on the ability to bind and activate MKP3. The initial velocities of *p*NPP hydrolysis by MKP3 were measured in the presence of fluorescein labeled or unlabeled ERK proteins. Open circles, filled circles, open triangles, filled triangles represent unlabeled wild type ERK, labeled wild type ERK, unlabeled D316/319N ERK, labeled D316/319N ERK, respectively.

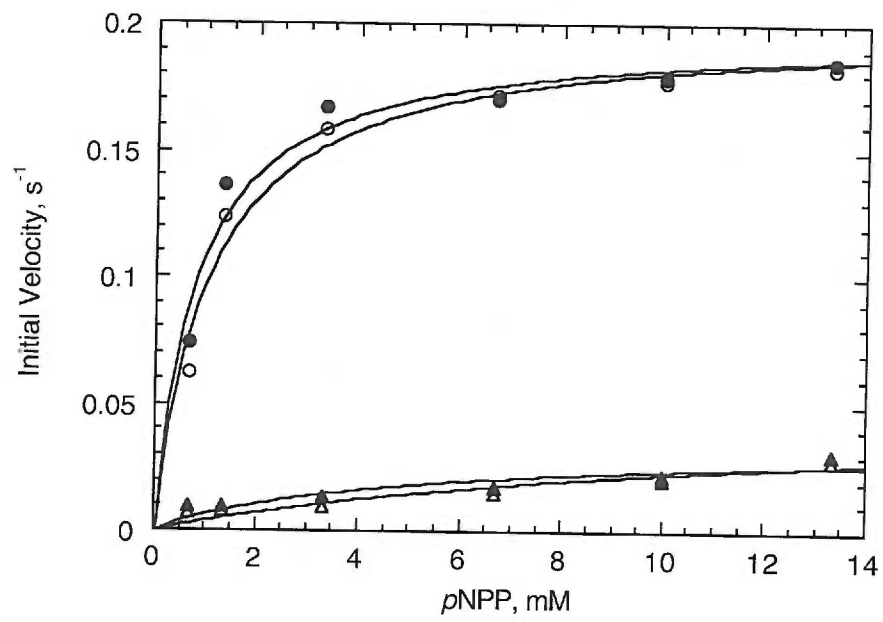


Figure 2. 5 Time-dependent dephosphorylation of pERK by MKP3, VHR, and an MKP3/VHR chimera. MKP3, VHR, and the MKP3/VHR chimera (100 nM) were incubated with phosphorylated ERK (1 μ M) at 25 °C for 0-15 min (TBA, pH 6.0 for VHR and MKP3/VHR chimera, pH 7.0 for MKP3). Dephosphorylation of pERK was determined by western blot analysis using antibodies specific to the dually-phosphorylated form of ERK, and the data were fitted to the integrated Michaelis-Menten equation (Eq. 2) as described in Materials and Methods. For MKP3 and MKP3/VHR chimera, the inhibition constants were taken into account as in Equation 3.

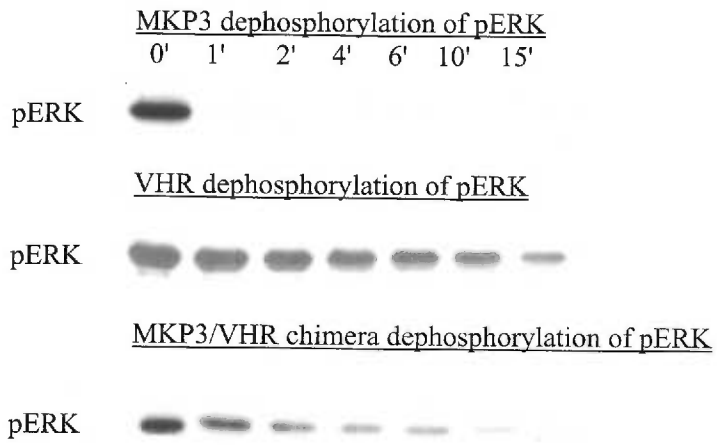


Figure 2. 6 Time-dependent dephosphorylation of pERK by VHR and the MKP3/VHR chimera using a radioactive kinase assay. VHR (A) and MKP3/VHR chimera (B) (0.1 μ M) were combined with 1 μ M pERK and incubated for up to 20 min at 25 °C. Aliquots were withdrawn at the indicated times and ERK kinase assays were performed as described in Materials and Methods. The data were fitted to the integrated Michaelis-Menten equation (Eq. 2). The graph is an average of three different experiments.

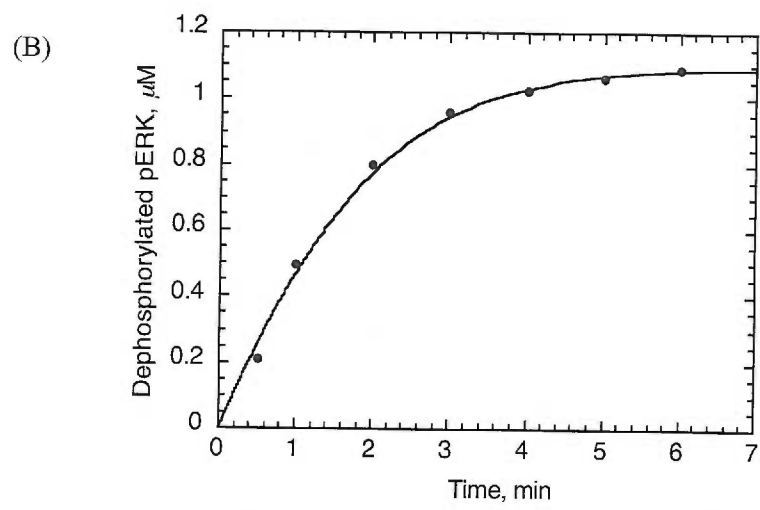
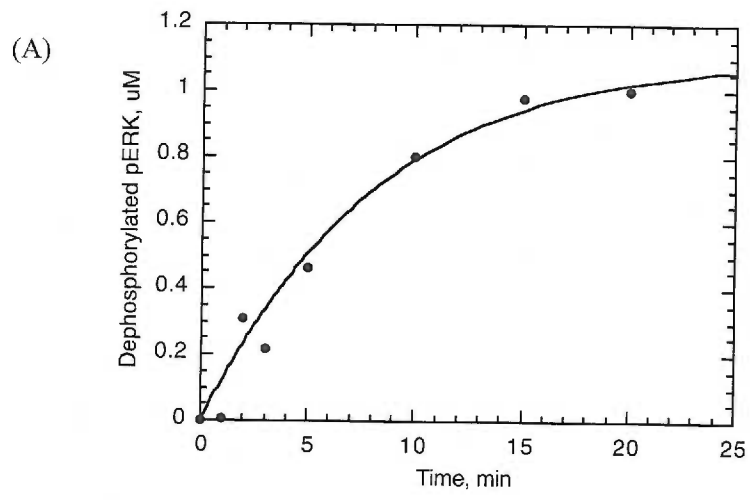


Figure 2. 7 Unphosphorylated ERK competes with phosphorylated ERK for binding at the N-terminal domain of MKP3. (A) Time-dependent dephosphorylation of pERK by MKP3. MKP3 (100 nM) was incubated with phosphorylated ERK (1 μ M) at 25 °C for 0-15 min (TBA, pH 7.0). Dephosphorylation of pERK was determined by western blot analysis using antibodies specific to the diphosphorylated form of ERK. For the dephosphorylation of pERK in the presence of unphosphorylated ERK (wild type and D316/319N), 10 μ M unphosphorylated ERK was preincubated with 100 nM MKP3 for 5 min at 25 °C, then reactions were initiated by adding pERK to the preincubated MKP3-ERK complex. (B) The catalytic activation of MKP3 in the presence of ERK or D316/319N ERK. 0.28 μ M MKP3 was incubated with 0.60 μ M of either wild type ERK or D316/319N ERK. The phosphatase substrate *p*NPP, ranging from 0 to 10 mM was used to examine the effect of ERK on the phosphatase activity of MKP3 (TBA, pH 7.0). The data were fitted using the Michaelis-Menten equation (Eq. 1). The D316/319N ERK double mutant did not activate MKP3. The graph is an average of three separate experiments. (C) Time-dependent ERK dephosphorylation by MKP3 and inhibition in the presence of unphosphorylated ERK or L4A H176E mutant. Data were generated and analyzed as in (A). MKP3 (100 nM) was incubated with phosphorylated ERK (1 μ M) at 25 °C for 0-20 min (filled circles). Open circles represent pERK dephosphorylation in the presence of 10 mM unphosphorylated ERK and the filled squares represent pERK dephosphorylation in the presence of 10 mM unphosphorylated L4A H176E mutant. The graph represents an average of two separate experiments.

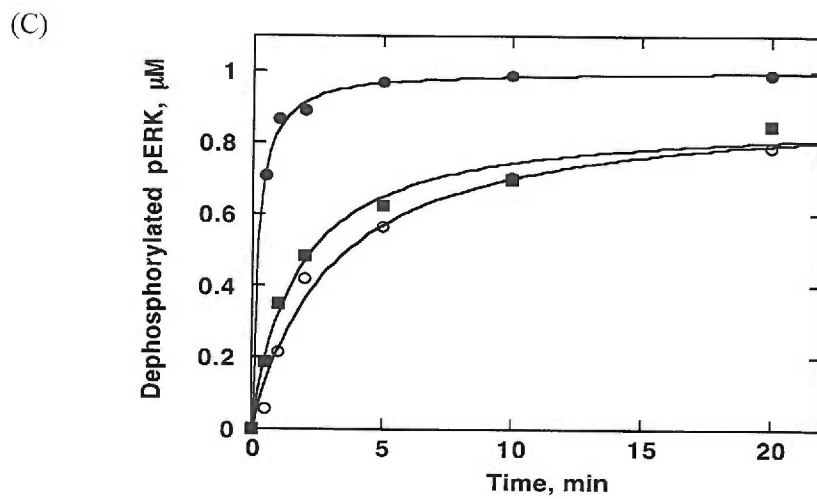
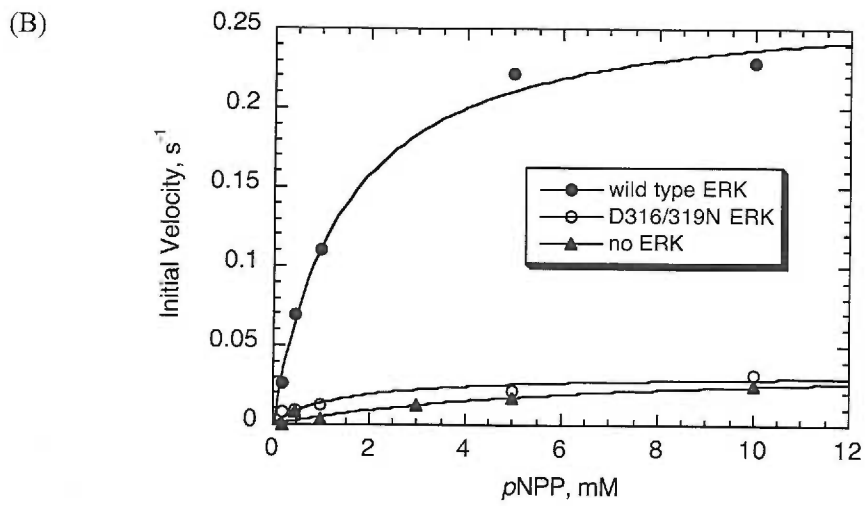
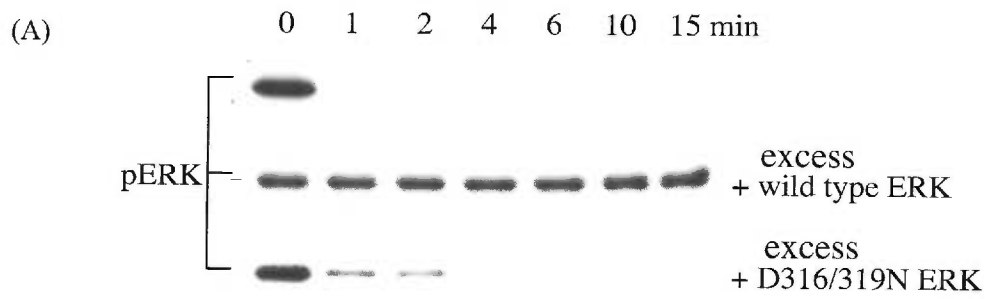


Figure 2. 8 Dephosphorylation of wild type and D316/319N mutant pERK by MKP3. Recombinant wild type and D316/319N mutant pERK at a final concentration of $1 \mu\text{M}$ were combined with $0.14 \mu\text{M}$ recombinant wild-type MKP3 in TBA, pH 7.0. Reactions were incubated at $25 \text{ }^\circ\text{C}$ for the indicated times prior to quenching. For the pERK dephosphorylation reaction by activated MKP3, MKP3 ($0.14 \mu\text{M}$) was pre-incubated with unphosphorylated ERK ($0.28 \mu\text{M}$) and used for dephosphorylating pERK. The rate of dephosphorylation was measured using integrated Michaelis-Menten equation including inhibition constant term (Eq. 3) as described in Materials and Methods.

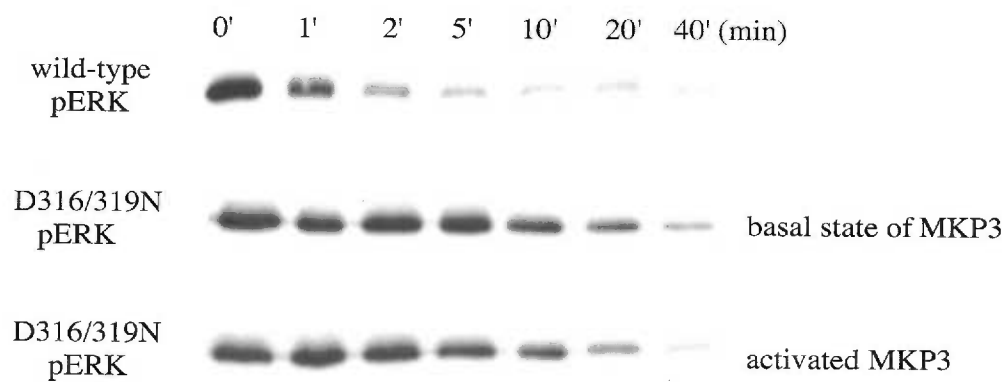


Figure 2. 9 Glutaraldehyde cross-linking of C293S MKP3 and pERK. (A-B) MKP3 (8 μ M), ERK (8 μ M), or 1:1 mixture of MKP3 and ERK (8 μ M each) were cross-linked with 5 mM glutaraldehyde up to 15 min at 25 °C. The reactions were terminated by adding glycine (pH 9.0) at a final concentration of 0.2 mM. The cross-linked species were determined with SDS-PAGE and western blotting with appropriate antibodies. (C) Coomassie staining of SDS-PAGE of cross-linked species.

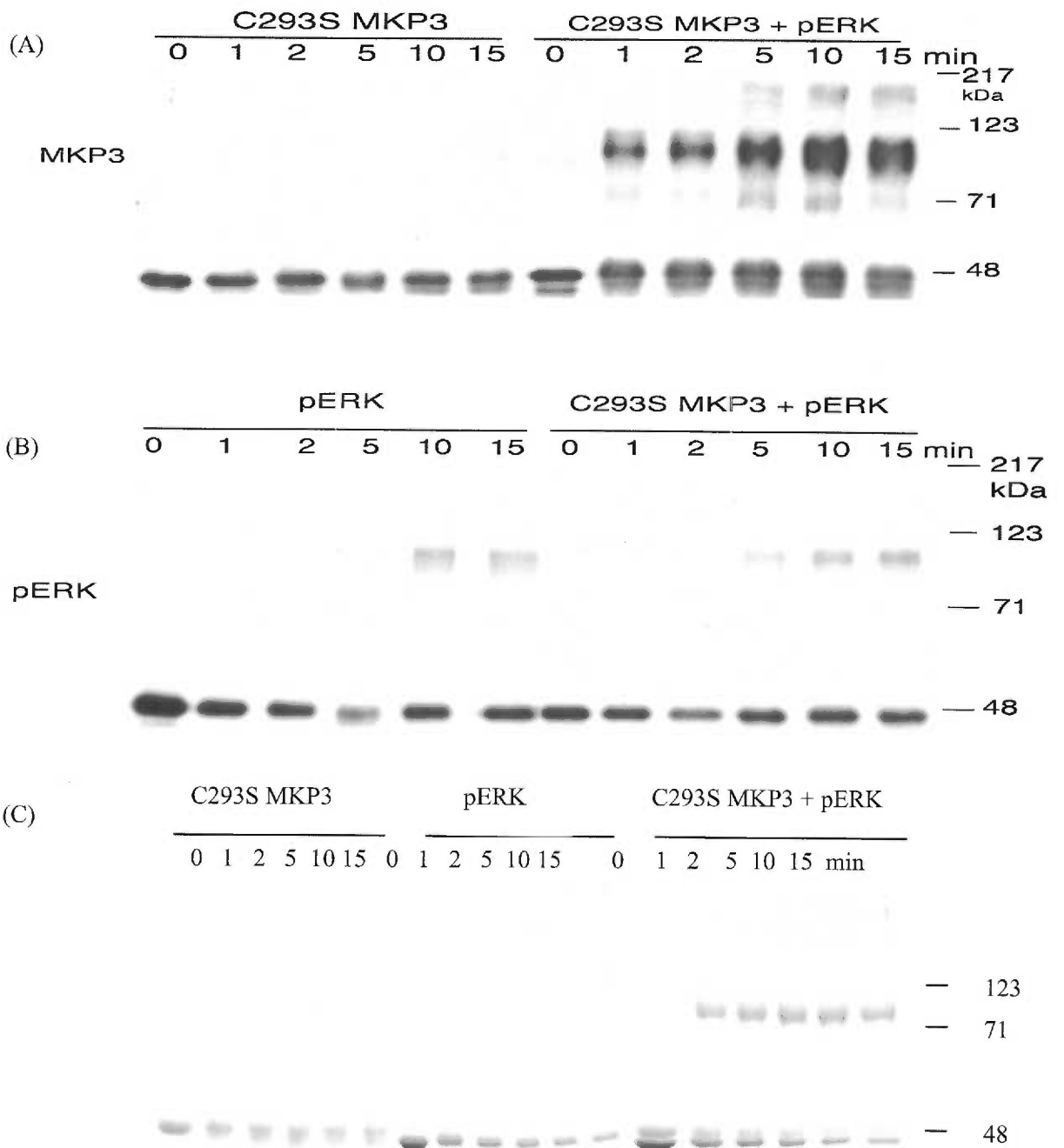


Figure 2. 10 Glutaraldehyde cross-linking of MKP3, ERK and the mixture of MKP3 and ERK. (A-B) MKP3 (8 μ M), ERK (8 μ M), or 1:1 mixture of MKP3 and ERK (8 μ M each) were cross-linked with 5 mM glutaraldehyde up to 15 min at 25 °C. The reactions were terminated by adding glycine (pH 9.0) at a final concentration of 0.2 mM. The cross-linked species were determined with SDS-PAGE and western blotting with appropriate antibodies. (C) Coomassie staining of SDS-PAGE of cross-linked species.

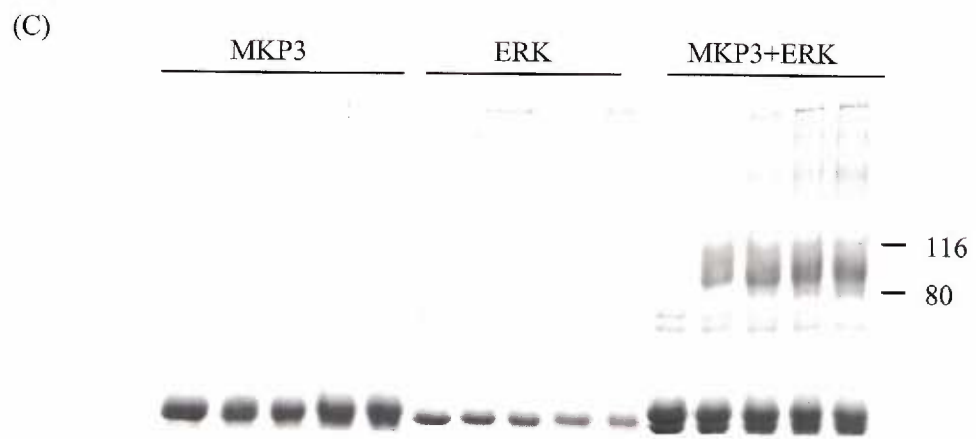
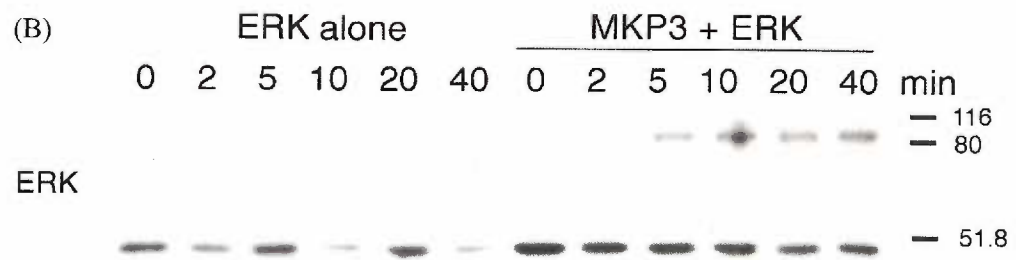
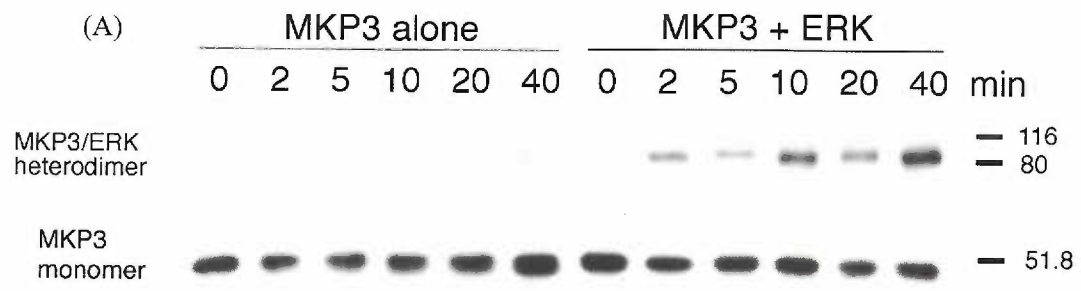


Figure 2. 11 Mobility differences in cross-linked species. ERK-MKP3, pERK-pERK, ERK-pERK cross-linked species were separated by SDS-PAGE and probed with antibody (polyclonal) that recognizes ERK.

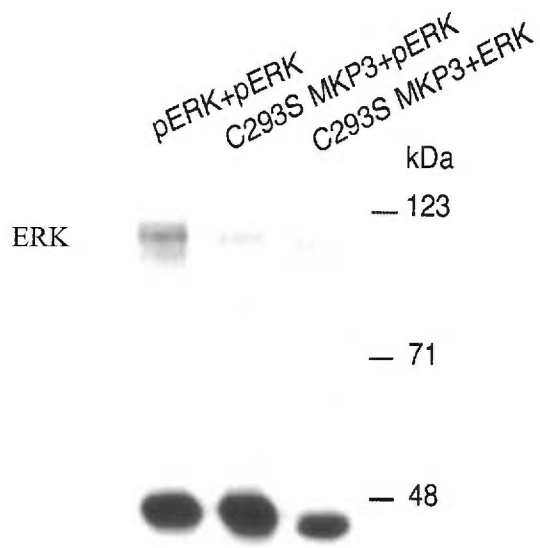


Figure 2. 12 Bis[sulfosuccinimidyl]suberate (BS³) cross-linking of MKP3, ERK, and the mixture of MKP3 and ERK. MKP3 (8 μ M), ERK (8 μ M), or 1:1 mixture of MKP3 and ERK (8 μ M each) were cross-linked with 0.2 mM up to 20 min at 25 °C. The reactions were terminated by adding glycine (pH 9.0) at a final concentration of 0.2 mM. The cross-linked species were determined with Coomassie staining of SDS-PAGE.

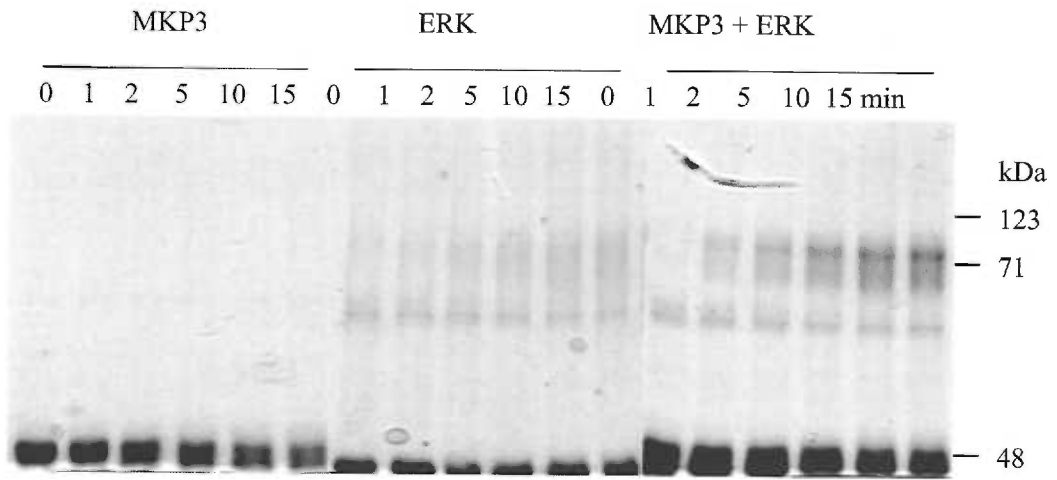


Figure 2. 13 Dephosphorylation of L4A H176E mutant pERK by MKP3. (A-B) Dissociation constants of wild type ERK and L4A H176E ERK to MKP3. The V/K values for *p*NPP hydrolysis at different ERK protein concentrations were measured and the concentration MKP3-bound ERK was determined as outlined in Methods. The bound ERK concentrations were plotted against free ERK concentration and the data were fitted to Eq. 4 to obtain the dissociation constant. Dissociation constants of wild type ERK and L4A H176E ERK to MKP3 were $0.27 \pm 0.06 \mu\text{M}$ and $0.20 \pm 0.07 \mu\text{M}$, respectively. These values are an average of three separate experiments. (C-D) Dephosphorylation of wild type and L4A H176E mutant pERK by MKP3. Recombinant wild type and L4A H176E mutant pERK at a final concentration of $1 \mu\text{M}$ were combined with $0.14 \mu\text{M}$ recombinant wild-type MKP3 in TBA, pH 7.0 and 25°C . The rate of dephosphorylation was measured using the integrated Michaelis-Menten equation including an inhibition constant term K_i (Eq. 3). V/K for wild type pERK dephosphorylation was $(3.1 \pm 1.9) \times 10^6 \text{M}^{-1}\text{s}^{-1}$ and that for the L4A H176E pERK dephosphorylation was $(0.88 \pm 0.23) \times 10^6 \text{M}^{-1}\text{s}^{-1}$. These values are an average of three separate experiments.

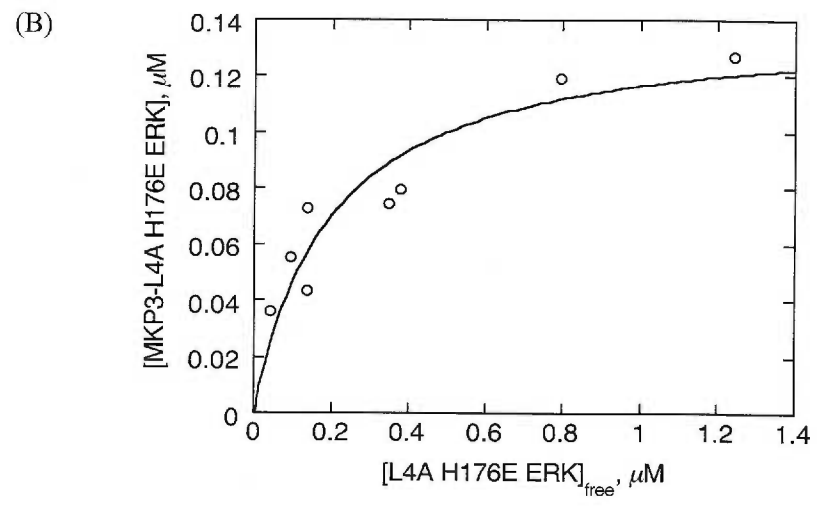
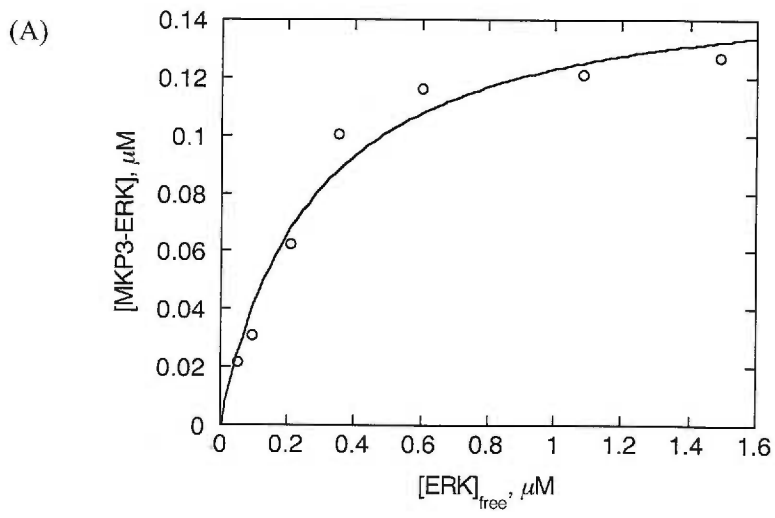
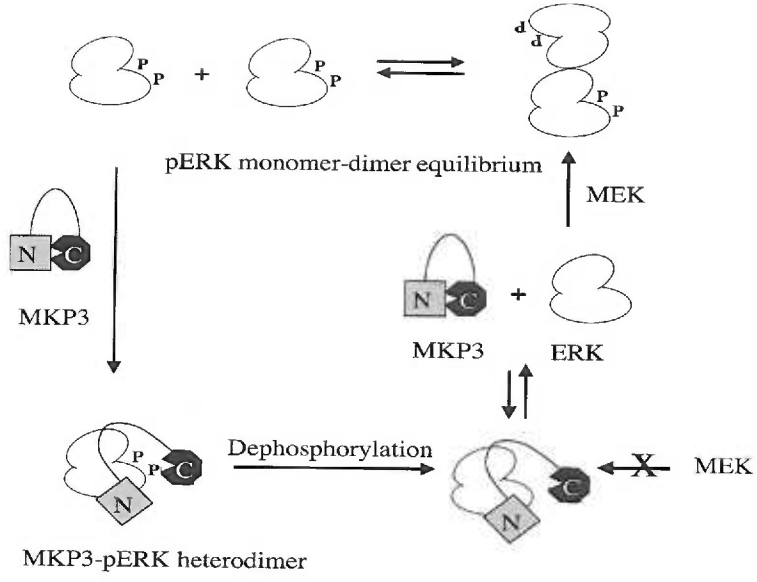


Fig 2. 14 Proposed model for pERK down-regulation involving the formation of a MKP3-pERK heterodimer and intramolecular dephosphorylation (see text for details).



Chapter 3

Probing the transition state structure of dual-specificity protein phosphatases using a physiological substrate mimic

(Submitted to *Biochemistry*, Apr 2004)

3.0 Preface

This chapter is a collaborative work between John Denu and Alvan Hengge (Utah State University) Labs. I performed the experiments in Figures 3.3, 3.4, 3.5, and inhibition studies with D92N VHR. Initial pH studies in Figure 3.4 were performed by Michael Jackson, a postdoc in Denu's Lab. Piotr K. Grzyska, a graduate student from Hengge's lab synthesized *m*NBP as shown in Figure 3.1 and 3.2, and determined isotope effects as shown in Table 3.1.

3.1 Introduction

Dual-specificity phosphatases (DSPs) constitute a large subfamily of the protein tyrosine phosphatases (PTPs). While PTPs dephosphorylate phosphotyrosine residues, DSPs efficiently dephosphorylate all three major types of phosphorylated residues found in eukaryotes: phosphoserine, phosphothreonine, and phosphotyrosine. Many DSPs downregulate mitogen activated protein kinases (MAPKs) by hydrolyzing phosphothreonine and phosphotyrosine residues within the activation loop TxY motif (94, 120). Although there is sparse sequence identity between the PTPs and DSPs, both families share a similar overall structure and general catalytic mechanism (14, 121). Utilizing the active-site motif HCxxGxxR(T/S) and a general acid catalyst (Asp), the general features of the mechanism involve the cysteine nucleophile attacking the phosphorus atom of a substrate to form a phosphoenzyme intermediate (Figure 1. 4) (15, 16). A general acid (conserved aspartic acid residue) donates a proton to the leaving group oxygen, releasing dephosphorylated substrate (40, 41, 122, 123). Subsequently, the cysteinyl-phosphate intermediate is hydrolyzed by a water molecule to generate inorganic phosphate.

Much of the detailed knowledge concerning the catalytic mechanism of PTPs and DSPs has been deduced from studies utilizing the artificial substrate *para*-nitrophenyl phosphate (*p*NPP) (Figure 3. 1). These studies included kinetic isotope effect (KIE) measurements to determine the transition-state structure for the initial phosphoryl transfer from substrate to enzyme. For the DSP VHR, and PTPs, YOP and PTP1, the measured KIEs for dephosphorylation of *p*NPP support a loose transition state with a large degree of bond cleavage to the leaving group, a metaphosphate-like structure of the transferring phosphoryl group, and very little bond formation to the nucleophile. These findings are similar to those of the uncatalyzed aqueous hydrolysis of the dianions of phosphate monoesters (44). For the enzymatic reactions with *p*NPP, KIEs in the leaving group are consistent with neutralization of charge in the transition state by proton transfer.

However, a fundamental question not addressed with the previous KIEs is how DSPs catalyze alkyl phosphate ester (phosphoserine/threonine) hydrolysis with similar efficiency to that of aryl phosphate esters, like *p*NPP or phosphotyrosine. For instance, VHR readily hydrolyzes aryl and alkyl phospho-monoesters whose reactivity (leaving group potential) can vary by as much as 9 orders of magnitude (124) (16). The common phosphatase substrate *p*NPP generates an excellent leaving group (*para*-nitrophenol) with a pK_a of 7.1, whereas phosphotyrosine and phosphoserine generate leaving groups with pK_a values of 10 and 14, respectively. How do DSPs compensate for the huge difference in reactivity based on leaving group pK_a ?

Because previous KIEs have been measured with *p*NPP, transition state information has been limited to aryl substrates with good leaving groups, ie. low pK_a . Recently, Grzyska *et al.* have used *m*-nitrobenzyl phosphate (*m*NBP, leaving group pK_a 14.9) to examine the transition-state structure for the solution hydrolysis reaction of this alkyl phosphate ester (125). The results for the hydrolysis of the monoanion of *m*NBP were most consistent with a pre-equilibrium proton transfer from the phosphoryl group to the ester oxygen atom, followed by rate-limiting P-O(R) bond fission. The transition state for *m*NBP hydrolysis (leaving group $pK_a = 14.9$) exhibits much less P-O(R) bond fission than the reaction of the more labile *p*NPP (leaving group $pK_a = 7.14$). This seemingly anti-Hammond behavior results from a weakening of the P-O(R) ester bond induced by protonation, an effect that calculations show to be much more pronounced for aryl phosphates than for alkyl phosphates (126).

To uncover differences in the transition state for the hydrolysis of aryl versus the alkyl esters by DSPs, we analyzed *m*-nitrobenzyl phosphate as substrate for human phosphatase VHR (*Vaccinia H1*-related), measured the KIEs and compared these results to those obtained previously for *p*NPP. Here, we demonstrate that VHR reacts with the dianionic form of *m*NBP. Previous pH analysis of the kinetic parameters showed that *p*NPP must be in the dianionic state for catalysis (41, 44). Compared to *p*NPP hydrolysis,

the value of the $^{18}(V/K)_{\text{bridge}}$ isotope effect is much smaller with *m*NBP indicating a much smaller degree of P-O bond fission in the transition state, the same trend observed in the uncatalyzed hydrolysis of the monoanion. While the enzyme utilizes the dianion form of the substrate, the mechanism shares the feature of proton transfer to the leaving group with the uncatalyzed monoanion hydrolysis. Lack of a normal isotope effect suggests that the VHR-catalyzed reaction may involve a discrete proton transfer step, from Asp-92 to the ester oxygen, preceding P-O(R) bond fission.

3.2 Materials and Methods

3.2.1 Materials

Alkaline phosphatase from chicken spleen was purchased from Sigma. Diethyl ether was used as purchased. The bis (cyclohexylammonium) salt of natural abundance, and isotopically labeled *m*-nitrobenzyl phosphate (*m*NBP) was synthesized as previously described (125), and *p*NPP was from Sigma as the disodium hexahydrate salt. VHR and D92N mutant were purified as previously described (41).

3.2.2 Assays

For the pH analysis, a three component buffer system consisting of 0.1 M acetate, 0.05 M Tris [tris(hydroxymethyl) aminomethane], and 0.05 M Bis-Tris [[bis(2-hydroxyethyl)imino] tris(hydroxymethyl)methane] was used to maintain a constant ionic strength throughout the pH range examined. All assays were performed at 25 °C. Assays using *p*NPP as a substrate were performed as described previously (41). The initial velocity of *m*NBP hydrolysis was measured using an inorganic phosphate detection assay described previously (127) with slight variation. Briefly, hydrolysis of *m*NBP (0 – 7 mM) was initiated by adding VHR (0.16 – 0.4 μM in 150 μL reaction volume), and the reaction was quenched with 850 μL of solution containing 1:6 ratio of 10 % ascorbic acid in H₂O and 0.42 % Ammonium Molybdate•4H₂O in 1 N H₂SO₄. The quenched reaction was incubated at 45 °C for 20 min and the release of phosphate by VHR was detected spectrophotometrically at 820 nm using a Shimadzu BioSpec-1601. The concentration of

released phosphate in the reaction was calculated based on a standard curve generated from known concentrations of free phosphate. The data were fitted to eq 3. 1 using the computer program Kaleidagraph (Abelbeck software). For the construction of the pH profiles, V/K values were determined at various pH values (pH 4.5 - pH 9.0), and the pH data were fitted to eq 3. 2 using Kaleidagraph (Abelbeck software). C is the pH-independent value of V/K , H is the proton concentration, and K_a , K_b , and K_c are the ionization constants of the groups involved in the reaction.

$$v = k_{\text{cat}}[E]_0 S / (S + K_m) \quad (3. 1)$$

$$v = C / [(1 + H/K_a)(1 + K_b/H)(1 + H/K_c)] \quad (3. 2)$$

3. 2. 3 Inhibition by *m*NBP

Using *p*NPP as substrate, the catalytic mutant of VHR (D92N) was used to measure an apparent inhibition constant for *m*NBP as a competitive inhibitor. At different concentrations of *m*NBP (0 – 6.0 mM), the initial velocities at fixed *p*NPP concentration (0.4 mM, low K_m condition) were measured as described previously (10). The apparent K_i was obtained using eq 3. 3.

$$v_{\text{inhibitor}} = v_{\text{no inhibitor}} / (1 + [I] / K_i) \quad (3. 3)$$

3. 2. 4 Isotope Effect Determinations

Figure 3.1 shows the substrate with the positions at which isotope effects were measured. ^{18}O Kinetic isotope effects were measured by isotope ratio mass spectrometry by the remote label method, using the nitrogen atom as a reporter for isotopic fractionation at the bridge or nonbridge oxygen atoms. The experimental procedures used to measure these isotope effects were similar to those previously reported to measure KIEs in phosphoryl transfer reactions in which the leaving group is *p*-nitrophenol (45).

The isotopic isomers of *m*-nitrobenzyl phosphate used for measurement of kinetic isotope effects are shown in Figure 3. 2. A mixture of isotopic isomers A and C was used for determination of $^{18}k_{\text{bridge}}$. Isomers B and C were mixed to reconstitute the natural abundance of ^{15}N and this mixture was used for determination of $^{18}k_{\text{nonbridge}}$. The isotopic abundance of the mixtures was determined by isotope ratio mass spectrometry. The unlabeled compound, containing the natural abundance of ^{15}N , was used to measure the ^{15}N isotope effect.

Isotope effects experiments were run at pH 6.0 and 7.15 using 0.2 M BisTris buffer containing 1mM DTT, at 30 °C. Temperature was maintained with a thermostatted heating block. The dicyclohexylammonium salt (43 mg) of the appropriate isotopically labeled form of the substrate was dissolved in 10ml of buffer that had been flushed with nitrogen for 30 min before reaction. Reactions were initiated by addition of 250 to 350 μL of enzyme (86 to 113 μM) and were monitored by ^{31}P NMR. After partial hydrolysis, reaction mixtures were extracted with diethyl ether four times (25mL) to separate the product *m*-nitrobenzyl alcohol. These ether layers were dried over magnesium sulfate and the ether removed by rotary evaporation. The *m*-nitrobenzyl alcohol was further purified by distillation at ~ 105 °C onto a cold finger apparatus before isotopic analysis by isotope ratio mass spectrometry using an ANCA-NT combustion system working in tandem with a Europa 20-20 isotope ratio mass spectrometer. The aqueous layer, containing the unreacted *m*-nitrobenzyl phosphate, was added to Tris buffer and brought to pH ~ 9 . About 1mg of commercial alkaline phosphatase was added to cleave the residual *m*-NBP. After more than 10 half-lives, this mixture was treated as described above to recover *m*-nitrobenzyl alcohol.

Isotope effects were calculated from the isotopic ratios at partial reaction in the product (*Rp*), in the residual substrate (*Rs*), and in the starting material (*Ro*).

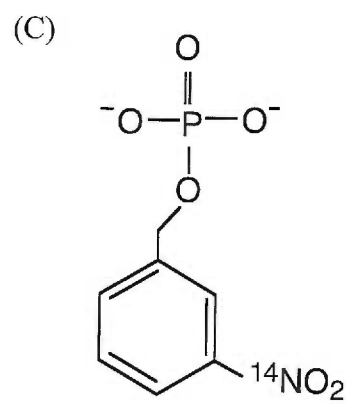
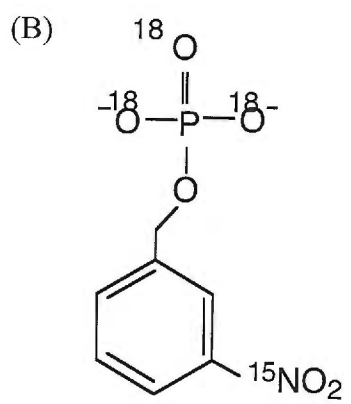
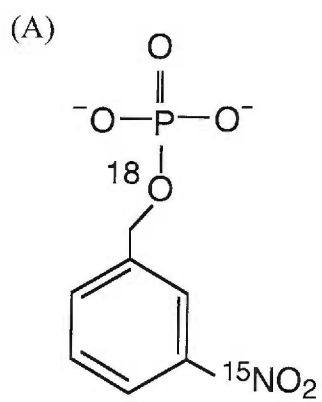
$$\text{KIE} = \log(1 - f) / \log[(1 - f)(\text{Rp}/\text{Ro})] \quad (3.4)$$

$$\text{KIE} = \log(1 - f) / \log[(1 - f)(R_s/R_o)] \quad (3.5)$$

Equations 3.4 and 3.5 were used to calculate the observed isotope effect either from R_p and R_o or from R_s and R_o , respectively, at the measured fraction of reaction. Experiments using natural abundance compound showed there is no measurable ^{15}N isotope effect. The ^{18}O isotope effects were corrected for levels of isotopic incorporation, as previously described (125). The independent calculation of each isotope effect using R_o and R_p and using R_o and R_s from eqs 4 and 5, respectively, provides an internal check of the results.

3.2.5 D_2O Solvent Isotope Effect

The V/K values were determined using a buffer consisting of 50 mM bis-tris in H_2O or D_2O . Buffer components were added directly to D_2O and the pD was adjusted with NaOD . Assays were performed as described for pH studies in Materials and Methods. The pD values were determined by adding 0.4 to the pH electrode reading (128).



3.3 Results & Discussion

First, we examined the ability of VHR to catalyze hydrolysis of the alkyl phosphate ester *m*NBP, with direct comparisons to *p*NPP as a substrate. Initial velocities as a function of *m*NBP concentration were measured, and from the resulting saturation curves (Figure 3. 3), the steady state kinetic constants were determined at pH 6. In spite of the difference of ~ 8 pK_a units between the leaving groups of *p*NPP ($pK_a = 7.1$) and *m*NBP ($pK_a = 14.9$), the V/K value with *m*NBP was only 2-fold lower than the value obtained with *p*NPP (Figure 3. 4). Similarly, the k_{cat} was ~ 2 -fold lower with *m*NBP compared with *p*NPP (Figure 3. 3).

In uncatalyzed hydrolysis reactions, the mono-anionic form of an alkyl phosphate is hydrolyzed much faster than the corresponding dianionic form. However, pH analyses of the V/K values showed that *p*NPP must be in the dianionic state for catalysis by PTPs (41, 44). To examine the formal possibility that similar catalytic efficiencies between *p*NPP and *m*NBP were due to a difference in the initial protonation state of the substrate, it was critical to determine whether the mono-anionic or dianionic form of *m*NBP was the catalytically reactive form. Using VHR and *m*NBP, the kinetic parameter V/K was determined as a function of pH. At each pH value, V/K values were determined by fitting initial velocities determined at varied [*m*NBP] to the Michaelis-Menten equation (eq 3. 1) as described in Materials and Methods. The data are presented in Figure 3. 4, along with the previously obtained pH profile for *p*NPP hydrolysis by VHR (41). Several data points with *p*NPP were re-performed to rule out any significant alterations that might arise from the use of different enzyme preparations. Within experimental error, the current data fell within the previously constructed V/K pH profile with *p*NPP. The pH profile with *m*NBP generated a curve that was very similar in overall shape to that of VHR using *p*NPP, where the plot rises with a slope of +2 on the acidic side and decreases with a slope of -1 on the basic side (Figure 3. 4). However, the *m*NBP pH profile is shifted significantly toward higher pH values on the acidic limb of the profile. Consistent

with previous interpretation, the plot indicates that two ionizable groups must be unprotonated, and one group must be protonated for optimal activity. From a previous analysis with *p*NPP (41), it was determined that two groups with pK_a values of 5.1 and 5.47 must be unprotonated, while a group with a pK_a value of 5.7 must be protonated for activity. The pK_a value of 5.1 represents pK_2 for the phosphate group of *p*NPP, and indicates that the dianion of *p*NPP is the reactive form of the substrate. The pK_a of 5.47 represents the catalytic cysteine (Cys-124) residue, and 5.7 represents the aspartic acid residue (Asp-92) of VHR (41).

When the substrate naphthylphosphate is employed instead of *p*NPP for the YOP PTP, a similar pH-dependent rate shift was observed, consistent with the difference expected from the second pK_a of the two substrates (129). The second pK_a of *m*NBP is 6.2 (125), compared with 5.1 for *p*NPP. This suggests that the shift in the profiles in the present study reflect a change in the pK_2 of the phosphate from 5.1 to 6.2.

To demonstrate that the shift in the *m*NBP pH profile was consistent with the pK_a difference between *p*NPP and *m*NBP, the *m*NBP data were fitted to eq 3. 2 using the previously determined values for Asp-92 ($pK_{as} = 5.7$; must be protonated) and Cys-124 ($pK_{a3} = 5.47$ Cys-124; must be unprotonated) (41). The pK_{a1} value for substrate and the *C* value were allowed to float in the analysis, yielding a pK_a value of 5.7 for the substrate ionization, and the pH independent value, *C*, of $12,600 \text{ M}^{-1} \text{ s}^{-1}$. The calculated kinetic pK_{a1} value of 5.7 is reasonably close to the thermodynamic pK_2 of *m*NBP determined as 6.2. Using the same type of fitting analysis for the *p*NPP data, a fit to eq 3. 2 yielded a pK_a value of 4.93, which is very similar to the pK_2 of *p*NPP determined as 5.1. The pH independent value *C* was $5730 \text{ M}^{-1} \text{ s}^{-1}$. Poor fits (Chi squared > 0.45 versus 0.2 for the above model) were obtained for alternative models involving one deprotonated group and two protonated groups, as well as one model involving one unprotonated and one protonated group. Moreover, if we assume a model that involves an unprotonated Asp-92 and the monoanion of substrate, the fit yields a pH-independent value for *m*NBP that

is 23-fold lower than that with *p*NPP. Given that the k_{cat} values are only ~2-fold different between the two substrates, which is similar to the difference in V/K observed from the fit used in Figure 3. 4, this is an unlikely model. Collectively, the pH studies suggest that VHR utilizes the dianionic forms of both *p*NPP and *m*NBP for catalysis.

The data presented above suggests that both *p*NPP and *m*NBP react with VHR as the dianion, and that the catalytic efficiency with alkyl esters did not appear to stem from a utilization of the monoanion over the dianion, as might be predicted from solution chemistry. From computational studies, it has been proposed that alkyl phosphates might be more likely to react via the monoanion form (130, 131), although another computational study by Asthagiri *et al.* favors the dianion and loose transition state pathway for PTP catalyzed phospho-enzyme intermediate formation (132). If the true substrate were the monoanion of *m*NBP, then it may be possible that the proton from the phosphoryl group in the monoanion is transferred to the leaving group, facilitating P-O bond cleavage. In this model, protonation of the leaving group by the general acid catalyst Asp-92 may be dispensable for activity when sufficient quantities of the monoanion of *m*NBP are present to compensate for loss of Asp-92. To test this possibility, we determine the ability of the catalytic mutant D92N of VHR (41) to hydrolyze *m*NBP. We attempted to obtain measurable rates of *m*NBP hydrolysis with D92N VHR using the phosphate detection assay as described in Materials and Methods. Although reasonable rates of hydrolysis were observed with *p*NPP, negligible reaction rates were measurable with *m*NBP, and due to the detection limitations of the assay, accurate values could not be obtained. Based on the sensitivity of the assay, we calculated an upper limit of $0.14 \times 10^{-4} \text{ s}^{-1}$ on the rate of *m*NBP hydrolysis by the D92N VHR mutant. The reaction rate with *m*NBP by this mutant was ~ 3.5 orders of magnitude slower than the value of 0.05 s^{-1} measured with *p*NPP. This value is consistent with that calculated from on the slope (β) from the Brønsted plot of the k_{cat} value for D92N as a function of leaving group $\text{p}K_{\text{a}}$ with a series of aryl phosphate esters (16). For the D92N

VHR mutant, the Brønsted slope of -0.5 ± 0.07 predicts a reduction in rate of ~ 3.9 orders of magnitude when the leaving group is changed from *p*-nitrophenol to *m*-nitrobenzyl alcohol. Together, these data support a critical role for the Asp-92 in protonating leaving groups with high pK_a values, like *m*NBP, and phosphoserine/threonine, as previous studies have implied for aryl ester substrates. These data are consistent with the dianion of both *p*NPP and *m*NBP as the catalyzed substrate.

The proposal that a phosphatase should prefer the monoanion form of its substrate is based on the fact that in uncatalyzed hydrolysis, the monoanion is more reactive than the dianion. However, this difference in reactivity arises from the ability of a proton to easily transfer intramolecularly from the phosphoryl group to the leaving group in the reaction of the monoanion, while in the dianion, the leaving group departs as the alkoxide. Interestingly, the phosphoryl group is fully deprotonated in the transition states of both the monoanion and dianion reactions. The basic elements that facilitate the uncatalyzed monoanion over the dianion reaction are present in the enzymatic reaction when a proton is available to protonate the leaving group. But, in the case of the enzymatic reaction, the aspartic acid within the active site supplies the proton that is transferred to the leaving group, obviating the need to obtain the proton from the monoanion.

The extremely slow turnover rate of D92N VHR toward *m*NBP allowed us to examine whether VHR exhibits differential binding between the two ionized forms of *m*NBP. This was accomplished by utilizing *m*NBP as a competitive inhibitor of the *p*NPP hydrolysis reaction catalyzed by D92N VHR. The inhibition constant (K_i) of *m*NBP was determined as described in Materials and Methods. The K_i of *m*NBP was 2.68 ± 0.51 and 2.76 ± 0.84 mM at pH 5.5 and pH 7.0, respectively. Using the Henderson-Hasselbach equation, it was determined at pH 5.5 *m*NBP is 17% in the dianion form, and 83% in the monoanion form, while at pH 7.0, 86% is in the dianion form and 14 % in the monoanion form. Despite the different ratios of dianion versus

monoanion at the different pH values, the K_i values were similar, indicating that both the mono- and dianionic forms of *m*NBP bind with the same affinity to the D92N VHR mutant. Although the D92N mutant shows no preference for binding the monoanion over the dianion of *m*NBP, the affinity might be expected to decrease in the wildtype enzyme when the carboxylate is anionic. We have shown previously that at pH values high enough to completely ionize Asp-92, the D92N mutant displays higher V/K values than wild type enzyme (41), likely due to the higher K_m values resulting from charge repulsion between the carboxylate and dianionic form of substrate. Collectively, the data are consistent with the enzyme's ability to bind both ionized forms of substrate, but only the dianion is utilized as a substrate in the hydrolysis reaction. This is borne out by the observations from the previous and current pH profiles (41), which exhibit this substrate ionization in the V/K profile, but not in the k_{cat} profile.

To probe the transition state structure for phosphoryl transfer from *m*NBP to VHR, kinetic isotope effects for the VHR-catalyzed reaction of *m*NBP were measured and compared with previous data using *p*-nitrophenyl phosphate (*p*NPP) (Table 3. 1). All of the isotope effects in this study were measured by the competitive method and therefore are isotope effects on V/K . Thus these KIEs are those for the phosphoryl transfer from the substrate to form the phosphoenzyme intermediate. Isotope effects were measured at the pH optimum of 6.0, and the value for $^{18}(V/K)_{nonbridge}$ was also measured at higher pH where the rate is slower. Because the nonbridge isotope effect is also sensitive to the protonation state of the substrate, the observed value differs, but should give the same value for $^{18}(V/K)_{nonbridge}$ after correction for the protonation state of the substrate, if chemistry is fully rate-limiting.

Because the second pK_a for *m*NBP was determined to be 6.2 (125), an equilibrium population of both the monoanion and dianion species are present at both pH values used in the isotope effect experiments. The known ^{18}O EIE for deprotonation of phosphate esters (1.015) (133) allows correction of the observed values of $^{18}(V/K)_{nonbridge}$ for this

fractionation. The proper correction requires an assumption as to whether the substrate for catalysis is the monoanion or the dianion. While the experimental evidence discussed above indicates that the substrate is the dianion, some computational arguments have been presented (130, 131), which suggest that the monoanion reaction is more likely for a more basic alkyl phosphate substrate. However, a recent computational argument favoring the dianion and a highly dissociative transition state have been presented (132). We have corrected the observed $^{18}(V/K)_{\text{nonbridge}}$ KIE in Table 3. 1 assuming both possibilities, in an effort to examine whether the data favor one case or the other, independent of the kinetic data supporting the notion that the reactive form of the substrate is the dianion, as discussed above.

In the generally accepted mechanism for the uncatalyzed hydrolysis of the monoanion of phosphate esters, the proton is transferred from the phosphoryl group to the leaving group in the transition state, or in a pre-equilibrium step. The $^{18}k_{\text{nonbridge}}$ for the hydrolysis of the monoanion of *m*NBP reflects the deprotonation of the phosphoryl group. By contrast, in reactions of the dianion of a phosphate ester, the $^{18}k_{\text{nonbridge}}$ is very small and inverse, reflecting the loose transition state involving no proton transfers to or from the phosphoryl group. Due to the extremely slow rate of the uncatalyzed hydrolysis of the dianions of alkyl phosphate esters (134), the KIEs for the reaction of the dianion of *m*-NBP could not be measured. Experimental evidence indicates that alkyl phosphate dianions undergo hydrolysis by a mechanism and transition state similar to aryl phosphates (134), and thus, the reaction of the dianion of *m*NBP would be expected to exhibit a small inverse $^{18}k_{\text{nonbridge}}$ similar to that for the dianion of *p*NPP (0.9994)(45).

Correction of the observed value of $^{18}(V/K)_{\text{nonbridge}}$, assuming the catalytically active species is the monoanion results in values of 1.0137 ± 0.0003 at pH 6.0, and 1.0144 ± 0.0006 at pH 7.15. Both values are very similar to that obtained for the hydrolysis of the monoanion in solution. Similarly, correction assuming the dianion is the reactive species results in very small inverse values, expected if the transition state is

loose, which is supported by prior experiments. Thus, the $^{18}(V/K)_{\text{nonbridge}}$ KIEs do not distinguish whether the monoanion or the dianion is the substrate. Although the KIEs cannot distinguish these two possibilities, the kinetic data described above strongly point to the dianion as the reactive form of the substrate. If the monoanion is the substrate, the similarity of $^{18}(V/K)_{\text{nonbridge}}$ to the full EIE for deprotonation indicates that this proton is essentially fully removed in the transition state (133). In this mechanistic scenario, the phosphoryl group of the substrate serves as the source of the proton that is transferred to the leaving group. However, the failure to observe a measurable rate of hydrolysis of *m*NBP with the D92N mutant indicates that it is this residue, and not the phosphoryl group of the substrate, that supplies the proton to the leaving group. It has been proposed that the carboxylate form of this residue merely provides stabilization of a bridge-protonated substrate (131). If such were the only role for this residue, and the proton source is the substrate, then one would expect a similar leaving group dependency in the D92N mutant as for the uncatalyzed reaction. However, the measured Brønsted slope of -0.5 is significantly larger than that for the uncatalyzed hydrolysis (-0.2 , (135)). Moreover, the monoanion as a substrate is also inconsistent with the pH-rate analysis that shows two groups must be deprotonated.

The $^{18}(V/K)_{\text{bridge}}$ KIE of 1.0004 is much smaller than that for the reaction using *p*NPP as the substrate, suggesting a much smaller degree of P-O bond fission in the transition state for the VHR-catalyzed reaction with *m*NBP compared to *p*NPP. It seems counterintuitive that a KIE at a position of bond fission in the *m*NBP reaction does not result in a significant normal value. This unexpected KIE difference is also observed in the uncatalyzed hydrolysis of the monoanions of these two esters, and can be explained by the relative contributions from the inverse isotope effect for protonation, and the normal one for P-O(R) bond fission. The difference between the values for *p*NPP and *m*NBP reveals differences arising from the timing of these events in the uncatalyzed hydrolysis (125), and perhaps in the enzymatic reaction as well.

In the reactions of both substrates, the observed $^{18}\text{O}_{\text{bridge}}$ is the product of that for P-O ester bond fission, and for protonation. In the case of pNPP, these maximal values are 1.034 and 0.985 respectively (45). The absence of a significant ^{15}N KIE indicates no charge on the leaving group in the transition state, which requires that proton transfer must be approximately as far advanced as P-O bond fission. Thus, the observed KIE will be the product $(1 + 0.034x) \times (1 - 0.015y)$, where x and y are the fractions of bond fission and protonation in the transition state. This is a simplification, since it assumes that the isotope effects will vary linearly with fractional bond orders. While the zero point energy factor will likely do so, the imaginary frequency factor will likely not, and the latter will probably be greater in an early transition state, for both the contribution from P-O fission and that from proton transfer. While only an approximation, this analysis gives a basis to place some general limits on possible transition states, and the synchronicity between proton transfer and P-O bond fission. To satisfy this criteria, and for protonation to not lag too far behind P-O fission, the normal $^{18}(\text{V}/\text{K})_{\text{bridge}}$ of 1.0118 requires that both P-O bond fission and protonation be well advanced (>50 %). In the case of mNBP, the leaving group is alkyl rather than aryl. Precedent for alkyl ^{18}O leaving group KIEs indicate the maximum value is higher. Leaving group ^{18}O kinetic isotope effect of up to 1.062 have been reported for the hydrazinolysis of methyl formate, when breakdown of the tetrahedral intermediate is rate-limiting (139). *Ab initio* calculations predict a similar maximum value for the alkyl phosphate, methyl phosphate (unpublished results). The isotope effect for protonation may be estimated from that for protonation of hydroxide, which is 0.96 (140). Thus, the observed $^{18}(\text{V}/\text{K})_{\text{bridge}}$ in the mNBP reaction will be approximated by the product $(1 + 0.06x) \times (1 - 0.04y)$, again, where x and y are the fractions of bond fission and protonation in the transition state. The negligible $^{18}(\text{V}/\text{K})_{\text{bridge}}$ observed (Table 1) requires that these two contributions cancel, which is only possible if protonation is ahead of P-O bond fission. If the reverse were true, or if both processes are equally progressed in the transition state, a normal $^{18}(\text{V}/\text{K})_{\text{bridge}}$ would result.

This is an unavoidable result of the fact that the isotope effect magnitude for P-O bond fission exceeds that of protonation, which is logical since the phosphoryl group involves bending and torsional modes not present in the phenol. For the same reason, ^{18}O fractionation factors between water and alcohols are 2 – 3 % normal.

Previously reported KIE results on the uncatalyzed hydrolysis of *m*NBP indicate a similar difference in P-O(R) bond fission between the aryl and alkyl phosphate ester substrates (125). In that case, a small inverse solvent isotope effect of 0.94 was observed, which was attributed to proton transfer occurring in a step before P-O ester bond fission. Could protonation of the ester oxygen atom also occur in a distinct step of the VHR-catalyzed reaction, rather than occurring simultaneously with P-O(R) bond fission? In such a scenario, proton transfer could occur from Asp-92, the reported general acid, and the resulting carboxyl group could stabilize the bridge-protonated form of the substrate.

To examine the possibility that protonation and P-O bond fission might be stepwise, or at least asynchronous with protonation ahead of P-O scission, the solvent deuterium isotope effect on V/K was measured for the VHR-catalyzed hydrolysis of *m*NBP. The classic general acid mechanism, which implies a proton in flight in the transition state of the rate-limiting step, predicts a normal solvent KIE. However, the reaction in which the transition state for proton transfer is either very early or late could result in a negligible solvent effect. In addition, a stepwise mechanism in which P-O bond fission is rate-limiting and occurs subsequent to proton transfer would exhibit only a fractionation factor, which, based on the data from the monoanion solution hydrolysis, would be inverse.

An important caveat is that solvent isotope effects on enzymatic reactions have been shown to be prone to artifacts resulting from viscosity effects, small global effects on structure, and pK_a shifts. To minimize such artifacts, we performed a pL (pD or pH)-dependent analysis of the solvent isotope effects on V/K , and compared these values between *p*NPP and *m*NBP. The V/K values for both *p*NPP (Figure 3. 5A) and *m*NBP

(Figure 3. 5B) were determined over a wide range in pL so that the maximum value could be easily ascertained from the pL profile, avoiding any differences in rates that were simply due to shifts in pK_a values between the two solvents. With *p*NPP, the solvent isotope effect $^D V/K$ was very small and slightly inverse at 0.92 ± 0.05 . However, with *m*NBP the $^D V/K$ value was large and inverse at 0.52 ± 0.07 . Both values were calculated from the peaks of the two plots (Figure 3. 5A & 3. 5B). Zhang *et al.* (124) reported a large inverse solvent effect using *p*NPP and VHR, and suggested a similar notion of a pre-equilibrium protonation of the ester oxygen. However, because their solvent effect was measured at a single pL value and by a different assay, it is difficult to compare their value with the values reported here. Our use of both *p*NPP and *m*NBP, as well as performing a complete pL dependence on the V/K values negates many, if not all, of the potential artifacts discussed above. These values indicate either a very early or late transition state for proton transfer, or a mechanism in which the proton is not in flight in the rate-limiting step, if proton transfer to the ester oxygen precedes P-O bond fission. Such very early or late transition states result in very small kinetic isotope effects that may be masked by fractionation factors to give an observed effect that can be inverse. An example is the acid-catalyzed hydrolysis of ortho esters, a reaction in which, like that under discussion here, involves protonation of the leaving group (141). The observed solvent KIE of 0.7 was ascribed to a KIE of near unity in a very late transition state for proton transfer from hydronium ion, and an inverse secondary isotope effect (141).

Interestingly, there is a significant difference in solvent effects between the two substrates in the enzymatic reaction (Figure 3. 5), while in the uncatlayzed hydrolysis of the monoanion, there is not (125). The different solvent KIEs between the two substrates might result from differences in the timing of proton transfer in the enzymatic reaction, such that in the *p*NPP reaction, a normal KIE component from proton transfer might partially offset the inverse effect from fractionation factors. In this scenario, proton transfer and P-O bond fission may be more closely coupled in the *p*NPP reaction, while

in the reaction of the more basic *m*NBP, protonation is ahead of P-O bond fission, which might be expected from the relative basicities of the two substrates. Alternatively, this difference might arise from stiffening of the torsional motion of the hydrogen/deuterium between aspartate and the bridge oxygen of substrate in the transition state. This stiffening would favor deuterium over hydrogen and would be more pronounced with *m*NBP, due to its greater basicity and the tightness of the resulting interaction. In support of this possibility, Cleland has reported that the fractionation factor of the S(H/D) of methanethiol shows a large dependence on the torsional force constant. In the phosphatase reaction, torsional restriction would have the advantage of keeping the proton in the correct position for reaction, which is essential for alkyl phosphoesters.

DSPs, as well as some PTPs, may allow for complementarity between leaving group lability, basicity of the ester oxygen and timing of proton transfer by aspartic acid, such that there is a continuum that falls between a stepwise and partially concerted mechanism for proton transfer and P-O cleavage, and ultimately, leads to similarity in the rates of ester hydrolysis. This basic idea was originally proposed by Kirby and co-workers in 1967 (135).

In summary, the results support an enzymatic mechanism that employs the dianionic form of *m*NBP as the substrate and where a proton donated by the general acid (Asp-92 in VHR) is transferred to the ester oxygen either in a step prior to significant P-O bond cleavage or in a concerted but asynchronous mechanism in which protonation is nearly complete in the transition state, and ahead of P-O bond fission (Figure 3. 6). The phosphoryl group is unprotonated in the transition state and the donated proton is fully transferred, or very nearly so, in the transition state for the reaction with both *p*NPP and *m*NBP (Figure 3. 6). Though the dianion is the enzymatic substrate, uncatalyzed monoanion hydrolysis shares the common feature of proton transfer to the leaving group, and the trend of less bond cleavage in the transition state of *m*NBP compared to that with *p*NPP. For uncatalyzed hydrolysis of the monoanions of *p*NPP and *m*NBP, protonation

of the bridge oxygen occurs in a pre-equilibrium step, weakening the P-O bond of the aryl ester to a greater extent than the alkyl phosphate. This leads to greater P-O bond fission in the transition state for hydrolysis of the aryl ester *p*NPP than that of the alkyl ester *m*NBP. Although protonation appears to weaken aryl phosphates more than alkyl phosphates, the higher basicity of the alkyl phosphates makes protonation more favorable, perhaps allowing the enzyme to better match leaving group potential with the timing of the proton transfer to the ester oxygen, such that diverse aryl and alkyl phosphoesters are turned over with similar catalytic efficiency.

3.4 Acknowledgement

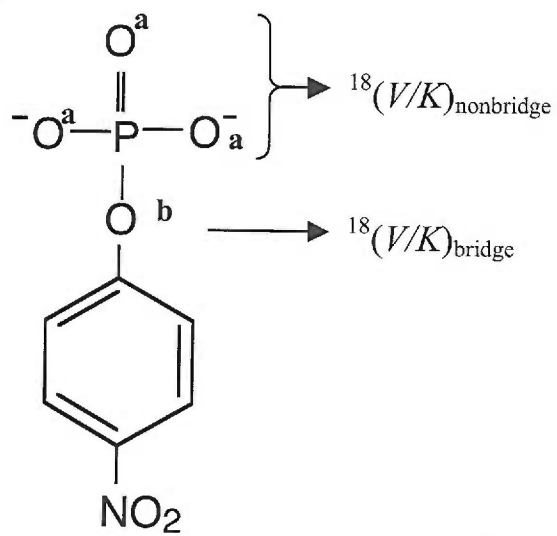
We thank W. W. Cleland for critical discussions.

Table 3. 1. Experimental values for $^{18}(V/K)_{\text{bridge}}$ and $^{18}(V/K)_{\text{nonbridge}}$. The standard errors are indicated in the last decimal place(s) in parentheses.

	$^{18}(V/K)_{\text{bridge}}$	$^{18}(V/K)_{\text{nonbridge}}$ (observed)	$^{18}(V/K)_{\text{nonbridge}}$ assuming the monoanion is the substrate	$^{18}(V/K)_{\text{nonbridge}}$ assuming the dianion is the substrate
<i>m</i> NBP VHR pH 6.0, 30°C	1.0004 (7)	1.0078 (3)	1.0137 (3)	0.9986 (3)
<i>m</i> NBP VHR pH 7.15, 30°C		1.0004 (6)	1.0141 (6)	0.9989 (6)
<i>m</i> NBP monoanion hydrolysis, pH 4.0, 115°C	0.9982 (7)	1.0149 (4)		
<i>p</i> NPP VHR pH 6, 30°C (44)	1.0118 (20)	1.0019 (3)	1.0156 (3)	1.0003 (3)
<i>p</i> NPP monoanion hydrolysis, pH 3.5, 95°C	1.0087 (3)	1.0184 (5)		

Figure 3. 1. The substrate (A) *p*-nitrophenyl phosphate (*p*NPP) and (B) *m*-nitrobenzyl phosphate (*m*NBP), showing the nomenclature for the positions at which isotope effects were measured. Nonbridging oxygen atoms are designated as a, the bridging oxygen as b.

(A)



(B)

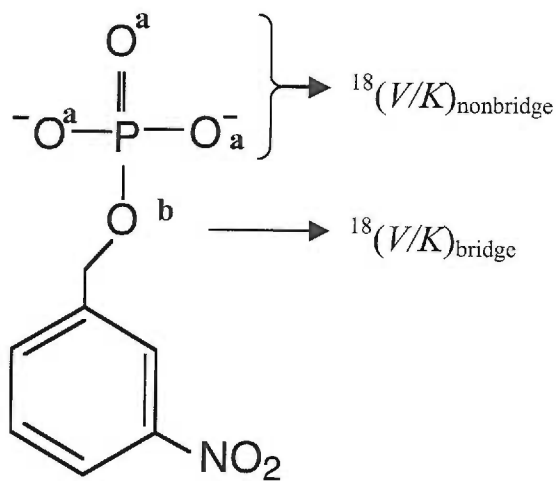


Figure 3. 2. Isotopic isomers synthesized for measurement of the bridge (A and C) and nonbridge (B and C) ^{18}O isotope effects.

Figure 3. 3. The initial velocities of *p*NPP (filled circles) and *m*NBP (open circles) hydrolysis by VHR. The initial velocities were measured at pH 6.0 at 25 °C using the phosphate detection assay as described in Materials and Methods. The solid line is a fit to the Michaelis-Menten equation.

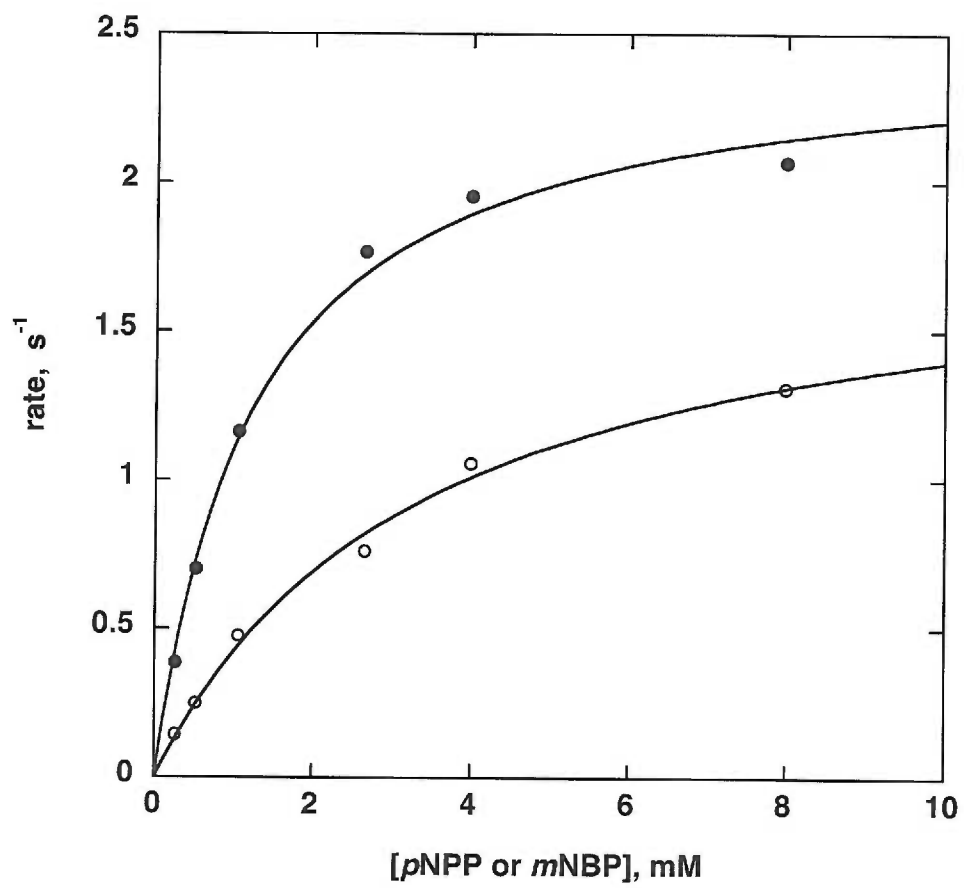


Figure 3. 4. pH dependency of the V/K value for VHR using p NPP and m NBP. The solid circles represent p NPP substrate and the open circles represent m NBP substrate. The p NPP data are from Denu *et al* (41). The data were fitted to eq 2. Assays were performed using TBA at 25 °C. See Materials and Methods for details. Results are summarized in the text.

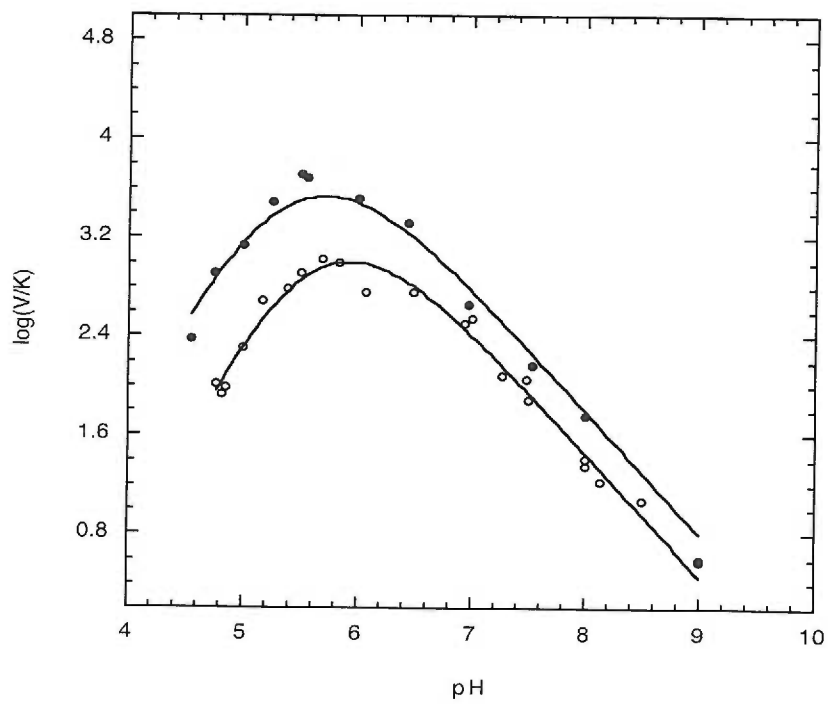
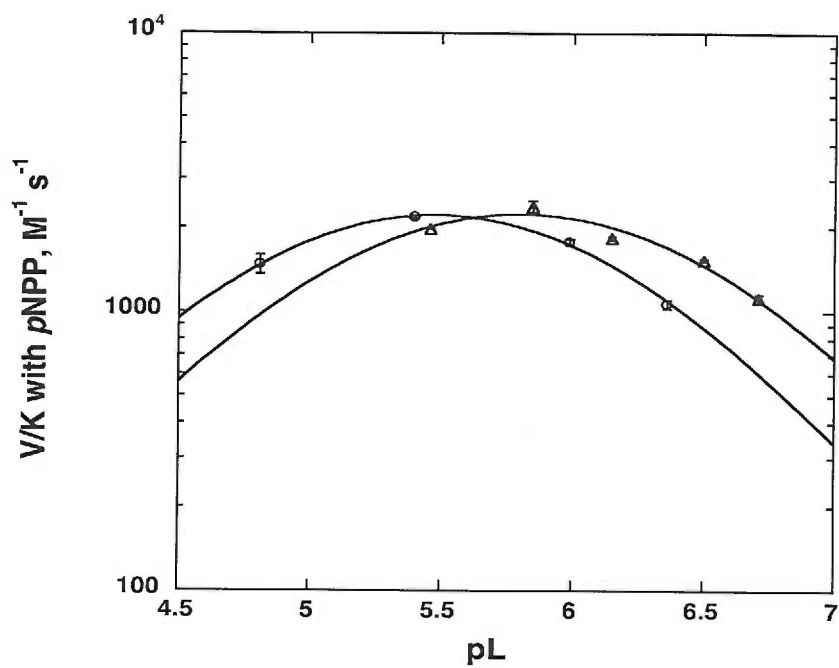


Figure 3. 5. Solvent kinetic isotope effects of VHR-catalyzed hydrolysis of (A) *p*NPP and (B) *m*NBP in H₂O (open circle) and D₂O (open triangle).

Hydrolyses of *p*NPP and *m*NBP were assayed in H₂O or D₂O consisting of 50 mM bis-tris from pL 4.5 to 7.5 at 25 °C. Error bars are standard deviations from no less than 3 separate determinations. Solid lines are the resulting fits to a bell-shape pH profile. See Materials and Methods for details.

(A)



(B)

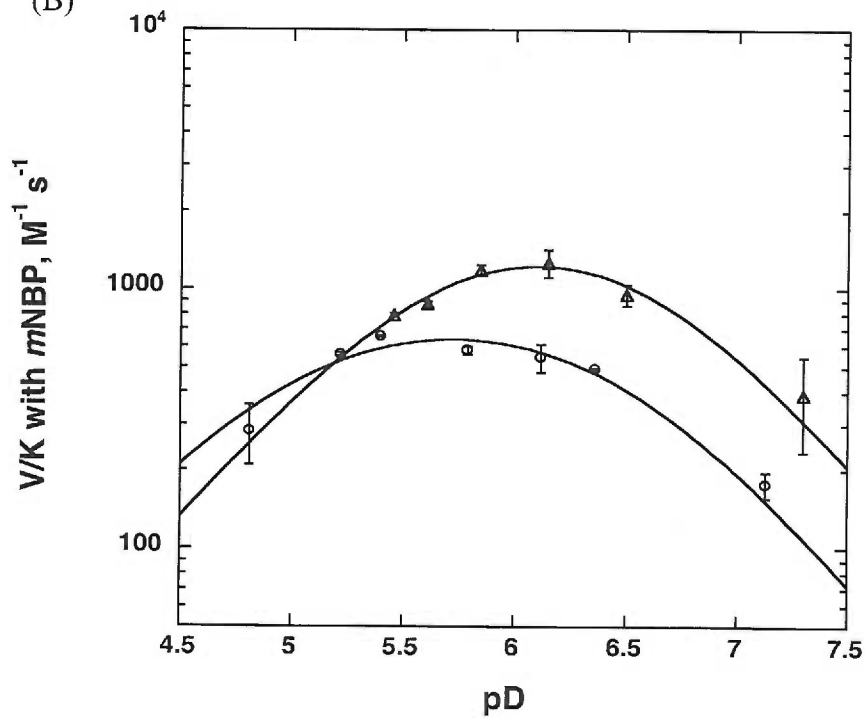
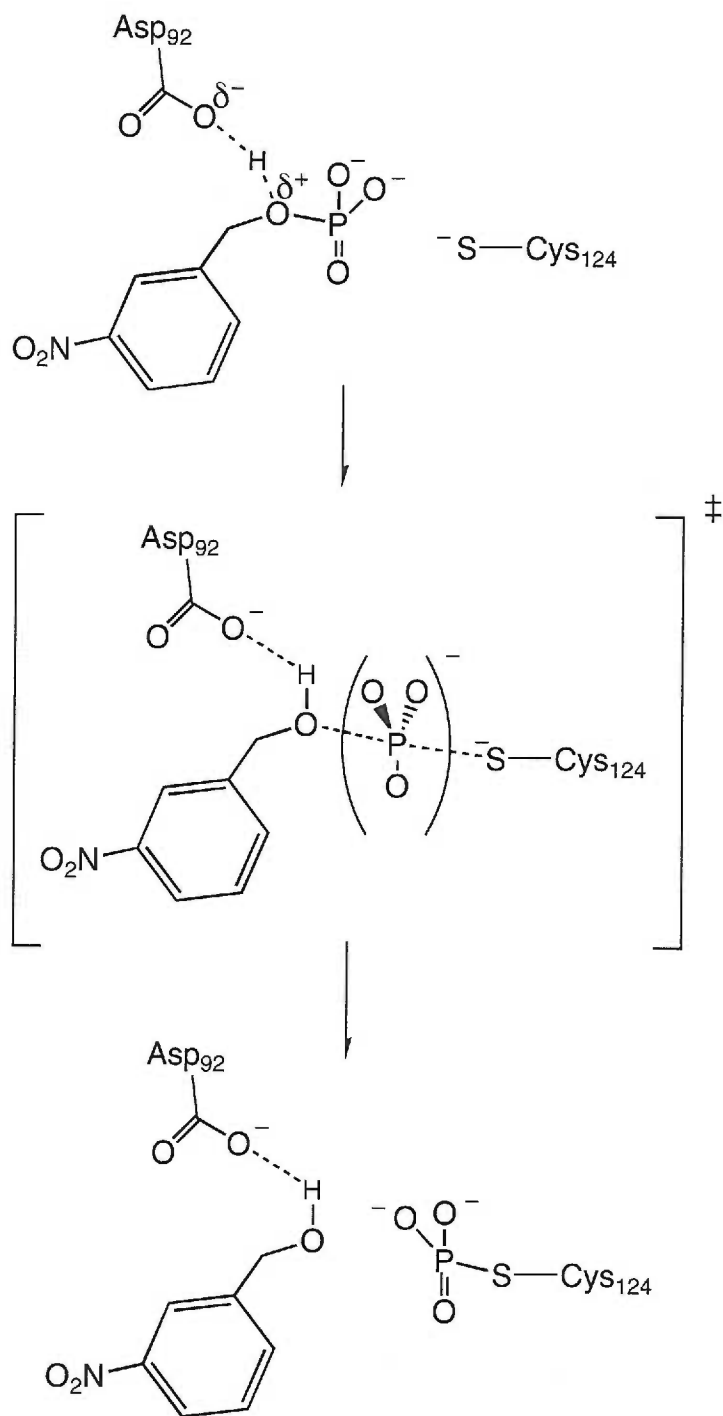


Figure 3. 6. Proposed transition state for VHR-catalyzed formation of the cysteinyl-phosphate enzyme intermediate from *m*NBP. Top figure shows an initial protonation step of the ester oxygen by Asp-92 (VHR numbering). Middle figure represents a highly dissociative (loose) transition state, where the P-O cleavage is nearly complete, and the proton is already transferred from Asp-92. Bottom figure shows the resulting phospho-enzyme intermediate generated from the nucleophile thiolate anion of Cys-124. Not pictured is the conserved Arg-133 which interacts with two oxygens of phosphate.



Chapter 4

Summary and Conclusions

We investigated the dephosphorylation mechanism of the dual-specificity phosphatases, MKP3 and VHR. Our goals were to elucidate the function of the N-terminal domain of MKP3 in the intramolecular dephosphorylation of pERK and to probe the transition state of VHR in dephosphorylation of *m*NBP. Both goals concern the reaction mechanisms of dual-specificity phosphatases with their physiological substrate or a substrate mimic.

4.1 Mechanism of pERK dephosphorylation by MKP3

The dual-specificity phosphatase MKP3 down-regulates mitogenic signaling by dephosphorylating ERK, an important enzyme in the MAP kinase signal transduction pathway. The mechanism of dephosphorylation by MKP3 has been studied with an artificial substrate, *p*NPP, as well as a physiological substrate, phosphorylated ERK (pERK). It has been shown that unphosphorylated ERK binding to the N-terminal domain of MKP3 increases the catalytic activity of MKP3 dramatically toward *p*NPP substrate. Without exogenous unphosphorylated ERK binding, *p*NPP dephosphorylation by MKP3 is very poor. On the other hand, MKP3 efficiently dephosphorylates pERK. While a great deal of work has addressed the catalytic mechanism of *p*NPP or pERK dephosphorylation by MKP3, the fundamental questions remain. Does MKP3 perform inter- or intramolecular dephosphorylation of pERK, and does the N-terminal domain of MKP3 have an important role in performing either type of dephosphorylation? The first question also addresses the stoichiometry of pERK:MKP3 complex.

Generation of an MKP3/VHR chimeric protein was an important strategy as we could eliminate the catalytic activation step as a necessary component for efficient dephosphorylation. The MKP3/VHR chimera displayed catalytic efficiencies that were similar to those of wild type VHR using *p*NPP as a substrate, and it was not activated upon binding of ERK to the N-terminal domain. This allowed us to evaluate the direct contribution of the N-terminal domain towards either inter- or intramolecular dephosphorylation of pERK. The ability of the MKP3/VHR chimera to dephosphorylate

pERK more efficiently than wild type VHR suggested that the N-terminal domain increases effective substrate concentration.

This observation led us to hypothesize that the pERK bound to the N-terminal domain of MKP3 is dephosphorylated by the catalytic domain of the same MKP3 molecule, which suggests an intramolecular dephosphorylation mechanism. In support of this, MKP3, when the N-terminal domain was occupied with unphosphorylated ERK, had almost no ability to dephosphorylate pERK. We used appropriate mutants of ERK in our studies. To make sure these mutants of ERK are structurally and functionally intact, we looked at their kinase activity as well as their ability to bind and activate MKP3. We determined the binding affinity of ERK proteins to MKP3 using both fluorescence anisotropy and an activation-based assay. We were the first group to show direct binding of ERK to MKP3 using the fluorescence anisotropy technique. Our data were consistent with an intramolecular dephosphorylation mechanism where pERK has to bind to the N-terminal domain of MKP3 to be effectively dephosphorylated by the catalytic domain of the same MKP3 molecule.

The stoichiometry of pERK bound to MKP3 was determined by chemical cross-linking using glutaraldehyde and bis[sulfosuccinimidyl]suberate. Coomassie staining and western analysis of the cross-linked species demonstrated that a monomer of MKP3 cross-linked with a monomer of pERK while MKP3 alone exists as a monomer and pERK alone exists in an equilibrium between dimeric and monomeric forms. Analytical ultracentrifugation performed in collaboration with Jeffery Hansen and Virgil Schirf at the University of Texas Health Science Center confirmed that MKP3 existed as a monomeric species with a calculated molecular weight of 41,347 kDa of a single ideal component. This was the first direct indication that MKP3 exists as a monomer. When MKP3 was combined with pERK, it produced a complex consistent with the molecular weight of a heterodimer. Consistent with the formation of a heterodimer complex

between MKP3 and pERK, MKP3 could dephosphorylate a dimerization-deficient mutant of pERK with a similar rate as wild type pERK.

In the above work, we determined the role of the N-terminal domain of MKP3 in intra- or intermolecular dephosphorylation of pERK and the stoichiometry of pERK bound to MKP3. We found that the N-terminal domain of MKP3 increases the effective substrate concentration in an intramolecular dephosphorylation reaction and that a monomer of MKP3 dephosphorylates a monomer of pERK in a heterodimeric Michaelis complex. From our findings, we propose that MKP3 binds to and dephosphorylates a monomer of pERK, pushing the equilibrium of pERK to a monomeric state. By forming a tight heterodimer complex, MKP3 could possibly prevent further activation of ERK by the upstream kinase MEK (see Figure 2. 14).

The questions remaining to be addressed from our studies are as follows. Since pERK exists in a dynamic equilibrium between monomer and dimer, it is difficult to distinguish whether MKP3 dephosphorylates a monomeric or dimeric form of pERK. Although we showed that MKP3 forms a heterodimer complex with a monomer of pERK and is able to dephosphorylate a dimerization-deficient mutant of pERK with a similar rate as wild type pERK, it does not rule out the possibility of MKP3 dephosphorylating a dimeric form of pERK. Generation of a chemically cross-linked or a genetically fused pERK dimer that is stable and functional would be useful in answering the above question. From our initial molecular modeling using available x-ray/NMR structures of VHR, pERK, the N-terminal domain of MKP3, and the C-terminal domain of MKP3, the linker and the N-terminal regions of MKP3 appear to overlap with the dimerization domain in pERK. Therefore, the interaction between MKP3 and pERK could possibly disrupt pERK dimer formation if MKP3 and pERK associate with higher affinity than that for pERK dimerization. Determining the regions in MKP3 that interact with pERK in a heterodimer complex as well as determining the K_d for pERK binding to MKP3 would be informative. Disruption of the pERK dimer might be another way of down-

regulating the mitogenic pathway by preventing ERK translocation to the nucleus since dimer formation is required for the nuclear translocation. In other studies, Zhao *et al.* (88) proposed the sequence of pERK dephosphorylation by MKP3 to be distributive, where MKP3 dissociates after first dephosphorylating the phosphotyrosine residue in pERK; however, further investigations are necessary to certainly rule out a processive mechanism since the question of simple dissociation of MKP3 from singly phosphorylated ERK is not addressed. In relation to this question, the order of dephosphorylation, that is, which one of the phosphotyrosine or phosphothreonine is dephosphorylated first needs to be examined.

4. 2 Transition state structure of VHR using a physiological substrate mimic (*m*NBP)

VHR was able to catalyze hydrolysis of *p*NPP (aryl phosphate ester) and *m*NBP (alkyl phosphate ester) with similar V/K values, although the leaving group pK_a values of the substrates differ by ~ 8 orders of magnitude. A pH analysis using the parameter V/K revealed similar pH profiles for both substrates, suggesting that VHR uses the dianionic forms of both *p*NPP and *m*NBP for catalysis. The observed shift in the *m*NBP pH profile was consistent with the pK_a difference between *p*NPP and *m*NBP (5.1 versus 6.2, respectively).

We could not measure rates of *m*NBP hydrolysis with the general acid VHR mutant D92N, indicating that aspartic acid is indispensable for protonating leaving groups with high pK_a values, and that the proton transferred to the leaving group is not coming from the *m*NBP substrate, which could have been predicted if the true substrate were the monoanion of phosphate. The D92N VHR mutant allowed us to examine whether VHR exhibits differential binding to mono- or dianionic forms of *m*NBP. At different pH values, that is, at different ratios of dianion versus monoanion, inhibition constants (K_i) of *m*NBP were similar, indicating that both forms of *m*NBP bind with the same affinity to D92N VHR.

Although the pH profile studies support the dianionic form of *m*NBP as substrate for VHR, we measured $^{18}(\text{V}/\text{K})_{\text{bridge}}$ KIEs with *m*NBP to probe the transition state structure for VHR using this substrate mimic. The measured $^{18}(\text{V}/\text{K})_{\text{bridge}}$ KIEs in the scissile bond in *m*NBP demonstrated less bond cleavage in the transition state compared to *p*NPP, a more labile substrate. Uncatalyzed hydrolysis of the monoanions of *p*NPP and *m*NBP also showed the same trend in KIE indicating that the protonation of the bridge oxygen occurs before P-O bond cleavage, weakening the P-O bond of the *m*NBP more than the *p*NPP. A large inverse isotope effect with *m*NBP in the VHR-catalyzed reaction supported protonation of the bridge oxygen by the conserved Asp-92 prior to P-O bond cleavage.

Our results demonstrated that the dianionic form of *m*NBP is employed as the substrate, and a proton from Asp-92 in VHR is transferred to the ester oxygen prior to P-O bond cleavage. Though the dianion is the enzymatic substrate, uncatalyzed monoanion hydrolysis also shares the common feature of proton transfer and P-O bond cleavage. Uncatalyzed hydrolysis of the monoanions of *p*NPP and *m*NBP revealed that protonation of the bridge oxygen weakens P-O bond of aryl phosphates such as *p*NPP more than that of alkyl phosphates such as *m*NBP. Yet, VHR displays a similar catalytic efficiency for diverse aryl and alkyl phosphoesters. This might be due to the higher basicity of the alkyl phosphates making protonation by Asp-92 of VHR more favorable, which could allow the enzyme to complement differences in leaving group $\text{p}K_{\text{a}}$ s of the substrates.

REFERENCES

1. Johnson, G.L. and R. Lapadat (2002) Mitogen-activated protein kinase pathways mediated by ERK, JNK, and p38 protein kinases, *Science* 298(5600) 1911-2.
2. Pouyssegur, J., V. Volmat, and P. Lenormand (2002) Fidelity and spatio-temporal control in MAP kinase (ERKs) signalling, *Biochem Pharmacol* 64(5-6) 755-63.
3. Pearson, G., et al. (2001) Mitogen-activated protein (MAP) kinase pathways: regulation and physiological functions, *Endocr Rev* 22(2) 153-83.
4. Egloff, M.P., et al. (1995) Crystal structure of the catalytic subunit of human protein phosphatase 1 and its complex with tungstate, *J Mol Biol* 254(5) 942-59.
5. Goldberg, J., et al. (1995) Three-dimensional structure of the catalytic subunit of protein serine/threonine phosphatase-1, *Nature* 376(6543) 745-53.
6. Griffith, J.P., et al. (1995) X-ray structure of calcineurin inhibited by the immunophilin-immunosuppressant FKBP12-FK506 complex, *Cell* 82(3) 507-22.
7. Kissinger, C.R., et al. (1995) Crystal structures of human calcineurin and the human FKBP12-FK506-calcineurin complex, *Nature* 378(6557) 641-4.
8. Mueller, E.G., et al. (1993) Purple acid phosphatase: a diiron enzyme that catalyzes a direct phospho group transfer to water, *J. Am. chem. Soc.* 115 2974-2975.
9. Martin, B.L. and D.J. Graves (1994) Isotope effects on the mechanism of calcineurin catalysis: kinetic solvent isotope and isotope exchange studies, *Biochim Biophys Acta* 1206(1) 136-42.
10. Wang, X.H., R. Y. N.; Whiting, A. K.; Que, L., Jr. (1999) Spectroscopic Characterization of a Ternary Phosphatase-Substrate-Fluoride Complex. Mechanistic Implications for Dinuclear Hydrolases, *J. Am. chem. Soc.* 121 9235-9236.

11. Williams, N.H., W. Cheung, and J. Chin (1998) Reactivity of Phosphate Diesters Doubly Coordinated to a Dinuclear Cobalt(III) Complex: Dependence of the reactivity on the basicity of the leaving group, *J. Am. chem. Soc.* 120 8079-8087.
12. Barford, D., A.K. Das, and M.P. Egloff (1998) The structure and mechanism of protein phosphatases: insights into catalysis and regulation, *Annu Rev Biophys Biomol Struct* 27 133-64.
13. Burke, T.R., Zhang, Z.-Y. (1998) Protein-tyrosine phosphatases: structure, mechanism, and inhibitor discovery., *Biopoly* 47 225-241.
14. Denu, J.M. and J.E. Dixon (1998) Protein tyrosine phosphatases: mechanisms of catalysis and regulation, *Curr Opin Chem Biol* 2(5) 633-41.
15. Pannifer, A.D., et al. (1998) Visualization of the cysteinyl-phosphate intermediate of a protein- tyrosine phosphatase by x-ray crystallography, *J Biol Chem* 273(17) 10454-62.
16. Denu, J.M., et al. (1996) Visualization of intermediate and transition-state structures in protein-tyrosine phosphatase catalysis, *Proc Natl Acad Sci U S A* 93(6) 2493-8.
17. Cho, H., et al. (1992) Isolation and structural elucidation of a novel phosphocysteine intermediate in the LAR protein tyrosine phosphatase enzymic pathway, *J. Am. chem. Soc.* 114 7296-7298.
18. Reynolds, R.A., et al. (1999) Crystal structure of the catalytic subunit of Cdc25B required for G2/M phase transition of the cell cycle, *J Mol Biol* 293(3) 559-68.
19. Fauman, E.B., et al. (1998) Crystal structure of the catalytic domain of the human cell cycle control phosphatase, Cdc25A, *Cell* 93(4) 617-25.
20. Rudolph, J. (2002) Catalytic mechanism of Cdc25, *Biochemistry* 41(49) 14613-23.
21. Coleman, J.E. (1992) Structure and mechanism of alkaline phosphatase, *Annu Rev Biophys Biomol Struct* 21 441-83.

22. Holtz, K.M. and E.R. Kantrowitz (1999) The mechanism of the alkaline phosphatase reaction: insights from NMR, crystallography and site-specific mutagenesis, *FEBS Lett* 462(1-2) 7-11.
23. Klabunde, T., et al. (1996) Mechanism of Fe(III)-Zn(II) purple acid phosphatase based on crystal structures, *J Mol Biol* 259(4) 737-48.
24. Klabunde, T. and B. Krebs (1997) The Dimetal Center in Purple Acid Phosphatases, *Structure & Bonding* 89 177-198.
25. Schwartz, J.H. and F. Lipmann (1961) Phosphate incorporation into alkaline phosphatase of E. coli, *Proc Natl Acad Sci U S A* 47 1996-2005.
26. Consortium, I.H.G.S. (2001) Initial sequencing and analysis of the human genome., *Nature* 409 860-921.
27. Ishibashi, T., et al. (1992) Expression cloning of a human dual-specificity phosphatase, *Proc Natl Acad Sci U S A* 89(24) 12170-4.
28. Guan, K.L., S.S. Broyles, and J.E. Dixon (1991) A Tyr/Ser protein phosphatase encoded by vaccinia virus, *Nature* 350(6316) 359-62.
29. Todd, J.L., K.G. Tanner, and J.M. Denu (1999) Extracellular regulated kinases (ERK) 1 and ERK2 are authentic substrates for the dual-specificity protein-tyrosine phosphatase VHR. A novel role in down-regulating the ERK pathway, *J Biol Chem* 274(19) 13271-80.
30. Todd, J.L., et al. (2002) Dual-specificity protein tyrosine phosphatase VHR down-regulates c-Jun N-terminal kinase (JNK), *Oncogene* 21(16) 2573-83.
31. Yuvaniyama, J., et al. (1996) Crystal structure of the dual specificity protein phosphatase VHR, *Science* 272(5266) 1328-31.
32. Barford, D., A.J. Flint, and N.K. Tonks (1994) Crystal structure of human protein tyrosine phosphatase 1B, *Science* 263(5152) 1397-404.
33. Jia, Z., et al. (1995) Structural basis for phosphotyrosine peptide recognition by protein tyrosine phosphatase 1B, *Science* 268(5218) 1754-8.

34. Stuckey, J.A., et al. (1994) Crystal structure of Yersinia protein tyrosine phosphatase at 2.5 Å and the complex with tungstate, *Nature* 370(6490) 571-5.
35. Schubert, H.L., et al. (1995) A ligand-induced conformational change in the Yersinia protein tyrosine phosphatase, *Protein Sci* 4(9) 1904-13.
36. Salmeen, A., et al. (2000) Molecular basis for the dephosphorylation of the activation segment of the insulin receptor by protein tyrosine phosphatase 1B, *Mol Cell* 6(6) 1401-12.
37. Schumacher, M.A., et al. (2002) Structural basis for the recognition of a bisphosphorylated MAP kinase peptide by human VHR protein Phosphatase, *Biochemistry* 41(9) 3009-17.
38. Lee, J.O., et al. (1999) Crystal structure of the PTEN tumor suppressor: implications for its phosphoinositide phosphatase activity and membrane association, *Cell* 99(3) 323-34.
39. Maehama, T. and J.E. Dixon (1998) The tumor suppressor, PTEN/MMAC1, dephosphorylates the lipid second messenger, phosphatidylinositol 3,4,5-trisphosphate, *J Biol Chem* 273(22) 13375-8.
40. Denu, J.M. and J.E. Dixon (1995) A catalytic mechanism for the dual-specific phosphatases, *Proc Natl Acad Sci U S A* 92(13) 5910-4.
41. Denu, J.M., et al. (1995) The catalytic role of aspartic acid-92 in a human dual-specific protein- tyrosine-phosphatase, *Biochemistry* 34(10) 3396-403.
42. Fjeld, C.C., et al. (2000) Mechanistic basis for catalytic activation of mitogen-activated protein kinase phosphatase 3 by extracellular signal-regulated kinase, *J Biol Chem* 275(10) 6749-57.
43. Hoff, R.H., et al. (2000) Effects on general acid catalysis from mutations of the invariant tryptophan and arginine residues in the protein tyrosine phosphatase from Yersinia, *Biochemistry* 39(1) 46-54.

44. Hengge, A.C., J.M. Denu, and J.E. Dixon (1996) Transition-state structures for the native dual-specific phosphatase VHR and D92N and S131A mutants. Contributions to the driving force for catalysis, *Biochemistry* 35(22) 7084-92.
45. Hengge, A.C. (2002) Isotope effects in the study of phosphoryl and sulfuryl transfer reactions, *Acc Chem Res* 35(2) 105-12.
46. Denu, J.M. and K.G. Tanner (1998) Specific and reversible inactivation of protein tyrosine phosphatases by hydrogen peroxide: evidence for a sulfenic acid intermediate and implications for redox regulation, *Biochemistry* 37(16) 5633-42.
47. Denu, J.M. and K.G. Tanner (2002) Redox regulation of protein tyrosine phosphatases by hydrogen peroxide: detecting sulfenic acid intermediates and examining reversible inactivation, *Methods Enzymol* 348 297-305.
48. Lee, S.R., et al. (1998) Reversible inactivation of protein-tyrosine phosphatase 1B in A431 cells stimulated with epidermal growth factor, *J Biol Chem* 273(25) 15366-72.
49. Meng, T.C., T. Fukada, and N.K. Tonks (2002) Reversible oxidation and inactivation of protein tyrosine phosphatases in vivo, *Mol Cell* 9(2) 387-99.
50. Leslie, N.R., et al. (2003) Redox regulation of PI 3-kinase signalling via inactivation of PTEN, *Embo J* 22(20) 5501-10.
51. Salmeen, A., et al. (2003) Redox regulation of protein tyrosine phosphatase 1B involves a sulphenyl-amide intermediate, *Nature* 423(6941) 769-73.
52. Savitsky, P.A. and T. Finkel (2002) Redox regulation of Cdc25C, *J Biol Chem* 277(23) 20535-40.
53. Xu, D., Rovira, II, and T. Finkel (2002) Oxidants painting the cysteine chapel: redox regulation of PTPs, *Dev Cell* 2(3) 251-2.
54. Finkel, T. (2000) Redox-dependent signal transduction, *FEBS Lett* 476(1-2) 52-4.
55. Finkel, T. (2003) Oxidant signals and oxidative stress, *Curr Opin Cell Biol* 15(2) 247-54.

56. Mourey, R.J., et al. (1996) A novel cytoplasmic dual specificity protein tyrosine phosphatase implicated in muscle and neuronal differentiation, *J Biol Chem* 271(7) 3795-802.
57. Muda, M., et al. (1996) MKP-3, a novel cytosolic protein-tyrosine phosphatase that exemplifies a new class of mitogen-activated protein kinase phosphatase, *J Biol Chem* 271(8) 4319-26.
58. Groom, L.A., et al. (1996) Differential regulation of the MAP, SAP and RK/p38 kinases by Pyst1, a novel cytosolic dual-specificity phosphatase, *Embo J* 15(14) 3621-32.
59. Camps, M., et al. (1998) Induction of the mitogen-activated protein kinase phosphatase MKP3 by nerve growth factor in differentiating PC12, *FEBS Lett* 425(2) 271-6.
60. Muda, M., et al. (1996) The dual specificity phosphatases M3/6 and MKP-3 are highly selective for inactivation of distinct mitogen-activated protein kinases, *J Biol Chem* 271(44) 27205-8.
61. Dowd, S., A.A. Sneddon, and S.M. Keyse (1998) Isolation of the human genes encoding the pyst1 and Pyst2 phosphatases: characterisation of Pyst2 as a cytosolic dual-specificity MAP kinase phosphatase and its catalytic activation by both MAP and SAP kinases, *J Cell Sci* 111(Pt 22)) 3389-99.
62. Keyse, S.M. and E.A. Emslie (1992) Oxidative stress and heat shock induce a human gene encoding a protein- tyrosine phosphatase, *Nature* 359(6396) 644-7.
63. Guan, K.L. and E. Butch (1995) Isolation and characterization of a novel dual specific phosphatase, HVH2, which selectively dephosphorylates the mitogen-activated protein kinase, *J Biol Chem* 270(13) 7197-203.
64. Rohan, P.J., et al. (1993) PAC-1: a mitogen-induced nuclear protein tyrosine phosphatase, *Science* 259(5102) 1763-6.

65. Ishibashi, T., et al. (1994) A novel dual specificity phosphatase induced by serum stimulation and heat shock, *J Biol Chem* 269(47) 29897-902.
66. Keyse, S.M. and M. Ginsburg (1993) Amino acid sequence similarity between CL100, a dual-specificity MAP kinase phosphatase and cdc25, *Trends Biochem Sci* 18(10) 377-8.
67. Kwak, S.P., et al. (1994) Isolation and characterization of a human dual specificity protein- tyrosine phosphatase gene, *J Biol Chem* 269(5) 3596-604.
68. Millar, J.B. and P. Russell (1992) The cdc25 M-phase inducer: an unconventional protein phosphatase, *Cell* 68(3) 407-10.
69. Wiland, A.M., et al. (1996) Purification and kinetic characterization of the mitogen-activated protein kinase phosphatase rVH6, *J Biol Chem* 271(52) 33486-92.
70. Muda, M., et al. (1998) The mitogen-activated protein kinase phosphatase-3 N-terminal noncatalytic region is responsible for tight substrate binding and enzymatic specificity, *J Biol Chem* 273(15) 9323-9.
71. Camps, M., et al. (1998) Catalytic activation of the phosphatase MKP-3 by ERK2 mitogen-activated protein kinase [see comments], *Science* 280(5367) 1262-5.
72. Brunner, D., et al. (1994) A gain-of-function mutation in Drosophila MAP kinase activates multiple receptor tyrosine kinase signaling pathways, *Cell* 76(5) 875-88.
73. Zhou, B. and Z.Y. Zhang (1999) Mechanism of mitogen-activated protein kinase phosphatase-3 activation by ERK2, *J Biol Chem* 274(50) 35526-34.
74. Rigas, J.D., et al. (2001) Transition state analysis and requirement of Asp-262 general acid/base catalyst for full activation of dual-specificity phosphatase MKP3 by extracellular regulated kinase, *Biochemistry* 40(14) 4398-406.
75. Slack, D.N., et al. (2001) Distinct binding determinants for ERK2/p38alpha and JNK map kinases mediate catalytic activation and substrate selectivity of map kinase phosphatase-1, *J Biol Chem* 276(19) 16491-500.

76. Hutter, D., et al. (2000) Catalytic activation of mitogen-activated protein (MAP) kinase phosphatase-1 by binding to p38 MAP kinase: critical role of the p38 C-terminal domain in its negative regulation, *Biochem J* 352(Pt 1) 155-163.
77. Wishart, M.J. and J.E. Dixon (2002) PTEN and myotubularin phosphatases: from 3-phosphoinositide dephosphorylation to disease, *Trends Cell Biol* 12(12) 579-85.
78. Leslie, N.R. and C.P. Downes (2002) PTEN: The down side of PI 3-kinase signalling, *Cell Signal* 14(4) 285-95.
79. Stewart, A.E., et al. (1999) Crystal structure of the MAPK phosphatase Pyst1 catalytic domain and implications for regulated activation, *Nat Struct Biol* 6(2) 174-81.
80. Farooq, A., et al. (2001) Solution structure of ERK2 binding domain of MAPK phosphatase MKP-3: structural insights into MKP-3 activation by ERK2, *Mol Cell* 7(2) 387-99.
81. Farooq, A., et al. (2003) Solution structure of the MAPK phosphatase PAC-1 catalytic domain. Insights into substrate-induced enzymatic activation of MKP, *Structure (Camb)* 11(2) 155-64.
82. Zhang, F., et al. (1994) Atomic structure of the MAP kinase ERK2 at 2.3 Å resolution, *Nature* 367(6465) 704-11.
83. Canagarajah, B.J., et al. (1997) Activation mechanism of the MAP kinase ERK2 by dual phosphorylation, *Cell* 90(5) 859-69.
84. Khokhlatchev, A.V., et al. (1998) Phosphorylation of the MAP kinase ERK2 promotes its homodimerization and nuclear translocation, *Cell* 93(4) 605-15.
85. Adachi, M., M. Fukuda, and E. Nishida (1999) Two co-existing mechanisms for nuclear import of MAP kinase: passive diffusion of a monomer and active transport of a dimer, *Embo J* 18(19) 5347-58.
86. Matsubayashi, Y., M. Fukuda, and E. Nishida (2001) Evidence for existence of a nuclear pore complex-mediated, cytosol- independent pathway of nuclear

- translocation of ERK MAP kinase in permeabilized cells, *J Biol Chem* 276(45) 41755-60.
87. Whitehurst, A.W., et al. (2002) ERK2 enters the nucleus by a carrier-independent mechanism, *Proc Natl Acad Sci U S A* 99(11) 7496-501.
 88. Zhao, Y. and Z.Y. Zhang (2001) The mechanism of dephosphorylation of extracellular signal-regulated kinase 2 by mitogen-activated protein kinase phosphatase 3, *J Biol Chem* 276(34) 32382-91.
 89. Clarke, P.R. (1994) Signal transduction. Switching off MAP kinases, *Curr Biol* 4(7) 647-50.
 90. Khokhlatchev, A., et al. (1997) Reconstitution of mitogen-activated protein kinase phosphorylation cascades in bacteria. Efficient synthesis of active protein kinases, *J Biol Chem* 272(17) 11057-62.
 91. Sun, H., et al. (1993) MKP-1 (3CH134), an immediate early gene product, is a dual specificity phosphatase that dephosphorylates MAP kinase in vivo, *Cell* 75(3) 487-93.
 92. Ward, Y., et al. (1994) Control of MAP kinase activation by the mitogen-induced threonine/tyrosine phosphatase PAC1, *Nature* 367(6464) 651-4.
 93. Kwak, S.P. and J.E. Dixon (1995) Multiple dual specificity protein tyrosine phosphatases are expressed and regulated differentially in liver cell lines, *J Biol Chem* 270(3) 1156-60.
 94. Keyse, S.M. (2000) Protein phosphatases and the regulation of mitogen-activated protein kinase signalling, *Curr Opin Cell Biol* 12(2) 186-92.
 95. Camps, M., A. Nichols, and S. Arkininstall (1999) Dual specificity phosphatases: a gene family for control of MAP kinase function, *Faseb J* 14(1) 6-16.
 96. Chu, Y., et al. (1996) The mitogen-activated protein kinase phosphatases PAC1, MKP-1, and MKP-2 have unique substrate specificities and reduced activity in vivo toward the ERK2 sevenmaker mutation, *J Biol Chem* 271(11) 6497-501.

97. Hirsch, D.D. and P.J. Stork (1997) Mitogen-activated protein kinase phosphatases inactivate stress-activated protein kinase pathways in vivo, *J Biol Chem* 272(7) 4568-75.
98. Zama, T., et al. (2002) A novel dual specificity phosphatase SKRP1 interacts with the MAPK kinase MKK7 and inactivates the JNK MAPK pathway. Implication for the precise regulation of the particular MAPK pathway, *J Biol Chem* 277(26) 23909-18.
99. Tanoue, T., et al. (2000) A conserved docking motif in MAP kinases common to substrates, activators and regulators, *Nat Cell Biol* 2(2) 110-6.
100. Denu, J.M., et al. (1995) The purification and characterization of a human dual-specific protein tyrosine phosphatase [published erratum appears in *J Biol Chem* 1995 Apr 28;270(17):10358], *J Biol Chem* 270(8) 3796-803.
101. Robbins, D.J., et al. (1994) MAP kinases ERK1 and ERK2: pleiotropic enzymes in a ubiquitous signaling network, *Adv Cancer Res* 63 93-116.
102. Denu, J.M., et al. (1995) The purification and characterization of a human dual-specific protein tyrosine phosphatase, *J Biol Chem* 270(8) 3796-803.
103. Wilsbacher, J.L. and M.H. Cobb (2001) Bacterial expression of activated mitogen-activated protein kinases, *Methods Enzymol* 332 387-400.
104. Alonso, A., et al. (2001) Inhibitory role for dual specificity phosphatase VHR in T cell antigen receptor and CD28-induced Erk and Jnk activation, *J Biol Chem* 276(7) 4766-71.
105. Zhou, B., et al. (2001) Multiple regions of MAP kinase phosphatase 3 are involved in its recognition and activation by ERK2, *J Biol Chem* 276(9) 6506-15.
106. Wolf, I., et al. (2001) Involvement of the activation loop of ERK in the detachment from cytosolic anchoring, *J Biol Chem* 276(27) 24490-7.

107. Flint, A.J., et al. (1997) Development of "substrate-trapping" mutants to identify physiological substrates of protein tyrosine phosphatases, *Proc Natl Acad Sci U S A* 94(5) 1680-5.
108. Garton, A.J., A.J. Flint, and N.K. Tonks (1996) Identification of p130(cas) as a substrate for the cytosolic protein tyrosine phosphatase PTP-PEST, *Mol Cell Biol* 16(11) 6408-18.
109. Brunet, A., et al. (1999) Nuclear translocation of p42/p44 mitogen-activated protein kinase is required for growth factor-induced gene expression and cell cycle entry, *Embo J* 18(3) 664-74.
110. Volmat, V., et al. (2001) The nucleus, a site for signal termination by sequestration and inactivation of p42/p44 MAP kinases, *J Cell Sci* 114(Pt 19) 3433-43.
111. Rubinfeld, H., T. Hanoch, and R. Seger (1999) Identification of a cytoplasmic-retention sequence in ERK2, *J Biol Chem* 274(43) 30349-52.
112. Adachi, M., M. Fukuda, and E. Nishida (2000) Nuclear export of MAP kinase (ERK) involves a MAP kinase kinase (MEK)-dependent active transport mechanism, *J Cell Biol* 148(5) 849-56.
113. Schmidt, C., et al. (1998) Mechanical stressing of integrin receptors induces enhanced tyrosine phosphorylation of cytoskeletally anchored proteins, *J Biol Chem* 273(9) 5081-5.
114. Bardwell, A.J., et al. (2001) A conserved docking site in MEKs mediates high-affinity binding to MAP kinases and cooperates with a scaffold protein to enhance signal transmission, *J Biol Chem* 276(13) 10374-86.
115. Xu, B., et al. (2001) Hydrophobic as well as charged residues in both MEK1 and ERK2 are important for their proper docking, *J Biol Chem* 276(28) 26509-15.

116. Fantz, D.A., et al. (2001) Docking sites on substrate proteins direct extracellular signal-regulated kinase to phosphorylate specific residues, *J Biol Chem* 276(29) 27256-65.
117. Bardwell, A.J., M. Abdollahi, and L. Bardwell (2003) Docking sites on mitogen-activated protein kinase (MAPK) kinases, MAPK phosphatases and the Elk-1 transcription factor compete for MAPK binding and are crucial for enzymic activity, *Biochem J* 370(Pt 3) 1077-85.
118. Zhang, J., et al. (2003) A bipartite mechanism for ERK2 recognition by its cognate regulators and substrates, *J Biol Chem* 278(32) 29901-12.
119. Muda, M., et al. (1997) Molecular cloning and functional characterization of a novel mitogen-activated protein kinase phosphatase, MKP-4, *J Biol Chem* 272(8) 5141-51.
120. Neel, B.G. and N.K. Tonks (1997) Protein tyrosine phosphatases in signal transduction, *Curr Opin Cell Biol* 9(2) 193-204.
121. Tonks, N.K. and B.G. Neel (2001) Combinatorial control of the specificity of protein tyrosine phosphatases, *Curr Opin Cell Biol* 13(2) 182-95.
122. Lohse, D.L., et al. (1997) Roles of aspartic acid-181 and serine-222 in intermediate formation and hydrolysis of the mammalian protein-tyrosine-phosphatase PTP1, *Biochemistry* 36(15) 4568-75.
123. Zhang, Z.Y., Y. Wang, and J.E. Dixon (1994) Dissecting the catalytic mechanism of protein-tyrosine phosphatases, *Proc Natl Acad Sci U S A* 91(5) 1624-7.
124. Zhang, Z.Y., L. Wu, and L. Chen (1995) Transition state and rate-limiting step of the reaction catalyzed by the human dual-specificity phosphatase, VHR, *Biochemistry* 34(49) 16088-96.
125. Grzyska, P.K., et al. (2003) Transition state differences in hydrolysis reactions of alkyl versus aryl phosphate monoester monoanions, *J Am Chem Soc* 125(43) 13106-11.

126. Bianciotto, M., J.C. Barthelat, and A. Vigroux (2002) Reactivity of phosphate monoester monoanions in aqueous solution. 1. Quantum mechanical calculations support the existence of "anionic zwitterion" $\text{MeO}^{+}(\text{H})\text{PO}^{3-}(2-)$ as a key intermediate in the dissociative hydrolysis of the methyl phosphate anion, *J Am Chem Soc* 124(25) 7573-87.
127. Ames, N.A. and D.T. Dubin (1960) The Role of Polyamine in the Neutralization of Bacteriophage Deoxyribonucleic Acid, *J Biol Chem* 235(3) 769-75.
128. Schowen, K.B. and R.L. Schowen (1982) Solvent isotope effects of enzyme systems, *Methods Enzymol* 87 551-606.
129. Zhang, Z.Y., et al. (1994) Nature of the rate-determining steps of the reaction catalyzed by the Yersinia protein-tyrosine phosphatase, *J Biol Chem* 269(11) 8140-5.
130. Kolmodin, K., P. Nordlund, and J. Aqvist, *Proteins: Structure, Function and Genetics*. Vol. 36. 1999. 370-9.
131. Hart, J.C., et al. (1998) An Alternative Role for the Conserved Asp Residue in Phosphoryl Transfer Reactions, *J. Am. chem. Soc.* 120 13535-6.
132. Asthagiri, D., et al. (2002) Density functional study of the mechanism of a tyrosine phosphatase: I. Intermediate formation, *J Am Chem Soc* 124(34) 10225-35.
133. Knight, W.B., P.M. Weiss, and W.W. Cleland (1986) Determination of equilibrium ^{18}O isotope effects on the deprotonation of phosphate and phosphate esters and the anomeric effect on deprotonation of glucose-6-phosphate, *J. Am. chem. Soc.* 108 2759-2761.
134. Lad, C., N.H. Williams, and R. Wolfenden (2003) The rate of hydrolysis of phosphomonoester dianions and the exceptional catalytic proficiencies of protein and inositol phosphatases, *Proc Natl Acad Sci U S A* 100(10) 5607-10.

135. Kirby, A.J. and A.G. Varvoglis (1967) The Reactivity of Phosphate Esters. Monoester Hydrolysis, *J. Am. Chem. Soc.* 89, 415-423.
136. Rishavy, M.A. and W.W. Cleland (1999) ^{13}C , ^{15}N , and ^{18}O equilibrium isotope effects and fractionation factors, *Can. J. Chem.* 77, 967-77.
137. Hengge, A.C., W.A. Edens, and H. Elsing (1994) Transition-State Structures for Phosphoryl-Transfer Reactions of *p*-Nitrophenyl Phosphate, *J. Am. chem. Soc.* 116, 5045-49.
138. Kim, Y., and Denu, J. M. "Protein Tyrosine Phosphatase Structure and Mechanism" Handbook of Cell Signaling, Vol 1, Elsevier Science (USA) 2003 (in press)
139. Sawyer, C. B., and Kirsch, J. F. (1973) Kinetic Isotope Effects for Reactions of Methyl Formate-Methoxyl- ^{18}O , *J. Am. chem. Soc.* 95, 7375-7381.
140. Green, M., and Taube, H. (1963) Isotopic Fractionation in the OH^- - H_2O Exchange Reaction, *J. Phys. Chem.* 67, 1565-1566
141. Kresge, A. J., and Preto, R. J. (1965) The Mechanism of Hydrolysis of Ortho Esters, *J. Am. chem. Soc.* 87, 4593-4596

Appendix

**A continuous, nonradioactive assay for histone acetyltransferases
(Analytical Biochemistry 280: 308-314, 2000)**

A. 1 Abstract

Histone acetyltransferases (HATs) catalyze the acetyl-group transfer from acetyl-CoA to the ϵ -amino group of specific lysine residues within core histone proteins. HATs and other chromatin remodeling enzymes have been recently shown to regulate gene activation within specific loci. To facilitate mechanistic studies, we have developed two continuous, non-radioactive assays for the prototypical GCN5 HAT. The CoASH generated in the HAT reactions was continuously measured by using a coupled enzyme system with either α -ketoglutarate dehydrogenase or pyruvate dehydrogenase. The CoASH-dependent oxidation of α -ketoglutarate or pyruvate is accompanied by the reduction of NAD to NADH, which was measured spectrophotometrically at 340 nm. The steady-state rate constants with substrates acetyl-CoA and a synthetic peptide (corresponding to the first 20 amino acids of H3 histone) were determined. The resulting rate constants were not significantly different between the two coupled assays, providing strong validation of these methods. Rate constants were also determined using the commonly-employed radioactive filter-binding assay and compared. The 1.5-5 fold lower values obtained in the radioactive end-point assay are discussed in terms of the technical problems and limitations of this assay. The coupled assays should be widely applicable since the production of CoASH is common to all HAT enzymes, regardless of protein substrate.

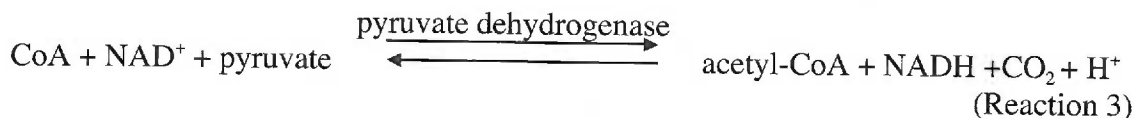
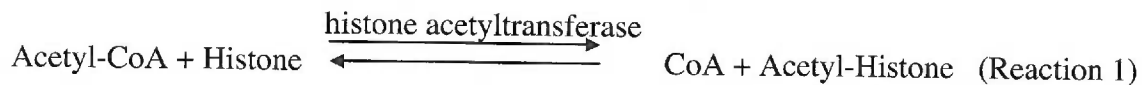
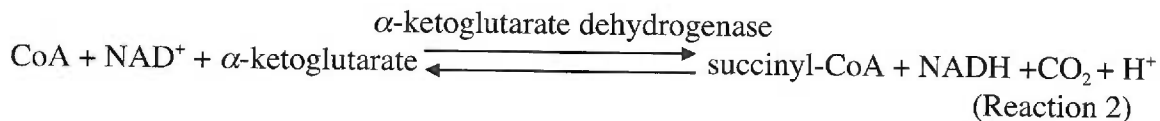
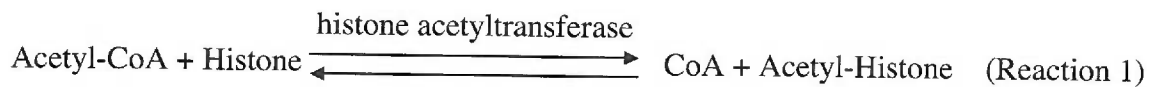
A. 2 Introduction

Histone acetyltransferases (HATs) are a family of enzymes which catalyze the transfer of an acetyl moiety from acetyl-CoA to the ϵ -amino group of lysine residues within core histone proteins. The acetylation of histones by HATs has an important role in transcriptional regulation by remodeling chromatin structure (1). In eukaryotes, approximately 146 base pairs of DNA wrap around an octamer of core histones to form the basic unit of chromatin, the nucleosome. This tightly packed DNA structure is transcriptionally repressive. HATs and other chromatin remodeling enzymes are proposed to generate an open, transcriptionally competent structure (2). Acetylation of histones neutralizes positively charged lysines in the amino-termini of histone proteins, thereby altering interactions between protein:protein and protein:DNA complexes. This loosening of chromatin structure allows access to transcription factors which initiate transcription of certain target genes (3). Several classes of HATs have been identified: p300/CBP (4), P/CAF (5), TAFII250 (6), and SRC-1 (7). Among HAT enzymes, yGCN5 (yeast GCN5), which is a P/CAF family member, has been the most characterized. The crystallographic molecular model (8) and biochemical studies (9) of yGCN5 have suggested that a conserved acidic residue, Glu-173, acts as a general base by deprotonating the ϵ -amino group of histone H3 substrate. The deprotonated ϵ -amino group then directly attacks the bound acetyl-CoA, resulting in transfer of an acetyl group to lysine. Except for a handful of biochemical studies, little is known concerning the mechanisms of catalysis, substrate specificity and regulation. Understanding the mechanism of HAT catalysis will provide deeper insight into the link between acetylation and gene activation. Thus, there is a great need for an efficient and accurate enzymatic assay to investigate the molecular mechanisms of the HATs.

Currently, histone acetyltransferase activity is measured using a discontinuous radioactive filter-binding assay (9). The filter-binding assay uses [3 H]-acetyl-CoA as a HAT substrate and the subsequent detection of [3 H]-acetyl-group transfer to histone

substrate is accomplished by liquid scintillation counting of [³H]-acetyl-histone retained on a phosphocellulose disk. Although the radioactive filter-binding assay is commonly employed for measuring HAT activity, it is technically problematic and is not ideal for kinetic analysis due to its discontinuous nature. The expense and the disposal of radioactive compounds can become prohibitive for routine enzymatic analyses. Also, the experimental procedure is relatively laborious and the data analysis is time-consuming. These complications and limitations led us to develop two continuous spectrophotometric assays for studying the enzymatic activities of HATs. The catalytic domain of yeast GCN5, the archetypal HAT, was employed in the development of these new assays.

These spectrophotometric assays continuously measure the amount of CoASH generated by the HAT reactions. The CoASH is determined by using a coupled enzyme system with either α -ketoglutarate dehydrogenase or pyruvate dehydrogenase. The CoASH-dependent oxidation of α -ketoglutarate or pyruvate is accompanied by the reduction of NAD to NADH, which can be measured spectrophotometrically at 340 nm.



In this study, we have demonstrated that these spectrophotometric assays are a simpler, less expensive and more accurate method for determining HAT activity,

compared to the filter-binding assay. Using these coupled assays we have determined the steady-state rate constants for yGCN5 and compared these values to those obtained by the filter-binding method. Furthermore, these assays should be widely applicable in biochemical investigations since the production of CoA is common to all HAT enzymes, regardless of the protein substrate.

A. 3 Materials and Methods

A. 3.1 Materials.

Histone H3 peptide, ARTKQTARKSTGGKAPPKQLC, corresponding to the 20 amino-terminal residues of human histone H3 and an additional carboxy-terminal cysteine was synthesized by the Protein Chemistry Core Lab at Baylor College of Medicine. Acetyl-CoA was from Boeringer Mannheim. Calf thymus histones were purchased from Calbiochem. [³H]Acetyl-CoA was from NEN Life Science Products. All other reagents were from Sigma.

A. 3.2 Purification of yGCN5.

The catalytic domain of yeast GCN5 (yGCN5) was recombinantly expressed and purified from bacteria as described previously (9), except for the following modifications. Following lysis by french pressure, the clarified yGCN5 preparation was dialyzed against MES buffer (20 mM MES, pH 6.0, 1 mM EDTA, 1 mM DTT, 10 % glycerol). The dialyzed sample was then subjected to SP-Sepharose (Amersham Pharmacia Biotech) ion-exchange chromatography, and eluted with a 0 - 0.8 M NaCl gradient. yGCN5 eluted at 400 mM NaCl. Pure fractions (assessed by SDS-polyacrylamide gel electrophoresis) were pooled and concentrated, and stored at -20 °C until use. Protein concentrations were determined by the method of Bradford (10).

A. 3.3 Spectrophotometric determination of yGCN5 activity.

yGCN5 histone acetyltransferase (HAT) activity was continuously measured by using either a Shimadzu Biospec-1601 UV/VIS spectrophotometer (Tokyo, Japan) or Multiskan Ascent microplate reader (LabSystems, Franklin MA). The HAT assay reaction mixtures contained 0.2 mM NAD, 0.2 mM thiamine pyrophosphate (TPP), 5

mM MgCl₂, 1 mM DTT, 2.4 mM α -ketoglutarate, 63 μ M acetyl-CoA, 60 μ M histone H3 peptide, 0.07 units of α -ketoglutarate dehydrogenase (one unit of dehydrogenases is defined by the manufacturer to be the conversion of 1.0 μ mole of β -NAD to β -NADH per minute at pH 7.4 at 30 °C in the presence of saturating levels of coenzyme A), 350 nM yGCN5, 100 mM sodium acetate, 50 mM Bis-Tris, and 50 mM Tris, pH 7.5, in a total volume of 300 μ L, unless otherwise noted. A ten-fold stock solution containing NAD, TPP, MgCl₂, DTT, and a ten-fold stock solution of α -ketoglutarate in 20 mM HEPES (pH 7.5) were prepared fresh daily. All assay components except yGCN5 were incubated at 25 °C for 5 min and the reaction was initiated by the addition of yGCN5. The rates were analyzed continuously for 5 min by measuring NADH production at 340 nm ($\epsilon_{340}^{\text{NADH}} = 6230 \text{ M}^{-1} \text{ cm}^{-1}$). The background rates resulting from the spontaneous formation of CoA were subtracted from the initial velocities derived from the yGCN5-catalyzed reactions. To determine the kinetic parameters for yGCN5, initial velocities were measured at various substrate concentrations. The data were fitted to the following equation using the computer software Kaleidagraph (Abelbeck Software).

$$v = ([E]_0 k_{\text{cat}} \cdot S) / (K_m + S)$$

When pyruvate dehydrogenase was used as a coupled enzyme, 0.03 units of pyruvate dehydrogenase and 2.4 mM pyruvate were employed in place of 0.07 units of α -ketoglutarate dehydrogenase and 2.4 mM α -ketoglutarate, respectively.

A. 3. 4 Radioactive filter-binding assay for measuring yGCN5 activity.

yGCN5 activity was measured using [³H]acetyl-CoA and histone H3 peptide as substrates. The radioactive filter-binding assay was performed as previously described (9). The reactions were allowed to proceed for 10 min at 22 °C. Assays were performed

in TBA buffer (pH 7.5) under the identical conditions employed with the spectrophotometric assays.

A. 3. 4 Product determinations by coupled reaction vs. filter-binding assay.

A HAT reaction containing [³H]acetyl-CoA, H3 peptide, and yGCN5 was allowed to proceed at 22 °C for 10 min before the reaction was terminated by heating the mixture for 2 min at 100 °C. Half of the heat-inactivated reaction mixture was spotted on the phosphocellulose disk to count [³H]acetyl-histone bound to the phosphocellulose disk, and the other half was added to a cuvette containing NAD, α-ketoglutarate, α-ketoglutarate dehydrogenase to measure the NADH production.

A. 4 Results and Discussion

yGCN5 uses acetyl-CoA to acetylate Lys-14 of H3 histone protein, and generates the products, acetylated -histone and CoA (Reaction 1). In the spectrophotometric coupled-assay, the CoA produced by yGCN5 is concomitantly used as a substrate for either α -ketoglutarate dehydrogenase or pyruvate dehydrogenase. Because of their ability to reduce NAD to NADH while oxidizing substrate (11), dehydrogenases have been employed for many spectrophotometric enzyme assays. The production of NADH is simply followed spectrophotometrically at 340 nm. Here, the usefulness of either α -ketoglutarate dehydrogenase or pyruvate dehydrogenase as a coupling enzyme system was examined. α -Ketoglutarate dehydrogenase oxidizes α -ketoglutarate to succinyl-CoA using CoA and NAD⁺, and generates the additional products NADH and CO₂ (Reaction 2). In a similar reaction, pyruvate dehydrogenase converts CoA, NAD⁺ and pyruvate to acetyl-CoA, NADH and CO₂ (Reaction 3).

The utility of the coupled assay was initially tested by measuring NADH formation at 340 nm due to yGCN5 histone acetyltransferase-dependent CoA production. Figure 1 shows the kinetic traces of the α -ketoglutarate dehydrogenase- and pyruvate dehydrogenase-coupled HAT reactions. Reactions were performed as described in the Materials and Methods section. In the absence of yGCN5, only slow background rates were observed; however, when the HAT reaction was initiated by the addition of yGCN5, robust steady-state initial velocities were observed. A short lag was observed with pyruvate dehydrogenase as the coupling enzyme at pH 7.5. No lag phase was observed for the α -ketoglutarate dehydrogenase coupled reaction. The higher reported K_m of CoA for pyruvate dehydrogenase (21 μ M) (12) compared to α -ketoglutarate dehydrogenase

(<0.1 μM) (13) suggested that the short lag might be due to the necessity of building up a critical level of CoA from the HAT reaction before a linear response is achieved. These short lag phases in the kinetic traces are not uncommon in enzyme-coupled reactions (14). This lag was not altered with increasing amounts of NAD, pyruvate, or pyruvate dehydrogenase. Interestingly, at pH 8.5 no lag was observed. Regardless, the initial velocities from both coupled reaction systems were calculated from the linear portion of the curves.

To verify that the coupled assays are accurate measures of yGCN5 activity and that the observed rates are not limited by the coupled reaction, the initial velocities were measured with increasing amounts of yGCN5. Figure 2 demonstrates that there was a linear relationship between NADH production and yGCN5 concentration; that is, the observed rate depends only on yGCN5 activity, and not α -ketoglutarate dehydrogenase or pyruvate dehydrogenase. To further demonstrate that the coupled assay system does not limit the observed rate, the concentrations of the coupled reaction components (e.g. NAD, pyruvate, α -ketoglutarate, pyruvate dehydrogenase, α -ketoglutarate dehydrogenase) were increased 2-3-fold and the HAT reactions were repeated. Increasing the concentrations of these coupled reaction components resulted in no change in observed rates, indicating that the original conditions were sufficient and that the coupled reaction does not limit the observed initial rate generated from the HAT reaction.

Having demonstrated that yGCN5 activity could be accurately measured using two different coupled enzyme systems, we attempted to use these spectrophotometric HAT assays to obtain the relevant steady-state rate constants. The concentration of histone H3 peptide was varied at saturating acetyl-CoA concentrations, and the initial

velocities were determined by measuring the continuous production of NADH at 340 nm. The slow background rates (absence of yGCN5) were subtracted from the rates determined in the presence of yGCN5. Under all conditions examined, the background rates were never larger than 10 % of the observed HAT-catalyzed reaction. The data (Figure 3 A & B) were then fitted to the Michaelis-Menten equation $v = ([E]_0 k_{cat} \bullet [S]) / (K_m + [S])$. Using the α -ketoglutarate dehydrogenase-coupled assay, the fit yielded a k_{cat} value of $0.45 \pm 0.07 \text{ s}^{-1}$, a K_m value of $130 \pm 52.9 \text{ }\mu\text{M}$ and a k_{cat}/K_m value of $3,058 \pm 678 \text{ M}^{-1} \text{ s}^{-1}$. With the pyruvate dehydrogenase coupled assay, the fit yielded a k_{cat} value of $0.43 \pm 0.03 \text{ s}^{-1}$, a K_m value of $114 \pm 24.4 \text{ }\mu\text{M}$ and a k_{cat}/K_m value of $3,708 \pm 575 \text{ M}^{-1} \text{ s}^{-1}$. As required, both enzyme coupled reactions yielded rate constants that were not significantly different, providing an additional check on the validity of these methods.

We also measured the ability of acetyl-CoA to saturate the HAT activity in the two coupled-assay systems. These experiments were performed at sub-saturating levels of H3 peptide ($60 \text{ }\mu\text{M}$, $K_m \sim 120 \text{ }\mu\text{M}$). The concentrations of acetyl-CoA were varied and the resulting initial velocities were fitted to the Michaelis Menten equation (Figure 4 A & B), yielding apparent k_{cat} values of 0.17 ± 0.01 and $0.18 \pm 0.01 \text{ s}^{-1}$ and apparent K_m values of 5.6 ± 1.6 and $5.1 \pm 1.5 \text{ }\mu\text{M}$, for α -ketoglutarate dehydrogenase and pyruvate dehydrogenase respectively. Indeed, acetyl-CoA was capable of saturating yGCN5 activity for both enzyme-coupled systems. Again, there is an excellent agreement between the two coupled assays.

In order to compare the radioactive filter-binding and coupled assays, the steady-state parameters were determined using the filter-binding assay. At saturating acetyl-CoA concentrations, H3 peptide concentrations were varied and the resulting data were fitted to the Michaelis-Menten equation, yielding a k_{cat} value of $0.30 \pm 0.03 \text{ s}^{-1}$, a K_m value of $566 \pm 95 \text{ }\mu\text{M}$ and a k_{cat}/K_m value of $539 \pm 36.2 \text{ M}^{-1} \text{ s}^{-1}$ (Table I). Also, a saturation curve for acetyl-CoA was determined at $60 \text{ }\mu\text{M}$ H3 peptide, yielding an apparent k_{cat} value of $0.040 \pm 0.001 \text{ s}^{-1}$, an apparent K_m value of $3.62 \pm 0.41 \text{ }\mu\text{M}$ and a k_{cat}/K_m value of

$11,000 \pm 1,072 \text{ M}^{-1} \text{ s}^{-1}$ (Table I). The data from all three different assays are summarized in Table I. Although there is excellent agreement between the two coupled assays, the radioactive filter-binding assay gave ~ 1.5 - 4 -fold lower values in k_{cat} and ~ 1.5 - 5 -fold higher K_{m} values compared to the two continuous assays.

This discrepancy in kinetic parameters between the two assays comes from the technical problems associated with the filter-binding assay. The filter binding assay relies on the ability of the product [^3H]acetylated H3 peptide to bind to the phosphocellulose disk, and depends upon accurate determination of the [^3H]-acetyl-CoA specific activity. The disks are washed extensively to remove excess [^3H]-acetyl-CoA and the amount of product produced is determined from liquid scintillation counting. It can be erroneous to assume that all of the radiolabelled product produced in the assay is bound to the phosphocellulose disk. If binding is less than complete, this can lead to an underestimation of the calculated rate constants. Also, if the specific radioactivity of [^3H]-acetyl-CoA is overestimated (due to contaminants containing [^3H] or partial hydrolysis of [^3H]-acetyl-CoA), the amount of product formed will be underestimated in the final calculations. To examine whether these problems existed in the filter-binding assay and were responsible for the small discrepancies between assays, we measured the amount of product formed using both the filter-binding assay and the coupled assay. After 10 min of reaction between [^3H]-acetyl-CoA, H3 peptide and yGCN5, the reaction was terminated by heat-inactivation of yGCN5 (100 °C for 2 min). To calculate the amount of product formed, half of the heat-inactivated reaction mixture was spotted onto the phosphocellulose disk and the other half was added to a sample containing the reaction components of the coupled assay. The amount of [^3H]-acetylated H3 peptide produced was then compared to the amount of NADH produced (i.e., CoA). Approximately 5-fold less product was measured with the filter-binding assay. Also, [^3H]-acetyl-CoA was used as a substrate in the coupled reaction to check whether the manufacturer's assigned concentration was accurate. The increase in absorbance at 340

nm due to CoA production by HAT indicated that only 67 % of the commercially-obtained [³H]acetyl-CoA was competent as a substrate for yGCN5. In the case of the H3 peptides used in this study, binding efficiency to the disks does not appear to explain the discrepancy between coupled and filter-binding assays, since both core histone proteins and H3 peptide yield similar k_{cat} values when used as substrates in the filter-binding assay. In other control experiments, we have determined that the lower counting efficiency of tritium bound to the disks can account for as much as 5-8 fold lower counts detected compared to those unbound. This quenching effect from the disks can result in a large underestimation of product formed. Collectively, these observations support the idea that the lower kinetic constants determined in the filter-binding assay can result from the technical difficulties (e.g., impure [³H]acetyl-CoA and variable counting efficiency) associated with this assay. Therefore, we suggest that extreme care must be taken to ensure the accuracy of measurements derived from HAT filter-binding assays. The two coupled assays developed here do not suffer from these technical problems.

In addition to peptides, calf thymus core histones are often used as HAT substrates. To investigate whether calf thymus histones could be used as a substrate in the coupled assays, we attempted to measure initial velocities. However, we observed only very slow rates with calf thymus histone. Based upon the predicted amount of product formed, we surmised that the coupling enzyme systems were inhibited by these histone preparations. To test whether these histone preparations inhibited the α -ketoglutarate dehydrogenase or pyruvate dehydrogenase reactions, calf thymus histones were added during the dehydrogenase reactions (Reactions 2 and 3). Addition of calf thymus histones almost completely inhibited the α -ketoglutarate dehydrogenase and the pyruvate dehydrogenase reactions. Interestingly, α -ketoglutarate dehydrogenase has been shown to precipitate in the presence of the nucleo-histones and other polycations (15). Therefore it is likely that both dehydrogenase enzymes are inhibited by the formation of a complex with histones.

In this study, we developed two continuous, non-radioactive assays for histone acetyltransferases using α -ketoglutarate dehydrogenase and pyruvate dehydrogenase as coupling enzymes. This assay is less labor intensive, less expensive, and is a safer and a more accurate way of measuring kinetic parameters for HATs than the commonly used radioactive filter-binding assay. These new assays are also amenable to high throughput analysis; we have used a microplate reader in this study to increase the capacity of our kinetic analyses. Although calf thymus histones could not be used as substrates, the coupled assays are not limited by the kinds of basic peptide/protein substrates that are required for efficient binding to the negatively-charged phosphocellulose disks. Moreover, due to the extreme heterogeneity, impurity and the various extents of acetylation, calf thymus histones are a poor choice for performing a detailed biochemical analysis, regardless of the type of assay used. We describe two coupled assays that are ideal for synthetic peptides (such as the H3 peptide ARTKQTARKSTGGKAPPKQLC) whose sequence and free lysine concentration can be well controlled. These continuous spectrophotometric assays will be widely applicable for studying the growing families of histone acetyltransferases.

A. 5 Acknowledgement

We thank Michael Langer for technical assistance.

Table I. Comparison of coupled assay to radioactive filter binding HAT assay

HAT assay: H3 Saturation	$k_{\text{cat}}, \text{s}^{-1}$	$K_m, \mu\text{M}$	$k_{\text{cat}}/K_m \text{ M}^{-1}\text{s}^{-1}$
Radioactive assay	0.30 ± 0.03	566.3 ± 94.8	539 ± 36.2
α -Ketoglutarate dehydrogenase	0.45 ± 0.07	130.2 ± 52.9	$3,460 \pm 678$
Pyruvate dehydrogenase	0.43 ± 0.03	113.7 ± 24.4	$3,708 \pm 575$

HAT assay: Acetyl-CoA Saturation	$*k_{\text{cat}}, \text{s}^{-1}$	$*K_m, \mu\text{M}$	$*k_{\text{cat}}/K_m \text{ M}^{-1}\text{s}^{-1}$
Radioactive assay	0.040 ± 0.001	3.62 ± 0.41	$11,000 \pm 1072$
α -Ketoglutarate dehydrogenase	0.17 ± 0.01	5.6 ± 1.6	$30,400 \pm 6,300$
Pyruvate dehydrogenase	0.18 ± 0.01	5.1 ± 1.5	$35,300 \pm 8,640$

* These are apparent values since sub-saturating levels of H3 peptide were used ($60 \mu\text{M}$, $K_m \sim 120 \mu\text{M}$).

Figure 1. Kinetic trace of yGCN5 histone acetyltransferase activity using the α -ketoglutarate dehydrogenase-coupled reaction (A) and the pyruvate dehydrogenase-coupled reaction (B). In both graphs, the lower trace indicates the reaction in the absence of yGCN5, and the upper trace indicates the reaction in the presence of yGCN5. Reactions were performed in TBA buffer (pH 7.5) at 22 °C as described in the Materials and Methods section. Initial velocities were determined from the linear portion of the curves.

Figure 1

Kim *et al.*, 1999

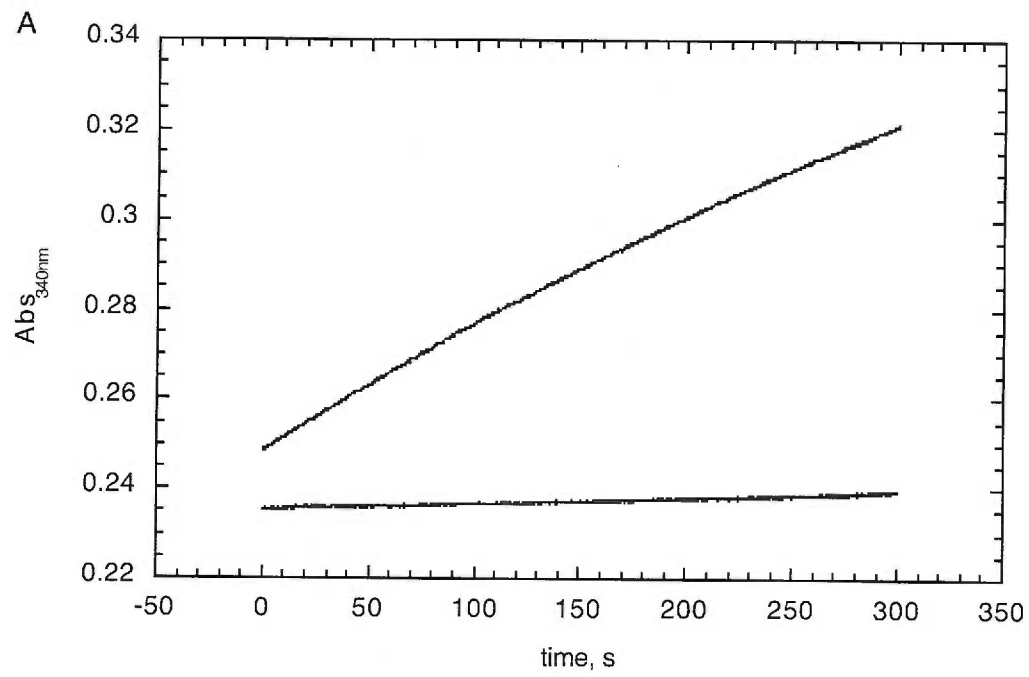


Figure 1

Kim *et al.*, 1999

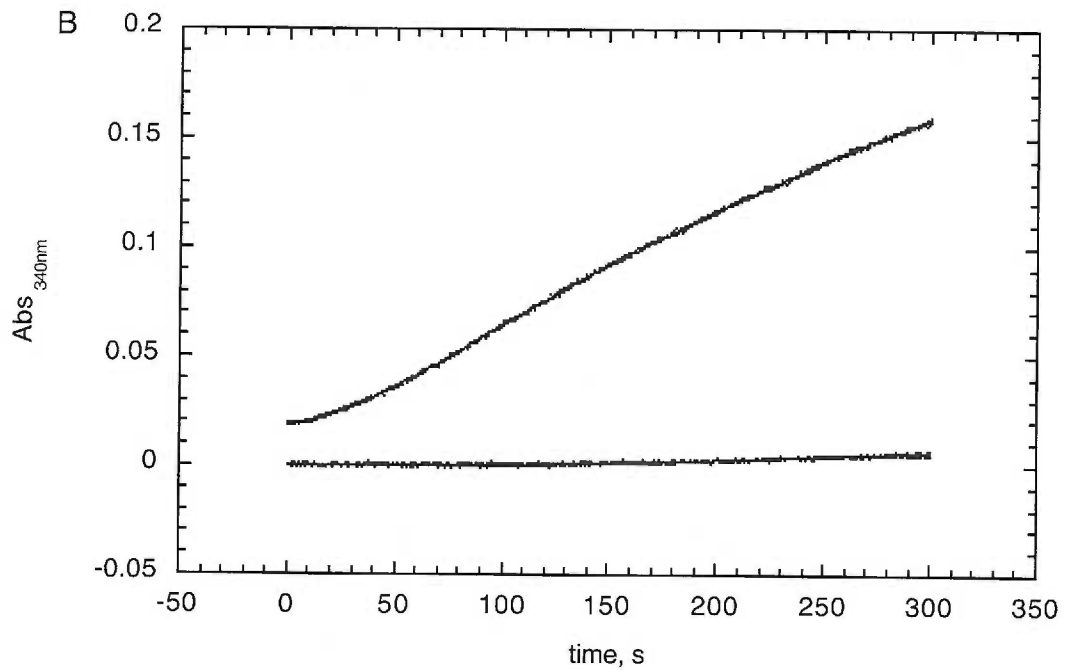


Figure 2. Linear dependence of the α -ketoglutarate dehydrogenase (A) and pyruvate dehydrogenase (B) coupled assays on yGCN5 concentration. Assays were conducted as described under the Materials and Methods section. Background rates measured in the absence of yGCN5 were subtracted from the yGCN5-catalyzed reactions. Absorbances at 340 nm were converted to pmoles NADH produced per minute.

Figure 2

Kim *et al.*, 1999

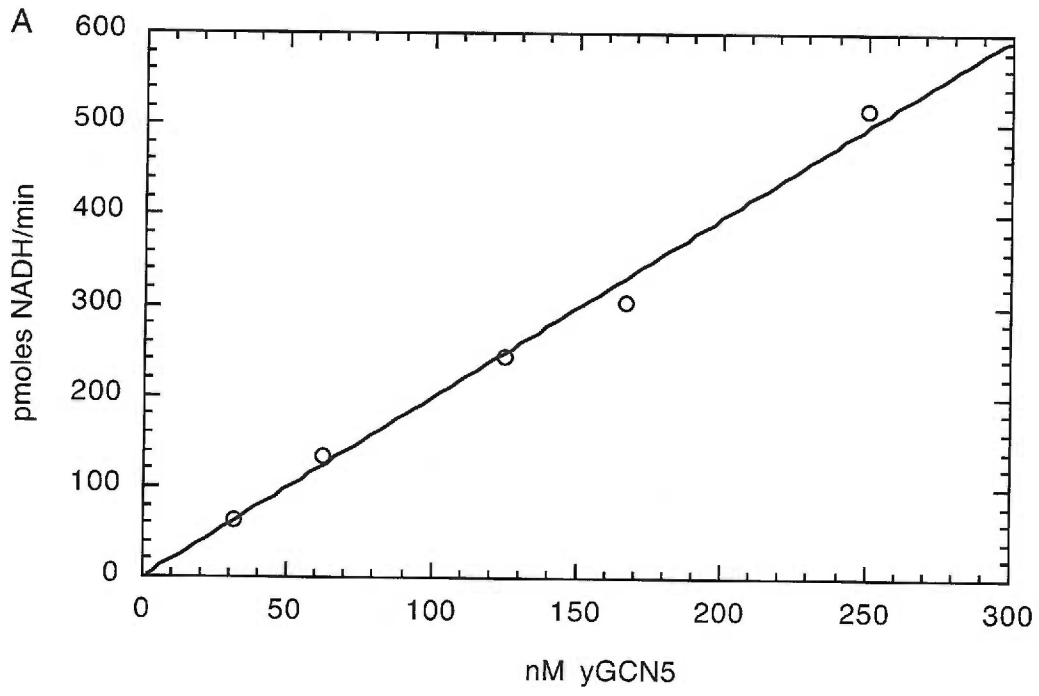


Figure 2

Kim *et al.*, 1999

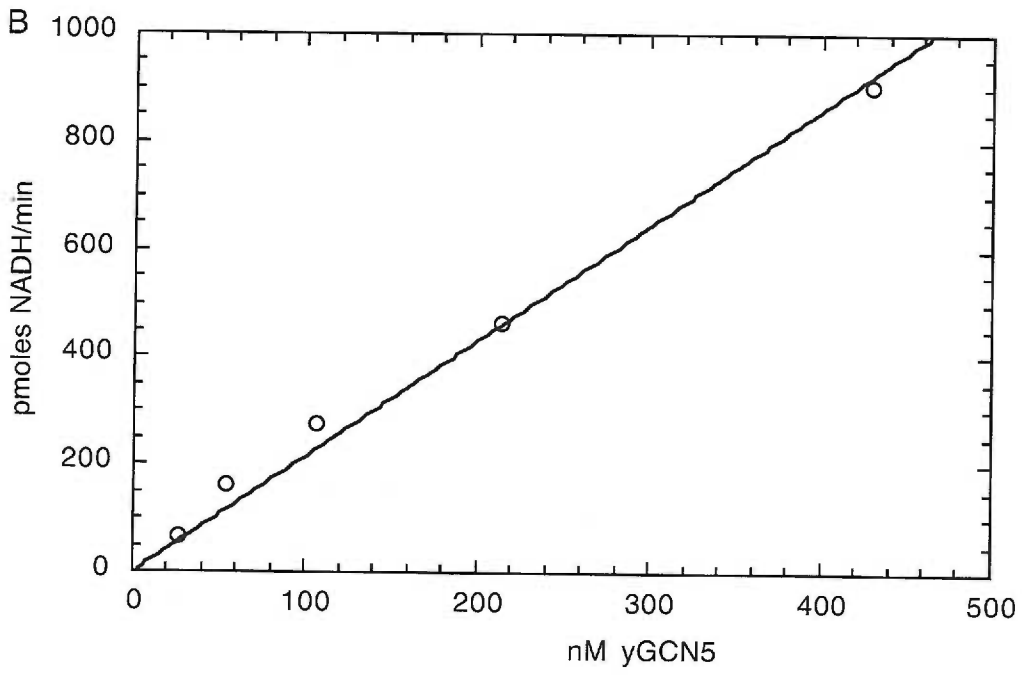


Figure 3. Histone H3 peptide saturation kinetics of yGCN5 using α -ketoglutarate dehydrogenase (A) and pyruvate dehydrogenase (B) coupled assays. Assays were performed as described in Materials and Methods section. For each assay, the histone H3 peptide concentrations were varied from 50 to 600 μM at saturating acetyl-CoA (63 μM). The background rates for each assay were subtracted from the yGCN5-catalyzed reactions. The data were fitted to the Michaelis Menten equation $v = ([E]_0 k_{\text{cat}} \bullet [S]) / (K_m + [S])$.

Figure 3

Kim *et al.*, 1999

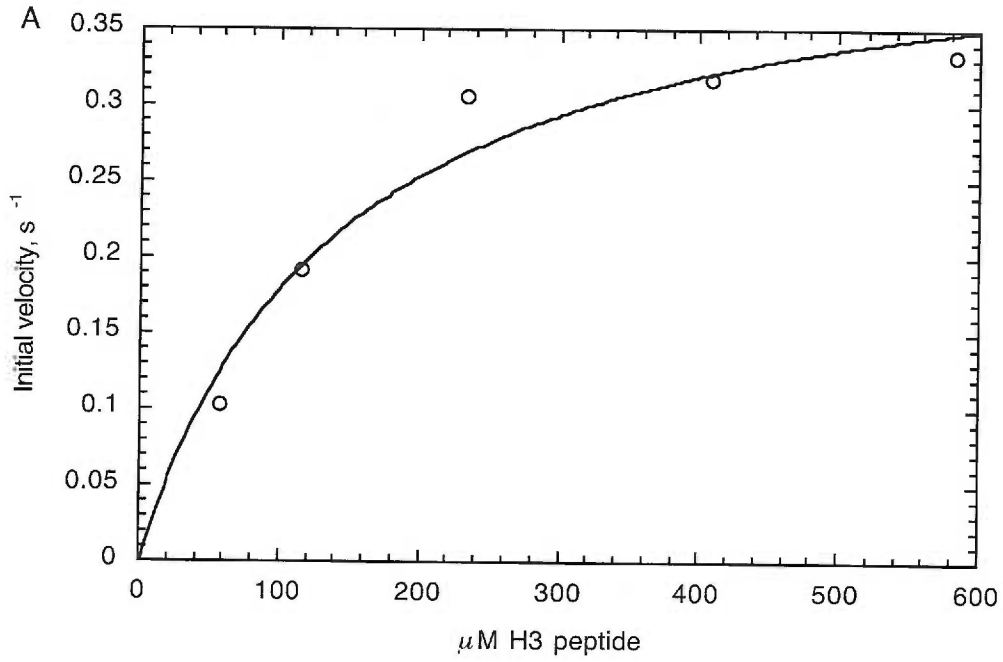


Figure 3

Kim *et al.*, 1999

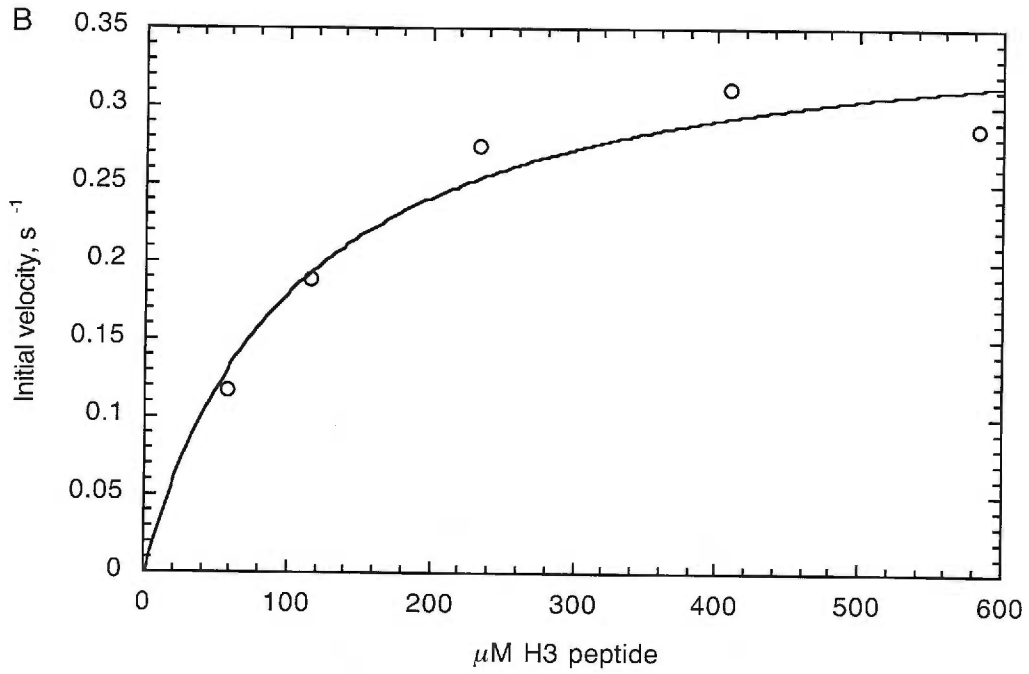


Figure 4. Acetyl-CoA saturation kinetics of yGCN5 using α -ketoglutarate dehydrogenase (A) and pyruvate dehydrogenase (B) coupled assays. Assays were performed as described in the Materials and Methods section. For each assay, the acetyl-CoA concentrations were varied from 5 to 90 μ M and the histone H3 peptide concentration was 60 μ M. The background rates for each assay were subtracted from the yGCN5-catalyzed reactions. The data were fitted to the Michaelis Menten equation $v = ([E]_0 k_{cat} \cdot [S]) / (K_m + [S])$.

Figure 4

Kim *et al.*, 1999

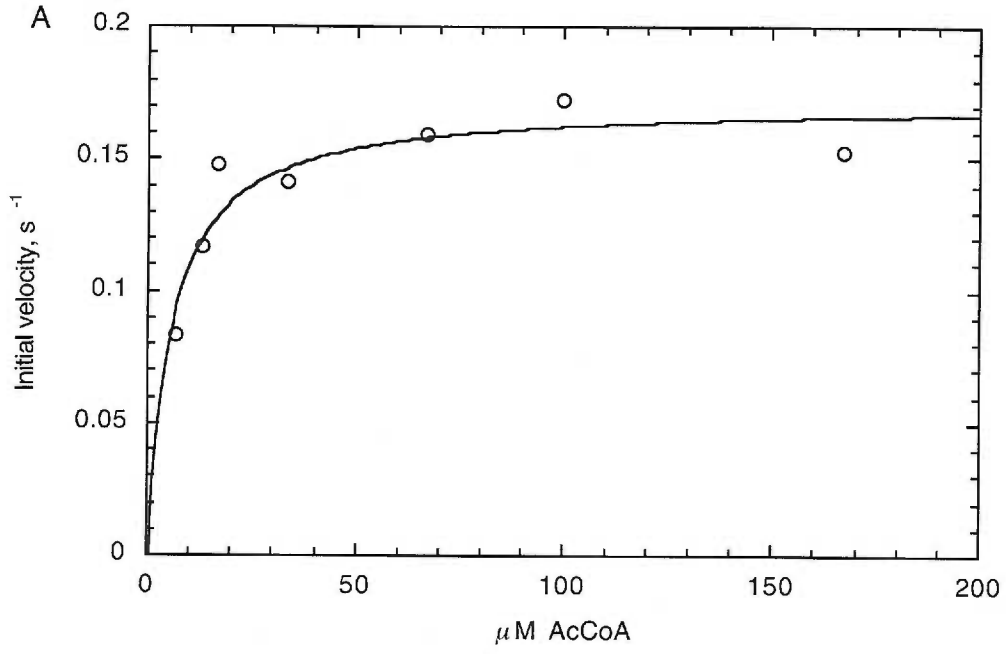
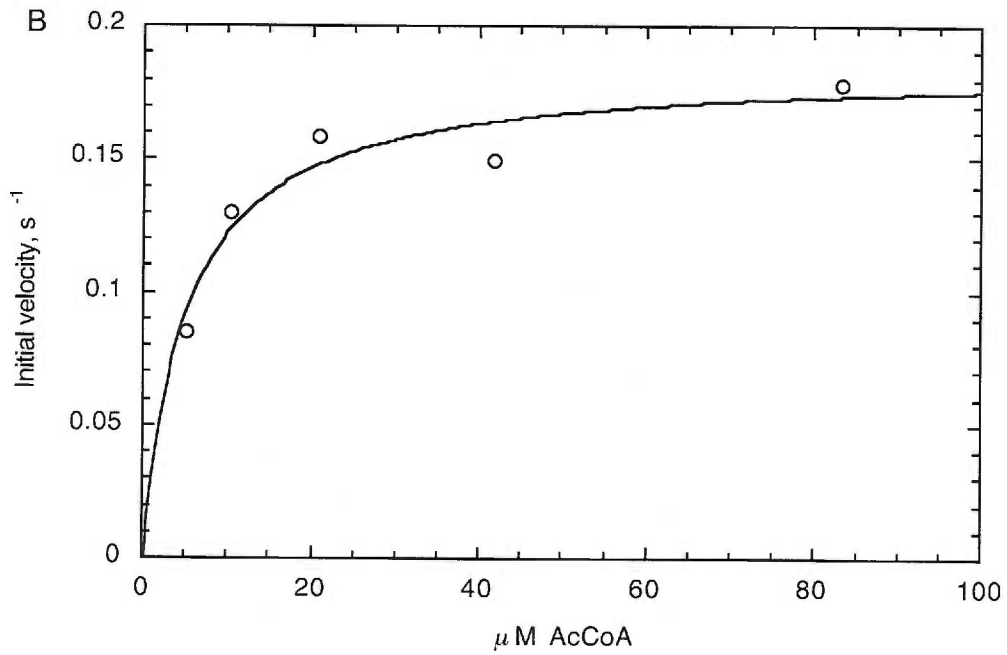


Figure 4

Kim *et al.*, 1999



References

1. Luo, R. X., and Dean, D. C. (1999) *J Natl Cancer Inst* **91**, 1288-94.
2. Grant, P. A., and Berger, S. L. (1999) *Semin Cell Dev Biol* **10**, 169-77.
3. Grunstein, M. (1997) *Nature* **389**, 349-52.
4. Bannister, A. J., and Kouzarides, T. (1996) *Nature* **384**, 641-3.
5. Yang, X. J., Ogryzko, V. V., Nishikawa, J., Howard, B. H., and Nakatani, Y. (1996) *Nature* **382**, 319-24.
6. Mizzen, C. A., Yang, X. J., Kokubo, T., Brownell, J. E., Bannister, A. J., Owen-Hughes, T., Workman, J., Wang, L., Berger, S. L., Kouzarides, T., Nakatani, Y., and Allis, C. D. (1996) *Cell* **87**, 1261-70.
7. Spencer, T. E., Jenster, G., Burcin, M. M., Allis, C. D., Zhou, J., Mizzen, C. A., McKenna, N. J., Onate, S. A., Tsai, S. Y., Tsai, M. J., and O'Malley, B. W. (1997) *Nature* **389**, 194-8.
8. Trievel, R. C., Rojas, J. R., Sterner, D. E., Venkataramani, R. N., Wang, L., Zhou, J., Allis, C. D., Berger, S. L., and Marmorstein, R. (1999) *Proc Natl Acad Sci U S A* **96**, 8931-6.
9. Tanner, K. G., Trievel, R. C., Kuo, M. H., Howard, R. M., Berger, S. L., Allis, C. D., Marmorstein, R., and Denu, J. M. (1999) *J Biol Chem* **274**, 18157-60.
10. Bradford, M. M. (1976) *Anal Biochem* **72**, 248-54.
11. Hunter, G. A., and Ferreira, G. C. (1995) *Anal Biochem* **226**, 221-4.
12. Hamada, M., Koike, K., Nakaula, Y., Hiraoka, T., and Koike, M. (1975) *J Biochem (Tokyo)* **77**, 1047-56.
13. Sanadi, D. R. (1969) *Methods in Enzymology* **13**, 55-61.

14. Rudolph, F. B., Baugher, B. W., and Beissner, R. S. (1979) *Methods in Enzymology* **63**, 22-42.
15. Scopes, R. K. (1994) *Protein Purification, Principles and Practice*, Springer, New York.